Ministry of Science and Higher Education of the Russian Federation
Siberian State Industrial University, Russia
Tsinghua Shenzhen International Graduate School, China
Samara National Research University, Russia
Institute of Strength Physics and Materials Science of
Siberian Branch of Russian Academy of Sciences, Russia
Polzunov Altai State Technical University, Russia
National Research Tomsk State University, Russia
World-Class Research and Academic Centre “Kuzbass”, Russia
University of Science & Technology Beijing, China
Huazhong University of Science and Technology, China
Tgl Technology Ltd, UK
Huanghe s&t university, China

MATERIALS IN EXTERNAL FIELDS (ISMEF 2022)

15 – 16 February 2022

Proceedings
of the 11th INTERNATIONAL ONLINE SYMPOSIUM

Novokuznetsk, 2022

UDC 669.017 : 539.2 (06)
BBC 22.9
M 39

M 39 Materials in external fields : proceedings of the 11th International online symposium on materials in external fields / under ed. of V.E. Gromov, Siberian state industrial university. – Novokuznetsk: SibSIU Publishing center, 2022. – 105 p. : drawings
ISBN 978-5-7806-0591-1

Conference proceedings contains scientific reports in the field of condensed matter physics based on scientific achievements arranged in the following sections: advanced technologies for surface hardening treatment, problems of strength, plasticity of materials under external energetic impacts, problems of materials operation in extreme conditions. The reports present results obtained by experimental methods and theoretical modeling. Relevance of the chosen areas is substantiated in various international conferences held annually, specialized publications, various international projects dedicated to the topics raised.

It is intended for specialists in strength and plasticity of materials under conditions of external energy impacts and may be used for scientific and technical workers, graduate students, and senior students.

ISBN 978-5-7806-0591-1

СОДЕРЖАНИЕ

Dear colleagues,

Today we are opening online the 11th International Symposium “Materials in External Fields”.

Since 2007 we have been continuing the tradition of joint discussion of international global problems. More than 50 scientists from China, Great Britain, South Korea, Russia, are taking part in our Symposium. On behalf of our university I welcome everyone to this event!

Results of the cutting-edge research and advanced technological solutions in the field of materials production and processing will be presented today. The prospects and trends of materials science development will be discussed.

Siberian State Industrial University, as a center of science and education in the south of Kuzbass, has vast experience and reputation in terms of materials science research, mainly in respect to metallurgy and mining. Our best schools and departments work in that field. This year we celebrate the 60th anniversary of the scientific school “Strength and plasticity of materials under external energy impacts”.

Let me express the hope that productive dialogue of scientists from different countries will become the basis for further cooperation!

Thank you!

Yuryev Alexey

SECTION 1. Advanced technologies for hardening surface treatment

UDC 544

SURFACE MODIFICATION OF POWDER COMPOSITION "Al-C" WITH 3,3,3-TRIFLUOROPROPYLTRIMETHOXYSILANE

Bulatnikov D. A., Grafov O. Yu., Popov D. A.

The Institute of Physical Chemistry and Electrochemistry RAS (IPCE RAS) Moscow, Russia

E-mail: bulatnikov@phyche.ac.ru

Abstract. The work has demonstrated the possibility of obtaining an antioxidant protective coating on the particles of powder composition "Al-C" by modification with 3,3,3-trifluoropropyltrimethoxysilane from acetone solution. Quantitative ratios of element states on the sample surface were determined by XPS-spectroscopy.

Keywords: Powder composition, mechanical alloying, modification, TFPTMS, protective coating

The method of mechanical alloying is a unique technique for obtaining energy-saturated compounds of heterogeneous components in the form of a powder [1]. To date powder compositions based on activated aluminum are of particular interest. Among them the system of "Al-C" composition is promising due to high energy release values in combination with the general availability of powder reagents and the simplicity of synthesizing the final material. At the same time, like the majority of aluminum-containing compositions, the system "Al-C" is sensitive to moisture, hence, for the possibility of practical application of the powder composition it is necessary to form a protective antioxidant coating on the activated particles.

The application of fluorine-containing coatings practically does not affect the value of the specific heat of combustion of the system, along with this it allows reducing the induction period.

Previously, it was shown in [2] that the near-surface layer of activated aluminum-containing powder compositions contains a significant content of hydroxide functional groups, the presence of which allows using alkoxysilanes as a modifier.

Thus, a 5% solution of 3,3,3 - trifluoropropyltrimethoxysilane (TFPTMS) in acetone was chosen to form a protective antioxidant coating. It is necessary to use only an anhydrous solvent that does not react with the modifier molecules to avoid hydrolysis of the alkoxysilane.

Figure 1 shows the mechanism of interaction of the modifier with the substrate surface.

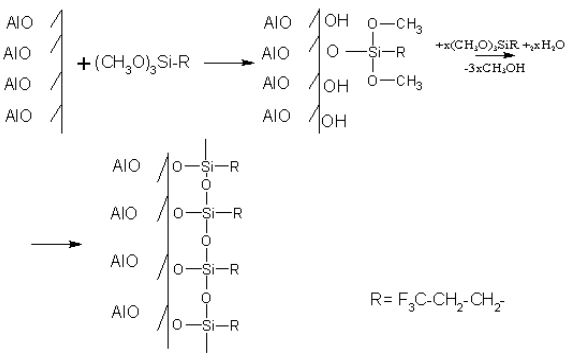

Figure 1 – Mechanism of interaction of fluorinated alkoxysilane with the oxidized surface of Al-C powder composition

As a result of the modification a system of Al-O-Si, Si-O-Si bonds is formed due to which the powder functionalization and protection against oxidation is provided.

The surface of the composite powder was studied by XPS spectroscopy. C1s-, O1s-, F1s-, Al2p- and Si2p-electron spectra were analyzed to study the qualitative and quantitative composition, but the most informative of them were the C1s- and O1s-electron spectra shown in the figure below.

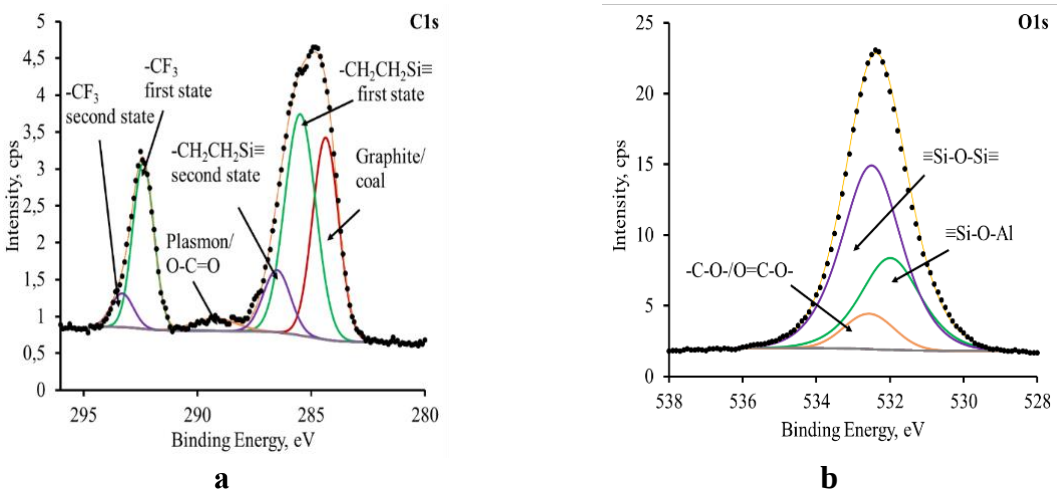

Figure 2 – XPS spectra of carbon C1s- (a) and oxygen O1s-electrons (b)

According to the results of XPS-research in the region of C1s-electrons carbon on the sample surface appears in several states: with 284.3 eV bond energy which can be correlated with graphite and coal, oxygen-containing derivatives -O-C=O with 289.1 eV bond energy and -C-O- and TFPTMS chain fragments: $-CH_2-CH_2-Si-$ with 285.5 eV bond energy and $-CF_3$ with 292.4 eV bond energy. The appearance of an additional peak in the case of $-CH_2-CH_2-CH_2-$ and $-CF_3$ is due to different surroundings of the atoms, leading to a change in the charge of the atoms due to redistribution of the electronic density on a number of molecules.

The oxygen O1s-electron spectrum is the most informative. It can be represented by a set of peaks, which can be correlated with the following states: the peak of a number of states: -C-O-, O=C-O, the -Si-O-Si- bond system in the energy region of 532.5 eV, and the -Si-O-Al bond system with an energy value of 532 eV. The presence of the peak responsible for the -Si-O-Al bond complex allows us to suggest the successful joining of TFPTMS on the surface of the composite powder.

Using the integral intensities under the peaks taking into account the cross sections of photoionization of electron shells, the ratios of the studied elements on the surface were calculated. It was shown that the quantitative content of the state responsible for the -Si-O-Al bond system is 6.74%, while, the content of the state responsible for the $-CF_3$ bond reaches 25.20%.

The results obtained testify to sufficiently high efficiency of TFPTMS for the possibility of its application as a surface modifier for composite powder of "Al-C".

REFERENCES

1. Koch C. C., Materials synthesis by mechanical alloying, Ann. Rev. Mater. Sci., 1989, Vol. 19, P. 121–143.

2. Bulatnikov D. A. Investigation of the compatibility of high-density energetic boron-containing composite powders with curable polymer matrices. Optimization of the physical and mechanical properties of the composite. Master’s thesis. MIREA - Russian Technological University (MITHT named after M. V. Lomonosov). Moscow. 2021. 86 c.

UDC 539.537;629.7.023.222

CHANGING OF A SURFACE CRATERS DENSITY ON QUARTZ PLATE SUFFERING HIGH-VELOCITY IMPACTS OF MICROPARTICLES BY DEPOSITION OF IN-SN-O BASED COATINGS

Tursunkhanova R.B.[1,2], Sergeev V.P. [1,2], Kalashnikov M.P.[1,2],
Sergeev O.V. [1], Neyfeld V.V[1]., Stuzhuk V.V.[3]

[1]*Institute of Strength Physics and Materials Science RAS, c.Tomsk, Russia*

[2]*National Research Tomsk Polytechnic University, c. Tomsk, Russia*

[3]*Rocket and Space Corporation Energia, c. Korolev, Russia*

E-mail: rbt1@tpu.ru

Abstract. To increase the resistivity of quartz glass against destruction from hyperspeed solid microparticles, In-Sn-O nanocomposite coatings deposited on the surface using magnetron sputtering. It is established that such coatings, slightly reducing the transparency of glasses in the visible region of the spectrum, but increasing the mechanical properties, lead to an increase in the resistance of glasses against the impact of high-speed iron microparticles.

Keywords: quartz, oxide coatings, high-speed impacts of microparticles.

During operation, spacecraft in outer space is exposed to extreme external factors (the impact of high-speed meteoroids and space debris particles, high and low temperatures, severe radiation exposure, etc.). Bombardment by high-speed particles poses an immediate threat to the safety of the spacecraft's flight, since it can cause its mechanical damage or even destruction. [1]. The most sensitive to the effects of this factor are the windows of the portholes, with the help of which observations of space objects are carried out. Thus, during the movement of spacecraft in low Earth orbits for 5-7 years, due to high-speed collisions with the flow of microparticles, erosion of the glass surface occurs, significantly complicating optical measurements of objects both on the Earth's surface and remote in outer space. Therefore, the protection of such transparent structures from meteorite impacts, space dust and debris are an urgent task. In [2,3] The resistance of nitride nanocomposite coatings based on the Si-Al-N system deposited on the quartz surface against the impact of hyperspeed microparticles and optical glasses is investigated. In this work, we focused on oxide coatings (ITO) based on the In-Sn-O system. At a certain concentration ratio of In and Sn and the deposition mode, they also become transparent in the visible region of the spectrum. The purpose of this work is to study the magnetron method of forming single-layer nanocomposite coatings based on In-Sn-O, which have simultaneously high values of transparency in the visible range of the spectrum, tensile strength and protective effect on the impact resistance of hyperspeed iron microparticles.

Deposition of coatings with a thickness of 5-6 mm was carried out on quartz glass plates of the KV brand. The coating process was formed by pulsed magnetron sputtering of a target based on indium-tin oxide on a vacuum installation "UVM-05 MD".

Mechanical tests of glass disks and determination of their strength for centrosymmetric bending were performed on the Instron-3369 deformation machine by the method of two coaxial rings for small test surface areas. During strength testing of the samples, destruction begins in the central zone. The cracking pattern during deformation of uncoated and In-Sn-O coated glass samples is shown (Figure 1 b, c). The value of the bending strength σ_{bB}, samples of

KV glass without coatings and with a coating based on the In-Sn-O system are presented in Table 1.

a b c

Figure 1 – Light transmission spectra (T) in the wavelength range of 200-800 nm of quartz glass (a) coated In-Sn-O (1) and uncoated (2), photographs of glass samples after tensile strength tests according to the centrosymmetric bending scheme uncoated (b) and coated In-Sn-O (c)

Table 1 – Average values of sample thickness <h> and tensile strength $<\sigma_{bB}>$ for centrosymmetric bending of KV glass samples without coating and with In-Sn-O coating

Coatings	**<h>, mm**	**$<\sigma_{bB}>$,**
Uncoated	–	46,0 ± 4,8
With In-Sn-O coating	5,6 ± 0,3	74,1 ± 6,1

The experimental method of firing samples of KV glasses with and without coating with spherical iron microparticles accelerated to a speed of 5-8 km/sec did not differ from the one previously described by us in [3].

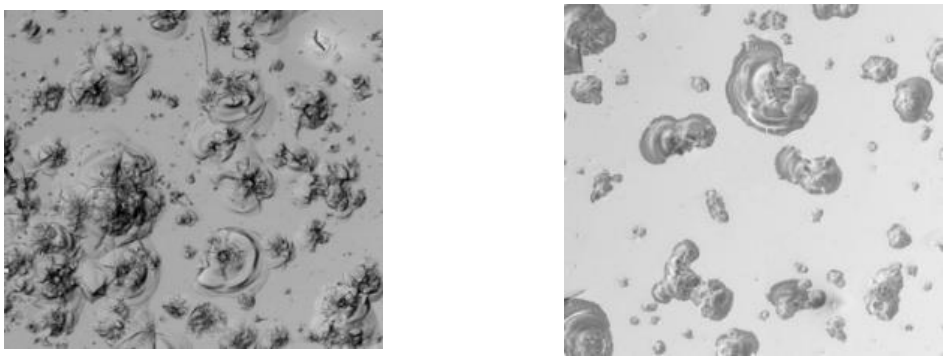

a b

Figure 2 – Image of craters on the surface of glass samples of the same area without coating (a) and with In-Sn-O coating (b) after firing

Figure 2 shows images of the surface of uncoated (a) coated glass samples located next to each other after the impact of the same flow of hyperspeed iron powder particles, where the difference in the surface density of craters, including local zones of microcracks, is clearly

visible. In addition, the surface density of the resulting craters on uncoated glasses ρ_0 (Figure 2 a) under the same test conditions on coated glasses In-Sn-O density ρ_I below (Figure 2 b). Counting the number of craters formed in one shot on the total area of the tested glasses shows that when coating In-Sn-O the relative decrease in the average value of the surface density of craters in comparison with uncoated glass is $\rho_0/\rho_I \approx 3{,}4$.

Thus, the experiments carried out made it possible to determine an increase in the tensile strength of coated glasses with centrosymmetric bending σ_{bB} with a slight decrease in the light transmittance in the visible region of the spectrum. It is established that the application of In-Sn-O coating on quartz glasses leads to a multiple decrease in the surface density of craters.

This research was performed under the government statement of work for ISPMS Project No FWRW-2021-0003. It was too supported by TPU development program.

REFERENCES

1. Silnikov M. V. и др. Numerical simulation of hypervelocity impact problem for spacecraft shielding elements // Acta Astronaut. Elsevier Ltd, 2018. T. 150, № August 2017. C. 56–62.

2. Sergeev V. и др. Magnetron sputtering of Si-Al-N nanocomposite coatings on quartz glasses for protection against impacts of high speed microparticles // Vacuum. Elsevier Ltd, 2017. V.143. P. 454 - 457.

3. Bozhko I.A.,et al. Investigation of the resistance of K-208 glasses with optically transparent Al-Si-N nanocomposite coatings to the impact of high-speed microparticles // Rus. Phys. J. 2019. V. 62, No. 3. P. 393 – 399.

UDC 621.785.53; 539.25

COMPLEX MODIFICATION OF STAINLESS HIGH-ALLOY STEEL - STRUCTURE AND PROPERTIES

Ivanov Yu.F., Petrikova E.A., Teresov A.D., Tolkachov O.S., Lopatin I.V.

Institute of High Current Electronics, Siberian Branch of the Russian Academy of Sciences
Tomsk, Russia

E-mail: yufi55@mail.ru

Abstract. As a result of the studies performed, the purpose of which was to establish the regularities of the steel 310 structure, mechanical and tribological properties evolution, subjected to a complex effect that combines irradiation with a pulsed electron beam and subsequent nitriding in a low-pressure gas discharge plasma, a processing mode that makes it possible to increase the hardness of steel (relative to the initial condition) by 11.2 times, wear resistance - by more than 700 times was identified.

Keywords: nitriding, pulsed electron beam, high-alloy steel, low-pressure gas discharge plasma, structure, properties.

Modification of the steel 310 (Fe-0.2C-23Cr-18Ni) surface layer was carried out by the pulsed electron-beam treatment ("SOLO" setup) methods [1]. It is shown that with an increase in the energy density of the electron beam, an increase in microhardness (from 1.7 GPa in the initial state to 2.4 GPa after irradiation at 30 J/cm^2) and wear parameter (from 1.9×10^{-4}

$mm^3/N \times m$ at 10 J/cm^2 up to 5.2×10^{-4} $mm^3/N \times m$ at 30 J/cm^2) of the specimen's surface layer. The steel wear parameter before irradiation is 4.9×10^{-4} $mm^3/N \times m$.

Nitriding was carried out ("QUINTA" setup) [1] of steel 310 specimens previously irradiated with a pulsed electron beam in a low-pressure gas discharge plasma by two methods: by heating the samples with plasma ions (hereinafter, method 1) and by heating the samples with plasma electrons (hereinafter, method 2).

It is shown that during nitriding according to method 1, the maximum microhardness, 19 GPa (exceeds the hardness of steel before modification by 11.2 times and the hardness of steel after irradiation with an electron beam by 8 times), and the minimum wear parameter, $k = 0.7 \times 10^{-6}$ $mm^3/N \times m$ (more than 700 times less than the steel wear parameter before modification and more than 750 times less than the steel wear parameter after electron beam irradiation) are observed on specimens irradiated at an electron beam energy density of 30 J/cm^2, 200 μs , 3 imp. and subsequent nitriding at a temperature of 520^0C for 3 hours.

The thickness of the hardened layer is 40 μm. It has been established that the specimens that demonstrated the highest values of hardness and wear resistance have the maximum (90.6%) content of nitride phases (chromium and iron nitrides) in the surface layer.

Transmission electron diffraction microscopy has shown that after nitriding at a temperature of 450^0C, iron and chromium nitrides are formed in the steel surface layer in the form of rounded nanosized particles. At nitriding temperatures of 520^0C and 600^0C, a lamellar-type structure is formed in the steel surface layer, formed by alternating parallel plates of iron nitride and chromium nitride.

The elion method of nitriding (method 2) leads to close (nitriding at 450^0C, 3 hours) or lower (nitriding at 520^0C, 3 hours and 600^0C, 5 hours) values of the steel surface layer microhardness, in relation to nitriding by the method one. During tribological tests, it was found that after nitriding at a temperature of 450^0C, 3 hours and 600^0C, 5 hours, the wear resistance of steel specimens modified according to method 1 is higher than the wear resistance of steel after nitriding according to method 2. Nitriding at a temperature of 520^0C, 3 hours leads to better results when using method 2, namely, the wear resistance of steel samples modified according to method 1 is lower than the wear resistance of steel after nitriding according to method 2 by 2.9 (ES = 10 J/cm^2) and 1.2 times (ES = 30 J/cm^2). It has been established that nitriding (method 2) at 450^0C and 520^0C temperatures for 3 hours of specimens previously irradiated with an electron beam (10 J/cm2, 200 μs, 3 pulses) is accompanied by the formation of a ceramic layer containing only iron and chromium nitrides. For the first time, during electron-ion-plasma nitriding (method 2), the phenomenon of blistering was discovered - the formation of bubbles on the surface of the material (Figure 1, a). It has been established, in the study of specimen's fracture surface previously irradiated with an electron beam and subjected to nitriding by two methods, that the destruction of steel surface layer nitriding according to method 1 proceeds mainly through a viscous mechanism; the destruction of the steel surface layer nitriding according to method 2 proceeds mainly by the quasi-brittle mechanism (Figure 1b).

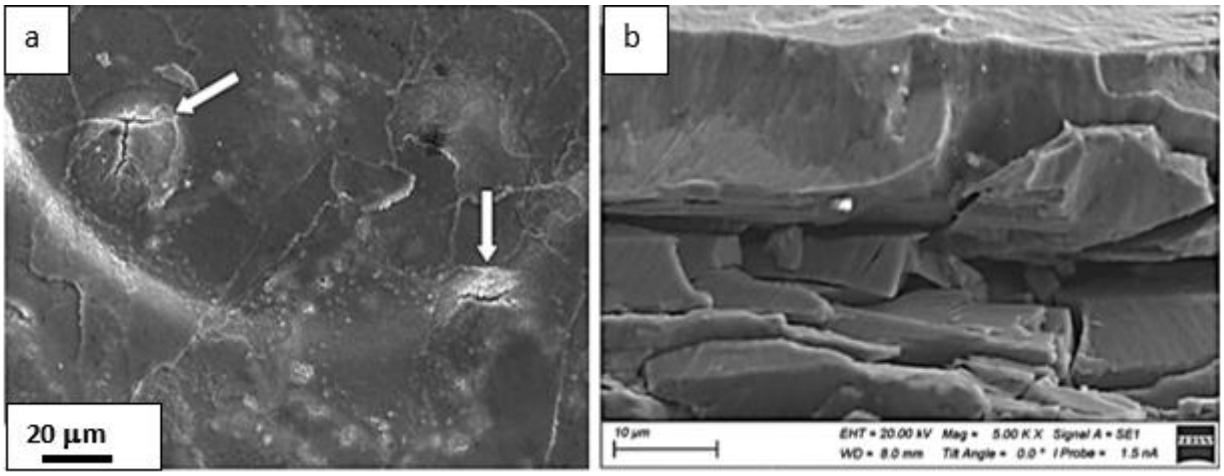

Figure 1 – Electron microscopic image of the steel 310 structure subjected to complex modification, combining irradiation with a pulsed electron beam (10 J/cm2, 200 µs, 3 pulses) (a) and (30 J/cm^2, 200 µs, 3 pulses) (b) and subsequent nitriding (520^{0}C, 3 hours) according to method 2; (a) modification surface (arrows indicate microcracks); (b) fracture surface.

Acknowledgements. The research was funded by RFBR and Tomsk region, project number 19-48-700010».

REFERENCES

1. Evolution of the steel surface layer structure subjected to electron-ion-plasma processing methods / Ed. N.N. Koval, Yu.F. Ivanov. Tomsk: NTL, 2016. 304 p.

UDC 539.6

MODEL OF THE FORMATION OF A HETEROGENEOUS PLASMA FLOW IN THE ELECTRIC EXPLOSION OF CONDUCTORS

V. Sarychev [1], A. Granovskii [1], S. Nevskii [1], V. Gromov [1]

[1] Siberian State Industrial University, Department of Nature Sciences, Novokuznetsk

E-mail: sarychev_vd@mail.ru, nevskiy.sergei@yandex.ru

Abstract. Using the method of high-speed shooting, it is revealed that there are three typical zones of a heterogeneous plasma flow in the end-type plasma accelerator. The relation between the coordinate of Zone 3 and time for various types of voltage is linear in logarithmical coordinates

Keywords: electric explosion of conductors, heterogeneous plasma fluxes, finite element method, conservation laws.

The experimental and theoretical studies on scattering of electric explosion products in the end-type plasma accelerator are carried out [1]. Using the method of high-speed imaging (10^6 shots per second), it is revealed that there are three zones in a heterogeneous plasma flow. Zone 1 is a plasma focus, in Zone 2 there is a 90 degree turn of a flow, whereas a plasma flow is parallel to the dielectric disk in Zone 3 (Figure 1).

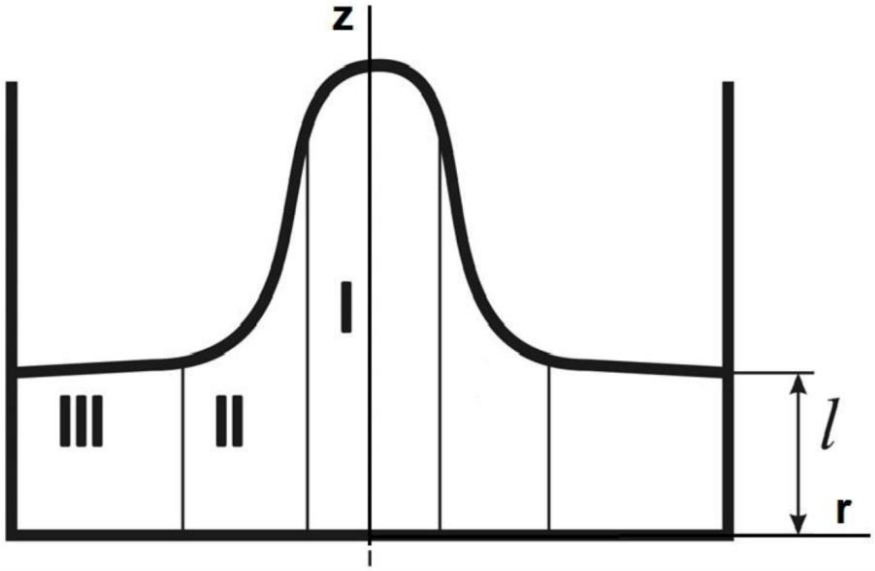

Figure 1. Scheme of plasma spread (I – plasma focus, II – zone of plasma flux turning, III – zone of parallel flow)

Following the concepts of plasma scattering when exposed to magnetic and gas-dynamic pressure, a mathematical model is proposed and provides an adequate explanation of plasma motion in Zone 3. It comprises equations of laws of mass and pulse conservation, as well as the first and second Kirchhoff's laws. The outcomes of modeling are in compliance with the experimental data. A numerical single-fluid magnetohydrodynamic model is developed for general description of formation and evolution of a plasma flow. It is based on Navier-Stokes and Maxwell's equations:

$$\begin{aligned} &\rho\left(\frac{\partial\vec{v}}{\partial t}+\vec{v}\nabla\vec{v}\right)=-\nabla p+\mu\Delta\vec{v}+\vec{F}_V;\\ &\nabla\cdot\vec{v}=0;\\ &\nabla\cdot\left(\sigma\nabla V+\sigma\frac{\partial\vec{A}}{\partial t}\right)=0;\\ &\sigma\frac{\partial\vec{A}}{\partial t}+\frac{1}{\mu_0}\nabla\times\left(\nabla\times\vec{A}\right)+\sigma\nabla V=0 \end{aligned} \tag{1}$$

where $\vec{v}$ – vector of velocity, p – pressure, ρ – density, μ – dynamic viscosity, $\vec{F}_V$ – volume forces, set by the sum of Lorentz force and gravitation: $\vec{F}=\vec{j}\times\vec{B}+\rho_0\vec{g}$. The distribution of temperatures in the field to be estimated was determined according to the equation of convection heat conductivity with a volume heat source.

$$\rho C_p\left(\frac{\partial T}{\partial t}+\vec{v}\nabla T\right)=\nabla\cdot(k\nabla T)+S_V \tag{2}$$

where T – temperature, C_p – specific thermal capacity, k – coefficient of thermal conductivity, S_V – volume sources of heat. Joule effect only can be considered as a volume heat source $S_V=\vec{j}\cdot\vec{E}$. The system of equations (1) and (2) was solved by the method of finite elements. The obtained patterns of plasma current distribution agree satisfactory with the results of high-speed imaging. They point at a jet in the central part of the electrode, which splits out with the distance from its surface (Figure 2)

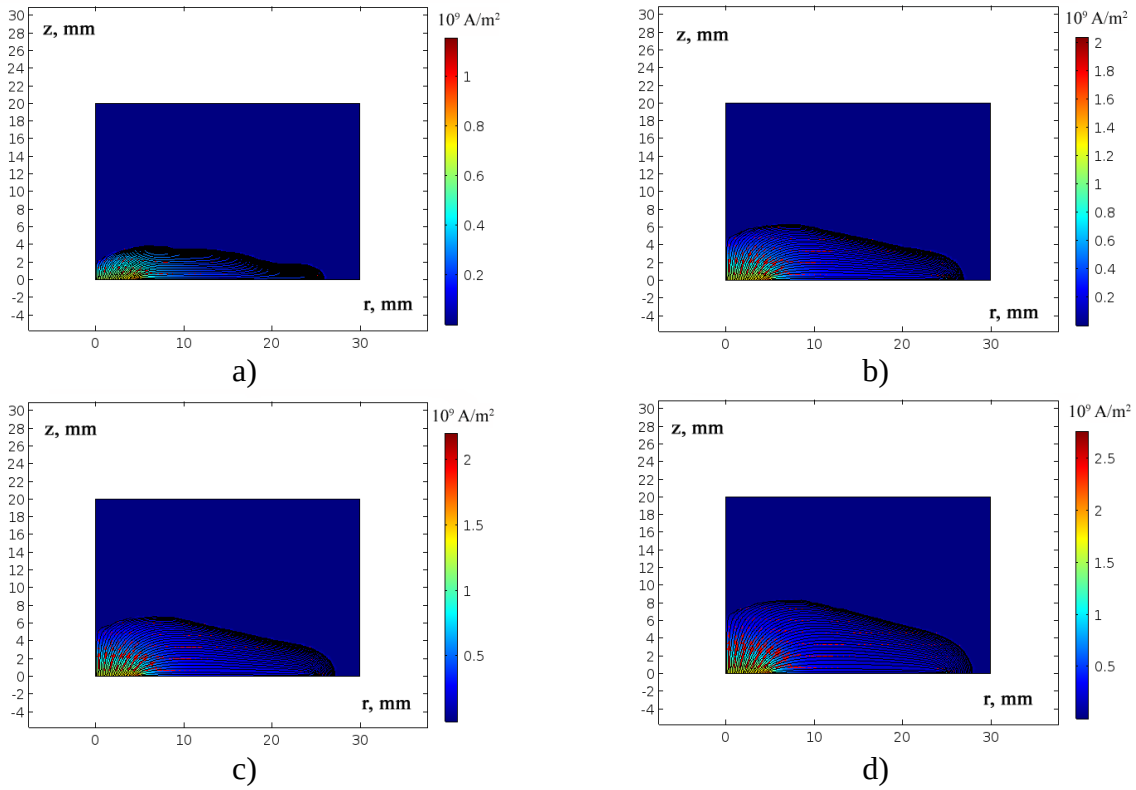

Figure 2 – Electric current distribution (a – 5 μs, b – 10 μs, c – 11 μs, d – 15 μs)

Acknowledgements. Work is executed at financial support of Russian Scientific Foundation (20-19-00452)

REFERENCES

1. Sarychev V. D. Modeling of the initial stages of the formation of heterogeneous plasma flows in the electric explosion of conductors/ V. D. Sarychev [et al] // Current Applied Physics. 2018. V 18. P. 1101-1107.

SECTION 2. Problems of strength, plasticity of materials under external energetic influences

UDC 669.620.17

ELECTROPLASTIC EFFECT UNDER TENSION IN TRIP STEEL

Stolyarov V.V.

Mechanical Engineering Research Institute of RAS

Moscow, Russia, vlstol@mail.ru

Abstract. In the work results of study of electroplastic effect in the metastable austenite-martensite TRIP steel under current of different modes and regimes are presented. Deformation behavior in form of stress-strain curves and mechanical properties has been investigated by tension. It has been shown strong current mode influence on ductility.

Keywords: electroplastic effect, pulse current, TRIP effect

Electroplastic effect (EPE) is a phenomenon consisting in a decrease in the flow stress when exposed to an electric current [1]. This allows to achieve increased deformability of the material during metal working treatment. On the tensile deformation diagram, the EPE manifestation is recorded, as a rule, in the form of downward stress jumps [2]. EPE has been studied in most detail for pure metals and coarse-grained single-phase alloys [3], as well as for titanium alloys, including those with shape memory [4]. It turned out that the action of the current can stimulate or suppress phase transformations [5]. This aspect is most interesting when applied to TRIP steels, in which the martensitic transformation is induced by plastic deformation. The aim of this work was to study the features of EPE manifestation in metastable austenitic-martensitic trip-steel under static tension and current action.

The object of the study was TRIP steel (23Cr15Ni5AMo3) in the form of a tape 0.3 mm thick. The phase composition of cold-rolled steel in the initial state was a mixture of cold-worked metastable austenite and deformation martensite in a ratio of 50/50. Specimens with a working section size of 0.3x3x30 mm^3 were tested for tension at a speed of $0.3x10^{-3}$ s^{-1} (0.6 mm / min) with the introduction of current in the following modes: 1 - without current; 2 - single pulses, current density j = 350 A / mm^2, $\tau = 0.5x10^{-3}$ s; 3 - multi-pulse current, j = 100 A / mm^2, τ = 100 ms, with a frequency of 1000 Hz; 4 - direct current, j = 12 A / mm^2. Note that, in the course of tension the actual current density increases due to a decrease in the initial cross section.

The mechanical properties of TRIP steel in the austenitic-martensitic state under tension with and without current are given in Table 1.

Table 1 – Mechanical properties of TRIP steel under various current modes

№	Current mode	Duration, min	Sample temperature, °C	UTS, MPa	YS, MPa	El, %
1	Without current	13.5	20	1650	1500	23
2	Single pulse current	8	20	1500	1190	12
3	Multipulse current	3	120	1465	1150	2,8
4	Direct current	2	130	1360	1150	2,0

Tension without current is accompanied by a yield tooth and an extended yield area, followed by a low abrupt strain hardening, which is caused by the TRIP effect (Figure 1a). Strength and ductility were the highest for this tension mode (Table 1). All subsequent modes

of current contribute to a decrease in strength and ductility, especially strong for multipulse and direct current. Single current pulses lead to the disappearance of the yield tooth, the appearance in the elastic region and at the stage of strain hardening of stress jumps downward with an amplitude of up to 50 and 140 MPa, respectively, without a significant increase in temperature (Figure1b).

Stress jumps are the result of the manifestation of the thermal effect in the elastic region and EPE in the elastoplastic zone.

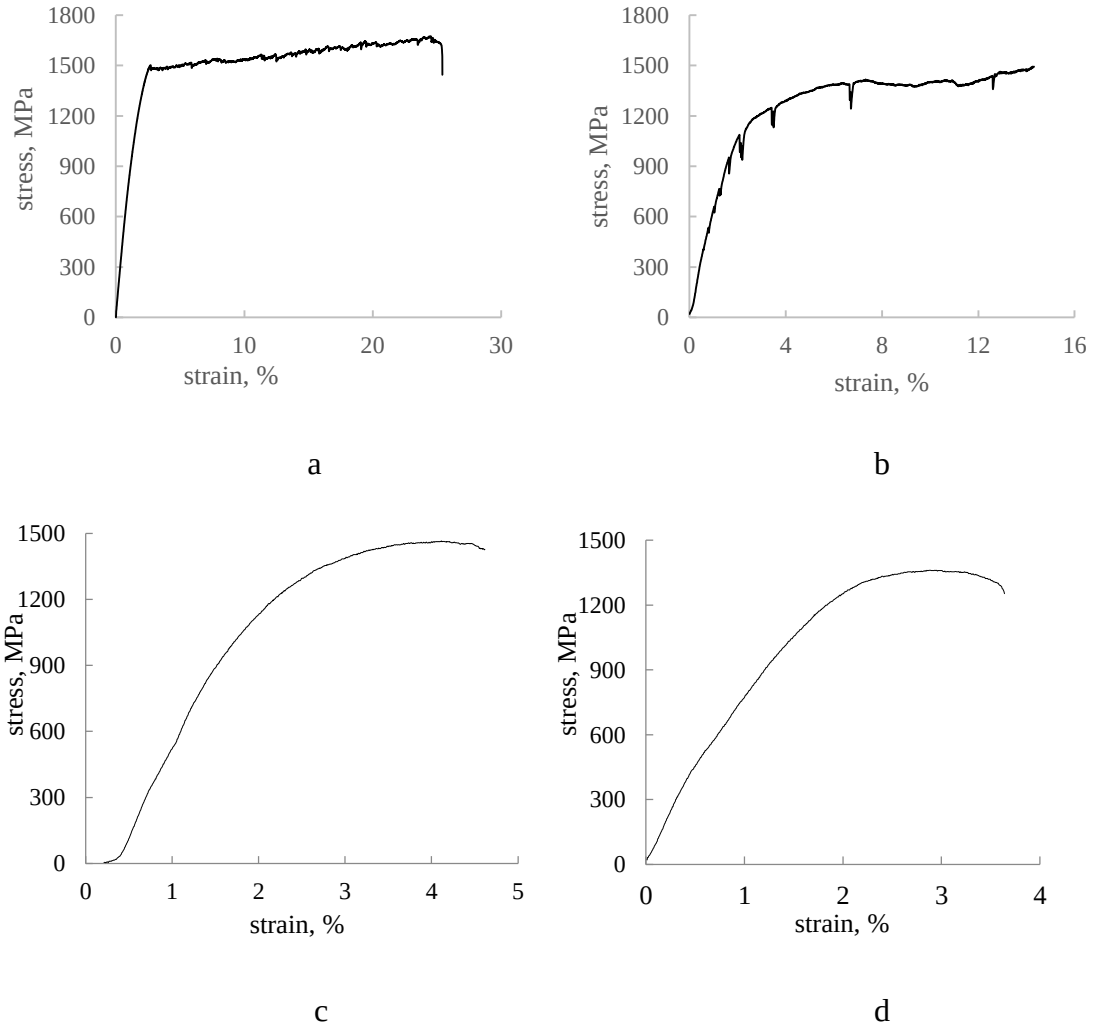

Figure 1 – Stress-strain curves of TRIP steel: a – without current; b – single pulse current; c – multipulse current; d –direct current.

When exposed to a multi-pulse and direct current, there are no stress jumps, and the strain hardening coefficient increases (Figure 1c, d). The static tension stress-strain curve takes on the form characteristic of stable austenitic steel, which is due to the large thermal effect (several hundred degrees). X-ray diffraction studies have shown that tension without current and with single current pulses most strongly increases the volume fraction of deformation martensite in the tested sample to 82%. Tension with multipulse current reduces the formation of martensite by up to 72%, and with direct current up to 50%.

Thus, the thermal effect accompanying the current suppresses the deformation austenite-martensitic transformation and, accordingly, the TRIP effect.

REFERENCES

1. Misochenko A.A., Stolyarov V.V., chapter 15, monograph "Advanced materials and technologies", v.1. 2015. 268-278.

2. Troitsky O.A, et al. Physical foundations and processing technologies of modern materials. v.1 - Moscow - Izhevsk. Institute of Computer Technology. - 2004.590p.

3. Conrad H. Electroplasticity in metals and ceramics // Mater. Sci & Eng., A287. 2000.276-287.

4. Stolyarov V.V., Influence of pulse current on deformation behavior during rolling and tension of Ti–Ni alloys // J. Alloys Compd. 577 2013. S275-S276.

5. Stolyarov V.V., Klyatskina E.A., Terentyev V.F. // Suppression of TRIP effect in metastable steel by electrical current, Lett. Mater. 6 (4). 2016. 355-359.

UDC 539.376

A REVIEW ON FABRICATION OF GRADIENT NANO-STRUCTURE SURFACE LAYER ON THE METALS BY MEANS OF ELECTRONPULSE–ULTRASONIC COUPLING PROCESS

G. Tang [1, 2], G. Song [1], H. Wang [1]

[1.] Tsinghua Shenzhen International Graduate school, Tsinghua University, China

[2.] TGL Technology Ltd. London, UK

Keywords: gradient nano-structure, electroplastic, electropulse-ultrasonic coupling, fatigue property, Thermal stability.

One of the biggest challenges in the service of materials is the surface damage and failure caused by wear, fatigue, corrosion, and thermal/cold instability. Surface roughness and microstructure is a key factor that directly affects the surface properties of the material. Our technology is a metal processing method based on the principle of electroplastic effects and ultrasonic impact effects coupling to significantly improve the overall performances of the processed workpiece. The fatigue properties of 304 stainless steel and thermal stability of Inconel 718 superalloy were systematically studied by electropulse-ultrasonic coupling (EU), ultrasonic process (U) and mechanical polishing (MP) process.

The gradient Nano/micro structures were prepared on the surface and subsurface of the material by EU and U process. The surface roughness was remarkably reduced and the surface hardness, the surface residual compressive stress and the fatigue resistance of the 304 steel are improved by the EU and U process. The results showed that the fatigue strength of EU processed samples increased from 280Mpa before processing to 593MPa, while the fatigue strength of samples with the same finish only after mechanical polishing was 369Mpa (Figure 1).

Slip and twinning are the two main competing mechanisms during the plastic deformation of metals. The critical slitting stress of twinning varies little, and is only related to the stacking fault energy of the material. The lower the stacking fault energy, the smaller the critical slitting stress of twinning. Most metallic materials undergo plastic deformation through dislocation slip. 304 stainless steel is a low stacking fault energy material, and it is easy to introduce nanotwin structure.

Introducing nanoscale twinning interfaces is recognized as an optimization an effective strategy for comprehensive mechanical properties of materials. with traditional Unlike nano-structured metals, this one has a high-density, low-energy state coherent interface. The nano-twinned metal not only has high strength, but also maintains good plasticity and mechanical stability and other excellent mechanical behavior, especially in the alternating cycle. It also exhibits high fatigue limit, long fatigue life and excellent fatigue characteristics such as cyclic stability independent of fatigue history sign, which is mainly attributed to its stable coherent interface characteristics and Unique dislocations interact with twin interfaces. Relevant mechanisms will be further explored in depth.

Thermal stability of Inconel 718 with surface nanocrystallization induced by EU and U process was also studied. The large deformation generated by ultrasonic rolling is coupled with the electroplastic effect, which promotes the improvement of plastic deformation capacity, and makes the accumulated deformation energy storage in the deformation area recombined with the energy of pulsed electrical stimulation, which accelerates dislocation motion and atomic diffusion and promote rapid recovery and recrystallization in the deformed region, thereby further refining the grains, and obtaining a deeper gradient nano-refinement layer (Figure 2). The nanocrystals obtained by this process have higher hardness and thermal stability, and the microhardness test also confirmed that compared with the U process, the EU sample has a finer grain distribution, higher performance and thermal stability. The thermal stability temperature can reach 700-750 °C (Figure 3), which is significantly improved compared to the service temperature (650 °C) of Inconel 718 superalloy.

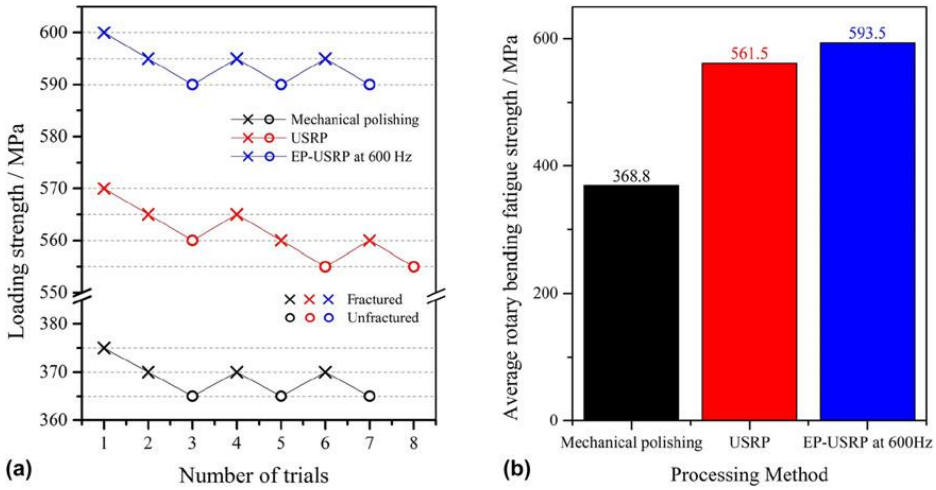

Figure 1 – 304 stainless steel: loading-failure up-and-down curves (a) and the average rotating fatigue strength (b) from the rotating bending fatigue test of the specimens processed by mechanical polishing, USRP, and EP-USRP at 600 Hz, respectively

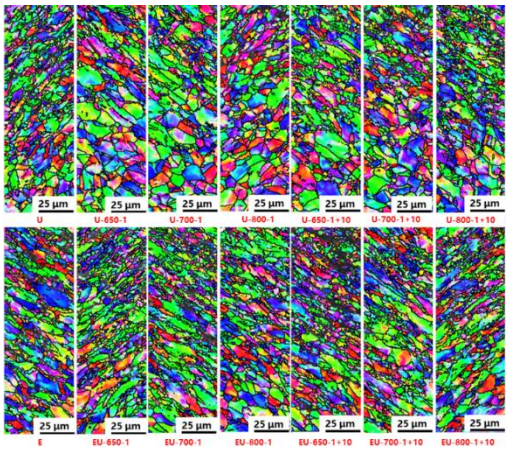

Figure 2 – Microstructure of Inconel 718 superalloy subjected to different heat treatments after ultrasonic processing (U) and Electropluse-utrasonic coupling processing (EU)

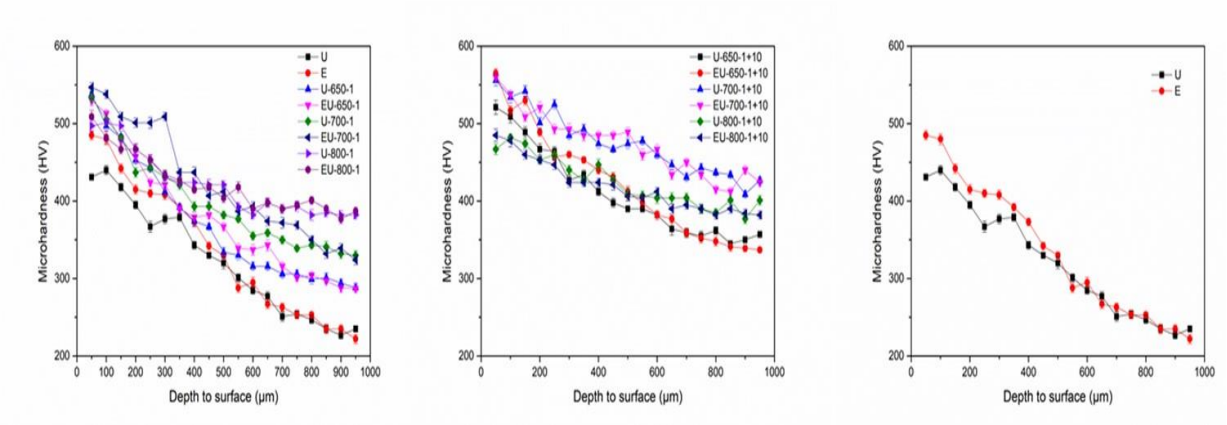

Figure 3 – Microhardness distributions on cross-section of Inconel 718 superalloy under different treatments

Acknowledgements. The authors are grateful for the contributions on partial experimental works from the graduated research group members, especially Zhiyan SUN, Xiaopei LI and Yongda YE.

REFERENCES:

1. Haibo Wang, Guoyi Tang, Guolin Song et al. J. Mater. Res., Vol. 33, No. 22, Nov 28, 2018
2. PAN Qingsong, CUI Fang, TAO Nairong, LU Lei. ACTA METALLURGICA SINICA, Vol.58 Jan. 2022
3. Wen Bin, Tian Yongjun ACTA METALLURGICA SINICA Vol.57 No.11 Nov. 2021
4. Qingsong PAN LIANGXUE ZHANG , LEI LU SCIENCE Vol 374, Issue 6570 pp. 984 98923 Sep 2021

UDC 620.193

DESTRUCTION OF A GROUNDED REACTOR ELECTRODE BY HIGH-VOLTAGE DISCHARGE IN LIQUID MEDIUM CONDITIONS

S.A. Glotov, G.G. Volokitin, YU.A. Krasnyatov, A.A. Alekseev

Tomsk State University of Architecture and Building, Tomsk, Russia

E-mail: sernatev@gmail.com

Annotation. In electric discharge technologies, the working tool is the electric discharge channel as a plasma formation. Due to the high energy parameters of this formation, such as temperature and pressure, the channel also carries a destructive force for the elements of the working chamber - the electrodes. Destruction manifests itself as erosion. The paper presents studies on changing the geometry of the hole (crater) of erosion.

Keywords: erosion, electrode, shock wave, vapor-gas cavity, cavitation phenomena, dimple, crater.

The whole variety of geometric shapes of the electrodes of electric discharge reactors (working chambers) can be reduced to one set: the tip - the plane. This form of electrodes is due to the conditions for creating a sharply inhomogeneous electric field in the interelectrode space. With this form of the electric field, the formation of an electric discharge channel is facilitated. Moreover, the “pointy” electrode is connected to the positive potential of the energy source, and the “flat” electrode is usually “grounded”.

Figure 1 shows the design of the electrode system of the electric discharge reactor. On the
Figure 2 shows the active element of the low-voltage electrode after it has been tested.

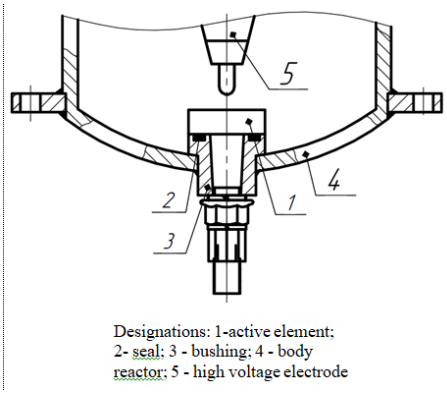

Figure 1 – Design of the electrode system of the electric discharge reactor

Figure 2 – Active element of the low-voltage electrode

This design makes it easy to remove the active element of the low-voltage (grounded) electrode as needed. The need to extract the active element may appear in the tasks of the experiment or for technological needs.

It should be noted that the erosion of the active element of the electrode was studied using a pulsed current generator, and the discharge was carried out in tap water. Based on the literature sources [1-3] and the conducted studies, it can be argued that the morphology of

erosion marks on the electrode (sample) is close if electric discharges existed in a gas or liquid medium. Those. in both cases, erosion holes were observed with the characteristic existence of a roller in the immediate vicinity of the hole. If the medium in the interelectrode space is represented by a solid electrically low-conductive body, then the erosion mechanism differs from the erosion mechanism in gas or liquid media. The difference in the mechanisms should be explained by the different degree of energy dissipation in the interelectrode space. The energy of a plasma formation is easily dissipated in a gas or liquid medium, but it is difficult if the medium is a solid body. Therefore, the erosion of electrodes can vary significantly - by two orders of magnitude. Figures 3 and 4 show samples subjected to electrical discharges.

As can be seen from these photographs, there is the formation of erosion holes with characteristic geometric dimensions - the diameter of the hole and its depth, as well as the presence of a roller near the erosion hole.

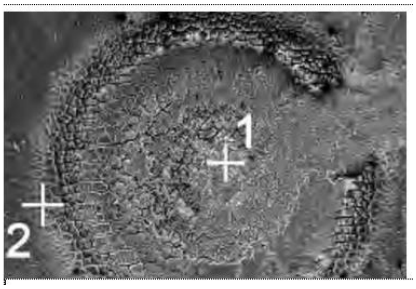

Figure3 – Photograph of a sample with erosion according to [2]

Figure 4 – Photograph of a sample with erosion according to these studies

As is known [3], erosion depends on the duration of loading, in this case, on the number of pulses received by the electrodes. Obviously, the greater the number of pulses, the higher the erosion value. In the above studies, the geometric parameters of the erosion hole (crater) were recorded - the diameter dl and the depth hl of the erosion hole, depending on the number of pulses applied, which is shown in Figure5.

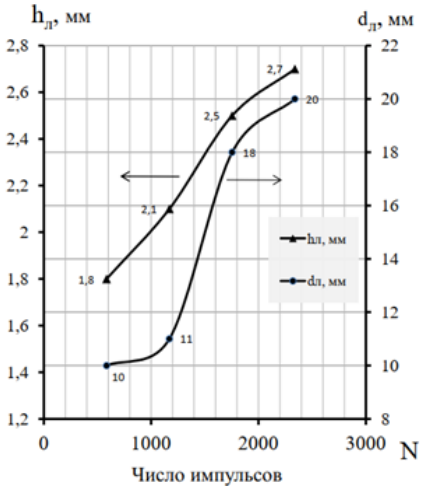

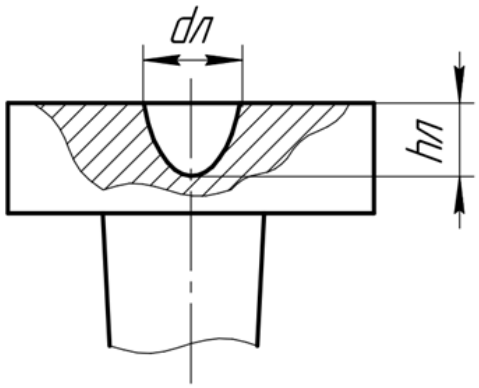

Figure 5 – Changing the diameter and depth of the erosion hole

As can be seen from the course of the curves in Figure 5, the erosion of the electrode in the initial period of time is determined by the deepening of the erosion hole with a slight change in its diameter and, starting from the number of pulses equal to 1200, there is a significant

expansion of the erosion hole and, from approximately 1800 pulses, erosion in diameter and in depth become proportional, as evidenced by the parallel course of the curves.

REFERENCES

1. Kurets V.I. Electropulse disintegration of materials / V.I. Kurets, A.F. Usov, V.A. Zuckerman. Apatity: publishing house of the Kola Scientific Center, 2002. 321p.

2. Gordienko P.S. Electrophysical model of electrode erosion under pulsed energy impact / P.S. Gordienko [et al.] // Electronic processing of materials. 2011. №3. pp. 15-27.

3. Kazub V.T. Kinetics and fundamentals of instrumentation for the processes of electric discharge extraction of biologically active compounds. Abstract Dis. D. in technical sciences / V.T. Kazub. Tambov State Technical University, 2002. 32p.

UDC 691.32

COMPUTATIONAL STUDY OF DEFORMATION AND FAILURE MECHANISMS OF HIGH E - LOW E COMPOSITES

A.A. Pazhin[1*], A.O. Chirkov[1], M.O. Eremin[2]

[1]National Research Tomsk State University Tomsk, Russian Federation

[2]Institute of Strength Physics and Materials Science SB RAS, Tomsk, Russian Federation,

*E-mail: alvian99@mail.ru

Ceramic materials based on zirconium carbide are widely used as protective thermal barrier coatings (refractory materials) aerospace and nuclear engineering [1-3]. Due to high corrosion resistance and the ability to maintain operational properties at high temperature. Mechanical properties such as elastic modulus and density make ceramics a direct competitor for classic constructional and functional materials like metals and their alloys. Ceramic materials based on carbides, borides, oxides are more preferred under specific type of loading. Meanwhile, ceramic materials have immanent brittleness in case that their type of chemical bond differs from classic metals. The latter yields the decreased resistance to tensile stresses. In the regions of bulk tension micro-damage and microfracture occur and later evaluate into magistral type of cracking. Since it is impossible to remove those ceramics properties described above, the new composite materials based on carbides, borides, oxides are designed increasing the crack resistance of original material.

The aforementioned problem is usually solved empirically. A huge number of different compositions of the origin material with hardening additives is designed and tested. But it is expensive. Due to the rapid development of high-performance computing technology, computer design and numerical experiment are widely used to estimate the physical-mechanical properties of the designed material in a wide range of loading conditions. In this work, fracture mechanism of ceramics based on zirconium carbide with the addition of low-modulus carbon particles is investigated. This type of composite in the literature was given the name High E – Low E (heteromodulus) composites [4-5].

Previous works carried out by the authors [6] have shown that fracture modeling of such a material using the yield/strength surface with single slope angle is not satisfactory. Now we propose a hypothesis of a piecewise linear yield surface which is more suitable for describing the mixed fracture mechanism of ceramic material. In this work, a model of uniaxial loading of heteromodulus composites is created using various slopes of the yield surface for the region of tensile and compressive stresses respectively. Drucker-Prager equation of yield surface [7] was

employed as a model basis. It allows considering the difference in material response to the stress sigh.

Main goal of this work is to develop the numerical technique for estimating the material crack resistance based on computational analysis of deformation and fracture of material mesovolume. Structural models are designed on the basis of SEM patterns of the material microstructure. Modelling is performed using the finite-difference method under the condition of plane strain. Verification with the experimental data indicates that piecewise-linear approximation of the yield surface allows to describe additional mechanisms in comparison with the single slope model.

REFERENCES

1. Katoh Y. Properties of zirconium carbide for nuclear fuel application / Y. Katoh [et al] // Journal of Nuclear Materials. 2013. №441. P.718-742
2. Shabalin I.L. Physicomechanical properties of ultrahigh temperature hereromodulus ceramics based on group 4 transition metal carbides / Shabalin I.L. [et al] // Advances in Applied Ceramics. 2010. №109. P.405-415
3. Dickerson M.B. Near net-shape, ultra-high melting, recession-resistant ZrC/W-based rocket nozzle liners via the displacive compensation of porosity (DCP) method / Dickerson M.B. // Journal of Materials Science. 2004. №39. P.6005-6015
4. Hasselman D.P.H., Becher P.F., Mazdiyasni K.S. Analysis of the Resistance of High-E, Low-E Brittle Composites to Failure by Thermal Shock / Hasselman D.P.H. // Material Science & Engineering Technology. 1980 №11. P.82-92.
5. Shabalin I.L Oxidation of titanium carbide–graphite hetero-modulus ceramics with low carbon content I. Phenomenological modeling of the ridge effect / Shabalin I.L, Roach D.L., Shabalin L.I // Journal of the European Ceramic Society 2008. №28. P.3165-3176
6. Pazhin A.A. Methematical modeling of deformation and fracture of zirconium carbide porous samples subjected to uniaxial compression / Pazhin A.A., Mirovoi Yu.A. // AIP conferences proceeding 2020. №2310. P.1-4
7. Drucker D.C. Soil mechanics and plastic analysis or limit design / Drucker D.C., Prager W. // Journal of applied Mathematics 1952. №10. P. 157-165

UDC 539 21:537

MODIFICATION OF PHYSICAL AND TECHNICAL CHARACTERISTICS OF METAL TWINNING UNDER EXTERNAL ENERGY INFLUENCES

V. S. Savenko

Mozyr State Pedagogical University named after I.P. Shamyakin Mozyr, Belarus

E-mail: savenko.vladimir195@gmail.com

Abstract. The article deals with theoretical and experimental aspects of electroplastic deformation by twinning of metals. The author defines the kinetic physical basis of the twinning development under the conditions of excitation of the electronic subsystem of metals, specifies physical models of new channels for the realization of twinning under the conditions of electroplasticity. The author also offers the mechanisms of the plasticizing effect of the surface electric charge and reveals the dynamic pinch effect to the elastic plastic deformation of

metals with the usage of the intrinsic magnetic field of the current, which causes ponderomotive factors.

Keywords: electroplastic deformation, ponderomotive action of current, pinch effect, skin effect, magnetic field, vortex electric field, pulsed current.

Plastic deformation by twinning is carried out when sliding is impossible, for example, with orientational inhibition and high loading rates, as well as at low temperatures. Twinning starts at tension concentrators, the development of twinning dislocations occurs at high rates, and strain tension at the boundaries of twin units often lead to the destruction of the material. Thus, if it were possible to control the development of twinning and reduce the tension concentration at the twin boundaries, then there would be a real opportunity to use twinning as a reserve of material plasticity [1–2].

The theoretical and experimental research results present the pulsed current effect with a density of 103 A/mm2 and a duration of 10-4 s, a frequency of 600-800 Hz on the implementation of electroplastic deformation of magnesium with a change in its kinetics due to a decrease in dislocation potential barriers and a decrease in starting tension for the breakdown of dislocations from stoppers.

We offer one of the possible mechanisms of the electron-plastic effect (EPE) - upon excitation of localized states of electrons on twinning dislocations under conditions of external energy influences (Figure 1).

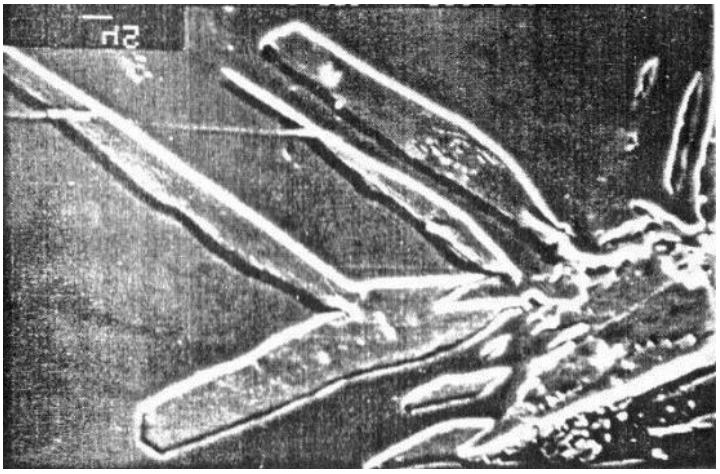

Fugure 1 – The system of twins that arose at the internal voltage concentrator when passing a current pulse with a density of 700 A/mm^2

Electrons are on the positive part of the deformation potential of dislocations:

$$\rho_+(r) = \frac{en_0B}{r} sin\varphi, \qquad B = \frac{Z_e b}{2\pi}\left(\frac{1-2\nu}{1-\nu}\right)$$

where φ is the angle between the vectors b and r, ν is Poisson's ratio, Z_e is the ion charge, and b is the Burgers vector.

External energy influences actuate localized electronic states at the potential, and, obviously, their wave functions are blurred. An increase in the electron density in the core of dislocations lowers the value of the Peierls-Nabarro potential barrier. The decrease in the steepness of the barrier relief also explains the mechanism of the magnetoplastic effect in *NaCl* and *Al*, the essence of which is the displacement of dislocations in unloaded crystals under the influence of a magnetic field. Before the crystal is placed in a magnetic field, the dislocations are in equilibrium, hanging in the long-range field of internal stresses on local barriers associated with point defects and the Peierls relief. By lowering the barrier by applying a

magnetic field, one can set the dislocations in motion. However, a similar mechanism can be applied to ionic and covalent crystals, while in metals the height of Peierls-Nabarro barriers is small and the activation volume for them is several orders of magnitude smaller than for potential barriers created by other dislocations and point defects.

The most probable mechanisms of the electromagnetic fields influence on the plastic deformation of metals should be carried out according to the crystal surface, since the excitation of the electronic subsystem of the crystal by an electromagnetic field leads to a change in its surface energy. When metals are deformed above the yield limit, moving dislocations, interacting with the free surface, acquire excess free energy, become unstable and tend to reach the surface of the crystal. It should be noted that the edge dislocation is attracted to the surface by the "mirror image" force, which is determined by a slowly varying logarithmic potential. At the same time, the emergence of a dislocation on the surface is accompanied by the appearance of a characteristic step. At the same time, the energy $b^2 \cdot \gamma$ is expended to create a new cell, where γ is the surface energy. This force is distributed towards the crystal axis over a dislocation half-width on the order of several *b*, and in the immediate vicinity of the surface it can prevail over the "mirror image" force. Therefore, a decrease in the surface energy of the metal will facilitate the emergence of dislocations of the same sign on the surface and will lead to an increase in the rate of plastic deformation and a decrease in deformation hardening. At the same time, an increase in the surface energy intensifies the work of surface dislocation sources by compensating for the "mirror image" force. As for metals, semimetals, and semiconductors, a change in the surface energy can be achieved by creating a Hall field in the crystal while simultaneously applying electric and magnetic fields in orthogonal directions.

A twin boundary is a set of twinning dislocations, each of which in this case interacts with a free surface having a different energy state. With an increase in the electric field tensity in the crystal during deformation, the range and generation of twinning dislocations increase with the predominance of the processes of excitation of dislocation sources with the stages of development of twins: the formation and transmission of twinning dislocations along the finished interface of twins. Twins usually originate on dislocation pileups and lead to diminution of internal tension. Under the conditions of electroplasticity, the diminution of internal tension occurs as a result of the development of new twins both on clusters of full dislocations and on clusters of twinning dislocations; in this case, dislocation clusters are discharged and the probability of brittle fracture in overtensioned areas of the material decreases. Thus, under conditions of electroplasticity, the simultaneous action of a strain above the limit and electrical impulses makes it possible to plasticize the material additionally due to twinning with an increase in the plasticity reserve.

REFERENCES

1. Savenko, V.S. (1999). Electroplastic effect under the simultaneous superposition and magnetic fields / V.S. Savenko // Journal of applied physics. – 1999. –№5. – P1–4.

2. Savenko, V.S. (2017). The contribution of ponderomotive factors to the realization of electroplastic deformation / V.S. Savenko, O.A. Troitsky, A.G. Silivonets // Izvestiya NAN RB, A series of physical and technical sciences. – 2017. –№ 1. – P. 85–91.

UDC 539.42

MODELING OF THE HIGH-VELOCITY STRIKER INTERACTION WITH A COMPOSITE

P. Radchenko, S. Batuev and A. Radchenko

Institute of Strength Physics and Materials Science of the Siberian Branch of the Russian Academy of Sciences, 2/4, pr. Akademicheskii, Tomsk, 634055, Russia

E-mail: andreyradchenko8@gmail.com

Abstract. The interaction of elongated (5 – 20 caliber) cylindrical steel strikers with orthotropic plates made of the organic plastic composite (Armos) at the velocity up to 2000 m/s is numerically investigated. Modeling is performed by the finite element method in a three-dimensional statement within the phenomenological approach of continuum mechanics using the original software EFES. The behavior of an anisotropic barrier material is described within the elastic-brittle model. The Tsai-Wu tensor polynomial criterion is used as a fracture criterion. The influence of the orientation of elastic and strength properties of the orthotropic composite and the nutation angle on the plate fracture and striker penetration are investigated.

Keywords: impact; anisotropic material; fracture; modeling; nutation angle

Property optimization of materials for their effective use in various structures is an urgent task of materials science and technologies for tailored materials. It is clear that a material should be designed with consideration for conditions (loads) under which it will operate. The latter govern the physical and mechanical properties and their orientation. Let us consider four cases of orientation of the orthotropic organic plastic properties with respect to the striker direction: initial orientation ($\gamma = 0^\circ$) and reorientation of the axes of symmetry of the material by 45, 90, and 135º relative to axis OY in the counterclockwise direction. Properties of the reoriented materials will be obtained from the initial one subject to the ratios $\nu_{ik}/E_i = \nu_{ki}/E_k$.

The initial material ($\gamma = 0^\circ$) has the following elastic and strength characteristics [27]: $E_x = 48.6$ GPa, $E_y = 21.3$ GPa, $E_z = 7.14$ GPa, $c_x = 6000$ m/s, $c_y = 3970$ m/s, $c_z = 2300$ m/s, $\nu_{xy} = 0.28$, $\nu_{yz} = 0.26$, $\nu_{xz} = 0.25$, $\sigma_x^t = 2.67$ GPa, $\sigma_y^t = 1.18$ GPa, $\sigma_z^t = 0.39$ GPa, $\sigma_x^c = 0.37$ GPa, $\sigma_y^c = 0.5$ GPa, $\sigma_z^c = 1.94$ GPa, $\tau_{xy} = 0.975$ GPa, $\tau_{yz} = 0.8$ GPa, and $\tau_{xz} = 0.607$ GPa. Here, E_x, E_y, E_z and c_x, c_y, c_z are Young's moduli and sound velocities in the corresponding directions; $\nu_{xy}, \nu_{yz}, \nu_{xz}$ are Poisson's ratios; σ_x^t, σ_x^c, τ_{xy} are the tensile, compressive and shear strength parameters.

Figure 1 shows the distribution of isolines in the fracture zone of the barrier material in section ZOX at the time instant 25 μs for the four variants of property orientation. The barrier fracture is initiated by an impact compression wave and develops under tensile stresses arising in unloading waves and due to the striker penetration. The fracture zone is elongated in the direction of the minimum compressive strength. It arrives at the rear surface of the plate to 25 μs only in the material with $\gamma = 90^\circ$, because the compressive strength along axis Z is minimum in this case. In the initial material ($\gamma = 0^\circ$), the fracture zone localizes in the upper

part of the barrier; at $\gamma = 45^\circ$ and 135º the fracture zone covers 4/5 of the plate thickness. This is associated both with the material strength in the corresponding direction and with the dependence of the wave velocity on the direction in the anisotropic material. The compression wave velocity is maximum along axis X at $\gamma = 0^\circ$ and along axis Z at $\gamma = 90^\circ$. At the initial stage of interaction, the decisive factor in the fracture development belongs to wave processes: fracture is initiated by a compression wave. With time, fracture is governed by tensile stresses due to the striker penetration.

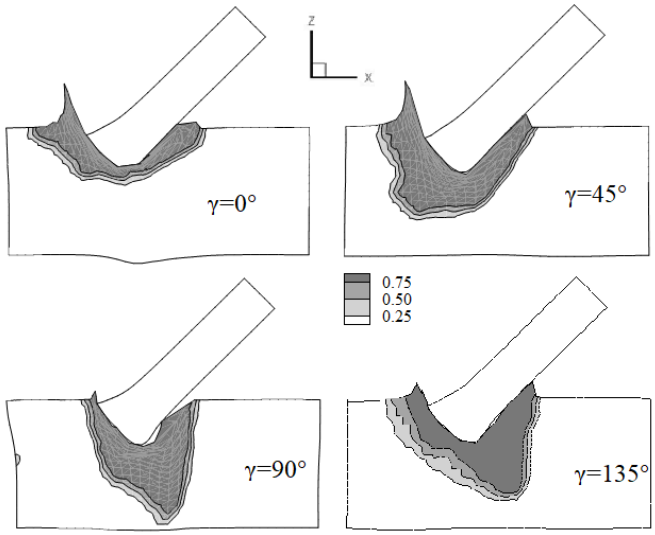

Figure 1 – Distribution of the relative fracture volume, $t = 25$ μs

The relative total volume of the fractured material (under compression and tension) is minimum for the barrier made of the initial material $(\gamma = 0^\circ)$. To the time instant 25 μs, it is 0.09% for the initial material, 50% and more at $\gamma = 45^\circ$, 33 and 44% at $\gamma = 90^\circ$ and 135º, respectively.

Values of the vertical v_z and horizontal v_x components of the center-of-mass velocity vector of the striker, its absolute value $|\mathbf{v}|$, and the angle α_t between axis Z and velocity vector at the time instant 25 μs are given in Table 2. The largest decrease in the vertical component of the center-of-mass velocity of the striker is seen to occur in the interaction with the barrier made of the initial material ($\gamma = 0^\circ$). In this case, the vertical component of the velocity decreases by 17% as compared to the initial value. For the material at $\gamma = 45^\circ$, the velocity change is minimum and comprises 12%. For materials with $\gamma = 90^\circ$ and 135º, the vertical component of the center-of-mass velocity is reduced by 14 and 15%, respectively.

After the wave processes attenuate, the dynamics of the stress-strain state of the barrier material will be determined by the striker penetration. The material will be mainly in tension in directions X and Y, in compression in direction Z. Therefore, fracture development in the barrier and the resulting resistance of the barrier to the striker penetration will be determined by the orientation of strength parameters.

The research was supported by RSF (project No. 22-21-00407).

UDC 532.42

NUMERICAL MODELING OF THE BEHAVIOR OF MATERIALS AND STRUCTURES UNDER PULSED LOADS

P. Radchenko, S. Batuev, A. Radchenko

Institute of Strength Physics and Materials Science of the Siberian Branch of the Russian Academy of Sciences, 2/4, pr. Akademicheskii, Tomsk, 634055, Russia

E-mail: andreyradchenko8@gmail.com

Abstract: In this work the results of numerical simulation of the interaction of an silica glass cylinder with a rigid wall, interaction of a steel ball with a silicate glass plate, oblique interaction of the cylindrical striker with an ogival head with a concrete barrier and interaction of the cylindrical striker with an ogival head with a concrete barrier are numerically investigated. The problems is solved numerically, by the finite element method, in a three-dimensional formulation within the framework of the phenomenological approach to the mechanics of a deformable solid using the author's software package EFES. To describe the processes of deformation, fracture and cracking, the JH-2 model was used, which makes it possible to take into account the large deformations, high strain rates and high pressures that occur in the material. The used calculation algorithm takes into account the formation of discontinuities in the material and the fragmentation of bodies with the formation of new free surfaces.

Keywords: model, fracture, strength, shock wave, unloading wave, stress

Glass is not an easy material for modeling, which has high strength characteristics in compression [1], but is less resistant to tension. With an increase in the rate of deformation, the strength of glass increases [2]. And the size of the tested specimens also affects the strength characteristics of the glass - specimens of a smaller size show a higher strength in comparison with larger specimens [3]. Also, the processes of cracking in glasses vary depending on the method of their manufacture [4].

The problem of interaction of an elongated cylindrical striker with a length of 95 mm and a diameter of 19 mm with a rigid wall is considered. The initial velocity of the cylinder is 4.2 m/s. Geometry of cylinder was divided into tetrahedral finite elements. The total number of finite elements in calculations approximately 22 millions.

Figure 1 shows a general view of the cylinder after interaction with a rigid wall at a time of 30 μs. The cylinder is covered with many cracks, at first they began to propagate from the region of interaction with the rigid wall, and then after the reflection of the compression wave from the rear surface. A main crack appears near the rear surface, which divides the cylinder into 2 parts.

Figure 1 – General view of the cylinder at the time 30 μs

The problem of interaction of a steel ball with a diameter of 3 mm and a plate of silicate glass with a thickness of 5 mm is considered. The initial velocity of the sphere is 750 m / s.

Geometry of interacting bodies was divided into tetrahedral finite elements. The total number of finite elements in calculations approximately 7.5E + 6.

Figure 2 shows the calculated configurations of the projectile and the barrier at different times and pressure isolines. Red corresponds to compression pressure and blue to tensile. Units of measurement on the pressure scale - MPa. In the presented configurations, completely fractured elements have already been removed from the computational grid. At the moment of time 10 μs, as a result of the release of the compression wave onto the free (rear) surface and reflection by the unloading wave, spall fracture is formed. On Figure 1 it can be seen that the volume of spall destruction increases with time. The striker is deformed and by the time of 50 μs it slows down to 700 m / s.

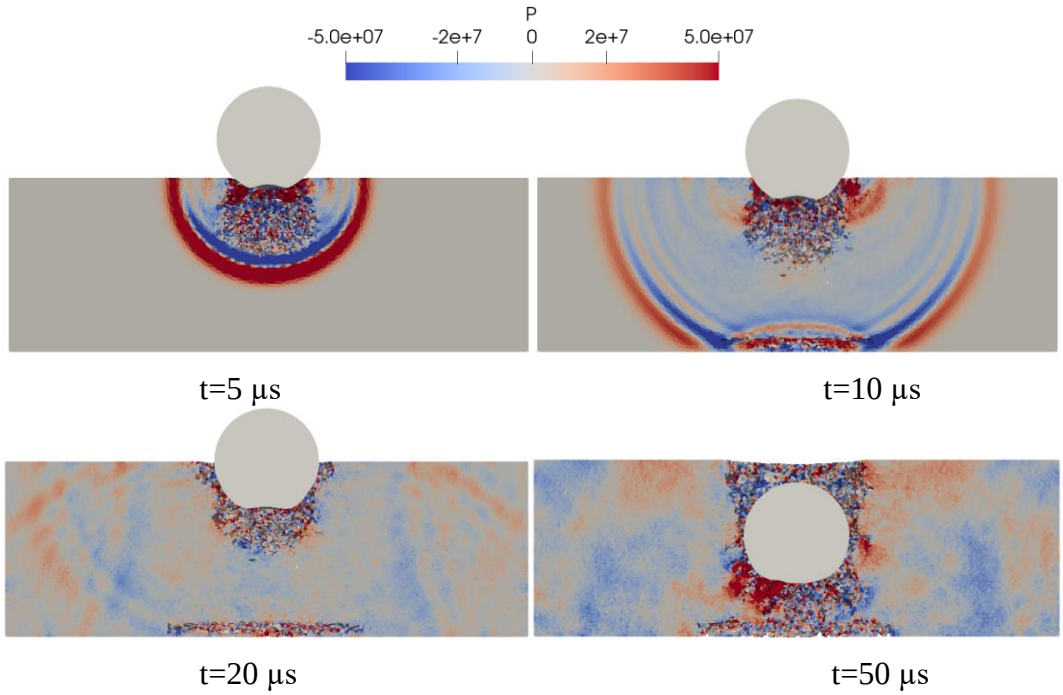

Figure 2 – General section view of pressure distribution during projectile and barrier interaction at various time points.

The used model describes well the behavior of brittle materials under high-speed loading. The obtained numerical results are in good agreement with the results obtained by other authors. The implemented calculation method allows predicting the behavior of glass and concrete under shock loads.

The research was supported by RSF (project No. 22-21-00407).

REFERENCES

1. Bridgman PW, Šimon I. Effects of very high pressures on glass. J Appl Phys 1953;24(4):405–13. http://aip.scitation.org/doi/10.1063/1.1721294.

2. Nie X, Chen WW, Wereszczak AA, Templeton DW. Effect of loading rate and surface conditions on the flexural strength of borosilicate glass. J Am Ceram Soc 2009;92(6):1287–95. http://doi.wiley.com/10.1111/j.1551-2916.2009.03019.x.

3. Anderson CE, Weiss CE, Chocron S. Impact experiments into borosilicate glass at three scale sizes 051011. J Appl Mech 2011;78(5).

4. A. Berenjian, G. Whittleston, History and manufacturing of glass, Am. J. Mater. Sci. 7 (1) (2017) 18–24.

UDK 538.9:537.63

INFLUENCE OF A CONSTANT MAGNETIC FIELD ON FATIGUE FRACTURE OF COMMERCIALLY PURE VT1-0 TITANIUM

Aksenova K.V., Shlyarov V.V., Zaguliaev D.V.

Siberian State Industrial University, Novokuznetsk,
E-mail: 19krestik91@mail.ru

Abstract. High-cycle fatigue tests to failure of commercially pure VT1-0 titanium under normal conditions (without a magnetic field) and under the influence of a constant magnetic field of various value (up to 1 T) were carried out. The multiple increase in the fatigue life of titanium by 1.6, 2.2 and 2.6 times after exposure to a magnetic field of 0.3, 0.4 and 0.5 T, respectively, was established.

Keywords: titanium VT1-0, constant magnetic field, fatigue, fracture.

It is known that external energy impacts on solids subjected to deformation can significantly change both the kinetics of the process and the integral, strength and plastic characteristics. Studies have shown that electropulse machining can extend the fatigue life of titanium [1] and aluminum [2]. The treatment of metals and alloys by electric and magnetic fields, short high-amplitude electric current pulses, affecting the deformation substructure, can change the distribution of internal stresses, phase composition, grain structure and, ultimately, significantly reduce the resistance to deformation. After treatment of the hard titanium alloy TC4 with a magnetic field of 3 T, an increase in the strength of the material by 7.6% is observed, which, according to the authors of [3], is explained by dislocation hardening. It should be noted that there are no studies in scientific periodicals aimed at establishing the physical nature of the influence of magnetic fields on the fatigue life of titanium, which indicates the relevance of the proposed studies.

The purpose of this work is to determine the number of cycles to failure of titanium specimens subjected to fatigue loading to failure under normal conditions (without a magnetic field) and under the influence of a constant magnetic field of various values (up to 1 T).

Samples of commercially pure titanium grade VT1-0 were used as the research material. High-cycle fatigue tests according to the scheme of cyclic asymmetric cantilever bending with a loading frequency of 3.3 s^{-1} and simultaneous exposure to a magnetic field of different values (0.3-0.5 T) were carried out. The specimens for fatigue tests were in the form of a parallelepiped with parameters 4x12x130 mm^3. The crack was simulated by two notches in the form of a semicircle with radii of 22 mm. During the fatigue tests, the number of cycles before the destruction of the prepared titanium samples was determined under normal conditions (without a magnetic field) and under the influence of a constant magnetic field of various magnitudes. For each value of magnetic induction, at least 10 samples were tested.

According to the results of fatigue testing of titanium samples, it was revealed that exposure to a constant magnetic field leads to a significant increase in fatigue life (table 1). The maximum increase in the number of cycles to failure by 163% is achieved after exposure to a magnetic field of 0.5 T.

Table 1 – The average number of cycles to failure of titanium specimens

Magnetic field induction B, T	0	0.3	0.4	0.5
Number of cycles to failure, N	121478±8086	199105±16143	270492±23957	319828±39519

Thus, the work established a multiple increase in the fatigue life of commercially pure titanium VT1-0 by 1.6, 2.2 and 2.6 times after exposure to a magnetic field of 0.3, 0.4 and 0.5 T, respectively. Taking into account the previous studies of the influence of a magnetic field on the microhardness and creep rate of titanium [4], it can be argued that a constant magnetic field is an effective way to modify the structure and optimize the properties of a material.

The study is supported by the grant of the Russian Scientific Foundation (project 21-79-00118).

REFERENCES:

1. Levitin V.V., Loskutov S.V. The effect of a current pulse on the fatigue of titanium alloy // Solid State Communications. – 2004. – V. 131(3-4). – P. 181-183.

2. Mohin M., Toofanny H., Babutskyi A., Lewis A., Xu Y. Effect of electromagnetic treatment on fatigue resistance of 2011 aluminum alloy // Journal of Multiscale Modelling. – 2016. – V. 7(3). – 1650004.

3. Li G.R., Li Y.M., Wang F.F., Wang H.M. Microstructure and performance of solid TC4 titanium alloy subjected to the high pulsed magnetic field treatment / G.R. Li, // Journal of Alloys and Compounds. – 2015. – V. 644. – P. 750-756.

4. Zagulyaev D.V., Konovalov S.V., Shlyarov V.V., Chen X. Influence of constant magnetic field on plastic characteristics of paramagnetic metals // Materials Research Express. – 2019. – V. 6(9). – 096523

UDC 621.791

INFLUENCE OF THE WELDING MATERIALS COMPOSITION ON THE WELD POOL FLUIDITY DURING FUNCTIONALLY ORGANIZED COMPOSITIONS FORMATION

R. S. Mikheev[1*], I. E. Kalashnikov[2], L. I. Kobeleva[2,]

[1] *Bauman Moscow State Technical Univercity, Moscow, Russia*
[2] *Baikov Institute* of Metallurgy and Materials Science of RussianAcademy of Sciences, Moscow, Russia

[*]E-mail: mikheev.roman@mail.ru; mikheev@bmstu.ru

Abstract. The results of studies of the influence of the new composite filler rods composition of on the weld pool fluidity are presented. Promising composite filler rods based on B83 babbitt alloy containing (Al-Bi) or $Ti_2NbAl_{(<100)}$ as a filler in an amount of 3% by weight were made by extrusion of a powder mixture of initial components. To assess the fluidity of a weld pool, the method of A.A. Erokhin. The influence of the reinforcement type in filler composite rods on the weld pool fluidity is determined.

Keywords: welding pool, fluidity, composite layers, functional organization, antifriction coatings, arc surfacing.

The performance of the mechanisms that are part of modern and promising machines is largely determined by the failure-free operation of the elements included in their composition, which form friction units [1, 2]. Since predominantly surface layers work in friction units, the functional organization of such parts due to the formation of layered compositions consisting of a steel base and a working composite coatings with improved tribotechnical properties is a very urgent task [3].

One of the economical and widely used methods for the formation of such coatings is the process of arc surfacing with a tungsten electrode in an inert gas [4]. In this case, a very important parameter that ensures the formation of high-quality layers is the weld pool fluidity, which is a complex set of properties that determines its ability to change its shape under the action of gravity and other forces, such as arc pressure, as well as the Marangoni effect. The classical methods used in foundry technology are not suitable for determining this parameter, since under the conditions of the welding process, unlike casting, liquid metal is characterized by a temperature gradient. In this regard, it is of practical interest to determine the fluidity of a such weld pool as a whole as an integral characteristic.

To assess the effect of the filler material composition on the weld pool fluidity, the work proposed and tested the method of A.A. Erokhin. In this method, the weld pool fluidity is estimated indirectly - by the violation of the symmetry of the cross section of a horizontal run obtained by surfacing on an inclined plane (angle of inclination α=35°) [5, 6]. The run section asymmetry is characterized by the area ratio F_2/F_1. Obviously, a higher value of F_2/F_1 corresponds to a better weld pool fluidity. In addition to determining F_1 and F_2, this method makes it possible to measure the values of the receding contact angles of inflow φ_1 and outflow φ_2 depending on the ratio of melt viscosity and surface tensions melt-gas, melt-solid, solid-gas [6]. The values of the these contact angles make it possible to approximately estimate the value of the equilibrium wetting angle θ [7].

In the work, the process of arc surfacing with a tungsten electrode in an argon environment of horizontal runs was carried out on a plate 180x120x5 mm in size, made of high-quality low-carbon steel 20 (GOST 1050). As a filler material, the developed composite rods with a diameter of 3 mm and a length of 300 mm based on the B83 antifriction alloy containing (Al-Bi) or $Ti_2NbAl_{(<100)}$ in an amount of 3 wt.% as a reinforcements were used. Composite filler rods were manufactured using the powder metallurgy technology by extrusion, which ensured the homogeneity of the structure and the isotropy of properties [8]. The surfacing process was carried out with technological parameters, ensuring the stability of the phase composition and structure, no burnout of alloying elements and minimal mixing of the base and deposited metal.

It has been established that the runs formed using composite filler rods of composition B83 + 3 wt.% (Al-Bi) in comparison with those obtained by rods B83 + 3 wt.% Ti_2NbAl are characterized by lower values of cross-sectional asymmetry: 2,43 versus 2,81 (Table 1). In addition, the values of the contact angles for runs containing Ti_2NbAl intermetallic particles decrease, which contributes to the spreading of the weld composite pool, and also improves the formation of satisfactory deposited layers.

Table 1 – Influence of the filler material composition on the weld pool fluidity: cross-sectional asymmetry F_2/F_1, contact angles of inflow φ_1 and outflow φ_2 and wetting contact angle θ of deposited runs.

Filler material composition, wt.%	**F_2/F_1**	**φ_1, °**	**φ_2, °**	**θ, °**
Б83 + 3 (Al-Bi)	2,43	57,7	159,5	101,6
Б83 + 3 Ti_2NbAl	2,81	40,3	115,6	80,5

Thus, experiments to assess the weld pool fluidity showed that the type of reinforcement has a significant effect on the formation of deposited layers. At the same reimforcement content (3 wt.%), the weld pool formed with the use of filler composite rods of the composition В83 + 3 wt.% Ti_2NbAl has greater values of the run cross section asymmetry and, consequently, fluidity, which makes it possible to increase the proportion of the reinforcement in the rods to achieve better tribotechnical properties of functionally organized layered compositions.

Acknowledgements. This research was supported by a grant from the Russian Science Foundation (project No. 22-29-00366).

REFERENCES

1. Jazykov A.E. Bearings and Oil Systems: tutorial/ A. E. Jazykov, V. N. Kazanskij, R. Sh. Buskunov. Cheljabinsk.: Cicero, 2010. 202 s.
2. Gaziev R. R. Repair of bearings of compressors using flame spraying / R. R. Gaziev [et. al.] // Neftegazovoe delo. 2012. № 5. P. 236−245.
3. Mikheev R. S. Aluminum-matrix composite materials reinforced with carbides for solving problems of new technology / R. S. Mikheev, T. A. Chernyshova. M.: Maska, 2013. 356 s.
4. Mikheev R. S. Innovative ways in the creation of antifriction composite coatings based on non-ferrous alloys with increased tribotechnical properties / R. S. Mikheev // Zagotovitel'nye proizvodstva v mashinostroenii. 2018. № 5. P. 204-210.
5. Erokhin A. A. Influence of fluidity of the pool on the geometric shape of the weld and the technological applicability of the welding process / A. A. Erokhin // Svarochnoe proizvodstvo. 1955. № 6. P. 5-9.
6. Berezovskiy B. M. Mathematical models of arc welding: In 3 volumes – Vol. 1. Mathematical modeling and information technology, weld pool models and seam formation / B. M. Berezovskiy. Cheljabinsk.: Izd-vo YuUrGU, 2002. 585 p.
7. Frolov Y. G. Course of colloid chemistry. Surface phenomena and disperse systems: textbook for universities / Y. G. Frolov. M.: Chemistry, 1988. 464 p.
8. Kalashnikov I. E. Technological modes of obtaining and properties of surfacing rods and antifriction coatings from a composite material based on an alloy of the SnSbCu system / I. E. Kalashnikov [et al] // Physics and Chemistry of Materials Processing. 2018. № 1. P. 33-21.

UDC 674.06–539.9:666

HIGH – ENERGY IMPACT OF PLASMA ENERGY ON THE MECHANICAL PROPERTIES OF SPRUCE AND PINE WOOD SAMPLES

V.A. Cheremnykh, G.G. Volokitin, A.A. Klopotov, Y.A. Abzaev, A.A. Alekseev

Tomsk State University of Architecture and Building,
Tomsk, Russia
E-mail: vacheremnykh@gmail.com

Abstract. This article presents the results of a study of the effect of plasma energy on the mechanical properties of pine and spruce wood. It was found that the impact of plasma energy does not have a significant effect on pine samples. However, the effect of plasma energy on the surface of spruce samples leads to an increase in the modulus of elasticity, the limit of proportionality and a change in the nature of destruction.

Keywords: wood, plasma energy, compressive strain**,** compressive strength, mechanical properties.

One of the most common building materials is wood [1]. The most popular types of wood for construction are spruce and pine. However, wood has disadvantages: rotting of wood, dependence of properties on humidity, heterogeneity of structure, defects, changes in physical and mechanical properties in height and radius of the trunk, anisotropy [2]. The improvement of physical, mechanical and biological properties can be the processing of wood with plasma energy [3, 4]. Plasma flows has a thermal effect on the product and at the same time forms a protective and decorative coating on the surface of wood [5].

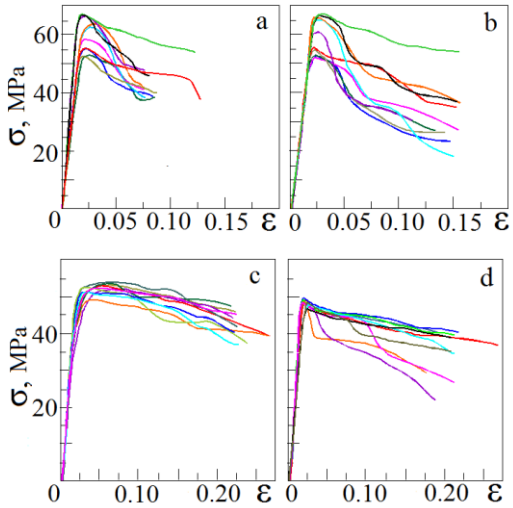

Figure 1 – Graphs of stress-strain dependence for wood samples:
a) untreated samples from pine,
b) treated with plasma energy from pine,
c) untreated samples from spruce,
d) treated with plasma energy from spruce

The purpose of this work is to study the effect of plasma energy on the mechanical properties of pine and spruce wood

For mechanical trials were made samples of pine and spruce in size 20×20×30 mm according to GOST 16483.10-73. Untreated (initial) samples and plasma energy-treated samples were considered. A direct arc plasmatron was used for high-energy impact on the surface of the samples [6]. The movement of wooden samples during plasma arc treatment occurred at a speed of 0.0735 m/s. The distance from the center of the plasmatron nozzle to the treated surface was 10 mm. The power of the plasmatron was 14.4 kW.

Mechanical trials were performed for uniaxial compression of samples along the grain.

The INSTRON 3382 testing machine was used for the trials. The speed of movement of the loading head of the test machine was accepted according to GOST 16483.10-73 and was 4 mm/min.

The graphs show the strain curves obtained by compressing samples of pine and spruce. The results of statistical processing of strain curves are presented in the table 1.

Analysis of the data given in the table showed that the high–energy impact on the surface of pine samples does not lead to significant changes in mechanical properties. The results of mechanical trials of samples from spruce showed that after reaching the compressive strength σ_m the process of strength reduction is less intense than in pine specimens (except for specimens with knots).

Table 1 – Mechanical properties of wood samples

№	Wood type	Type of sample processing	Compression modulus of elasticity *E*, [MPa]	Strain ε, [mm/mm]	Stress in a point of proportional limit $\sigma_{PL,}$ [MPa]	Compressive strength $\sigma_{m,}$ [MPa]
1	Pine	Untreated	4540±330	0.017±0.003	43±2	60±3
2	Pine	Plasma energy	4498±330	0.017±0.003	44±2	59±3
3	Spruce	Untreated	3026±330	0.049±0.003	31±2	52±3
4	Spruce	Plasma energy	3864±330	0.025±0.003	36±2	49±3

The strain curves of spruce samples are characterized by a more uniform distribution than the curves $\sigma=f(\varepsilon)$ of pine samples.

It was found that the impact on the surface of spruce samples using plasma flows leads to a noticeable change in mechanical properties: σ_{PL} – value increased by 14%, σ_m – value decrease in by 5%, E – value increased by 22%.

Thus, the study showed that the high–energy effect of plasma energy on the surface of samples from different types of wood has a noticeable improvement only on samples from spruce.

The work has been conducted with the financial support of the Government Assignment of the Ministry of Education and Science of the Russian Federation (project No. FEMN-2020-0004).

REFERENCES

1. Tsvetkov N. A. Mathematical modelling of renewable construction materials for green energy-efficient buildings at permafrost regions of Russia / N. A. Tsetkov [et. al.] // Environmental Challenges. 2021. V.4. 100101.

2. Ugolev B. N. Wood science and forest merchandising: textbook / B. N. Ugolev. M.: GOU VPO MGUL, 2007. 351 c.

3. Kunts O. A. Modification of the wood surface by plasma treatment / O. A. Kunts [et. al.] // XI International Scientific and practical conference Investments, urban planning, real estate as drivers of socio–economic development of the territory and improving the quality of life of the population. Tomsk: TSUAB, 2021. C. 359-366.

4. Koptev A. S. The effect of plasma exposure on the near–surface layers of wood / A. S. Koptev, A. A. Klopotov, G. G.Volokitin // 67th University Scientific and Technical Conference of Students and Young Scientists. Tomsk. 2021. C. 343-347.

5. Volokitin G. G. Plasma treatment of wood / G. G. Volokitin [et. al.] // Thermophysics and aeromechanics. 2016. Vol. 23. No. 1(97). C. 125-130.

6. Vlasov V. A. Plasma technologies for the creation and processing of building materials: monograph / V. A.Vlasov [et. al.]. Tomsk: NTL, 2018. 512 c.

UDC 538.9

PHYSICALLY-BASED SIMULATIONS FOR THE DEFORMATION BEHAVIOR OF ADDITIVELY MANUFACTURED ALUMINUM ALLOYS

E. Dymnich[1*], V. Romanova[1], R. Balokhonov[1], M. S. Mohebbi[2], V. Ploshikhin[2]

[1]Institute of Strength Physics and Materials Science, Siberian Branch of the Russian Academy of Sciences, Tomsk, Russia

[2]Airbus Endowed Chair for Integrative Simulation and Engineering of Materials and Processes, University of Bremen, Bremen, Germany

E-mail: dymnich@ispms.tsc.ru

Abstract. A physically-based computational approach was developed to evaluate the microstructure-to-property linkage of AlSi10Mg produced by Powder Bed Laser Beam Melting. Three-dimensional microstructural model was simulated by modelling a solidification process by cellular automata and a heat transfer by the Finite-Difference. Micromechanical analysis for the simulated microstructure was performed using crystal plasticity finite-element calculations. The stress and strain field analyses demonstrate an anisotropy of the grain-scale mechanical properties.

Keywords: Powder Bed Laser Beam Melting, aluminum alloys, micromechanics, Crystal Plasticity Finite-Element calculations, Cellular Automata Finite Difference model

A large body of experimental studies for Laser Powder Bed Laser Beam Melting (L-PBF) aluminum alloys reports the development of a complex anisotropic microstructure throughout all length scales. Due to high-gradient thermal processes inherent in L-PBF, a fine cellular-dendritic structure is formed at the intragrain level and the so-called fish-scale pattern is produced by laser tracks at the macroscale. The presence of a hierarchical structure affected by processing parameters in a multiple-valued manner dramatically complicates predicting the mechanical properties of L-PBF-produced parts. Particularly, an anisotropic mechanical response of L-PBF-produced parts loaded along different directions is the subject of extensive discussions. However, experimental data on the mechanical anisotropy reported by different authors are still contradictory. In each particular research, the specific anisotropic response was attributed to the microstructural effects. Thus, an accurate prediction of the processing-

microstructure-property relation of the L-PBF-produced aluminum alloys is a challenging task which requires a thorough understanding of the processes and mechanisms involved.

For predicting the deformation behavior of materials with polycrystalline structures, Crystal Plasticity (CP) simulations are widely used (e.g., [1, 2]), including some works focusing on the Additive Manufacturing (AM) materials [1, 2]. The majority of CP models for AM alloys involve homogenization schemes reproducing a macroscopic material response without direct association with stress-strain distributions at the micro- and mesoscales [3, 4]. While the homogenized constitutive equations are often solved by the finite-element method (FEM), an RVE can be approximated by only a few elements. Thus, the stress and strain fields are not represented in detail but the RVE stress-strain curve affected by the grain orientations and loading conditions is reproduced. Using the mean-field polycrystal plasticity modeling, Liu et al. [2] studied the grain shape and texture effects on the macroscopic strain-stress responses of loaded L-PBF AlSi10Mg alloys. Dong-Kyu Kim et al. [3] evaluated the stress-strain relationship of constituent phases of a L-PBF AlSi10Mg alloy within the CP framework. Again, the investigation took into account neither melt pool geometry nor a distribution of grains over melt pools.

The estimates of local stress-strain characteristics which can significantly deviate from the homogenized response are possible with the micromechanical CP simulations where grain geometry is explicitly introduced in the model. However, these simulations for additive materials are few [1-5]. The majority of these works are based on two-dimensional approximations or use an essential idealization of microstructural features.

As an example, Andani et al. [1] developed a micromechanical two-dimensional model of L-PBF fabricated metallic alloys to take into account the melt pool geometry but the grain morphology was still disregarded. Van Nuland et al. [35] developed a microstructural two-dimensional model for predicting the macroscopic yield behavior under various loading angles of an additively manufactured 316L stainless steel. The model covers grain shapes and orientations within several melt pools. Tang et al. [2] proposed a multi-scale modelling framework including synthetic microstructure generation approach covering realistic grain morphology and texture. The developed microstructure-based CP model aimed to unravel the complex structure-property relationship with the remarkable numerical examples being provided for a L-PBF Ti-6Al-4V alloy. In our previous work [6] the grain-scale stress-strain fields developing in a L-PBF aluminum alloy under different loading conditions were numerically studied. These simulations, however, failed to reproduce the whole processing-microstructure-property linkage.

A step forward along these lines is made in this investigation. The objective of this contribution is to develop a computational approach providing the whole processing-microstructure-property linkage, including physically-based simulation of grain structure evolution during L-PBF, subsequent micromechanical calculations for the microstructure deformation behavior at the grain scale and calculation of a homogenized response by averaging the mechanical properties over the RVE.

The funding provided by the German Research Foundation (Deutsche Forschungsgemeinschaft) [grant number PL 584/4-1] and the Government of the Russian Federation through the research assignment for ISPMS SB RAS (№FWRW-2021-/0002/) are acknowledged.

REFERENCES

1. Andani M. T. Micromechanics modeling of metallic alloys 3D printed by selective laser melting / M. T. Andani [et al.] // Mater. Des. 137. 2018. P. 204-213.
2. Tang H. Multi-Scale modelling of structure-property relationship in additively manufactured metallic materials / Tang H. [et al.] // Int. J. Mech. Sci. 194. 2021. P. 106185.
3. Kim D.-K. Evaluation of the stress-strain relationship of constituent phases in AlSi10Mg alloy produced by selective laser melting using crystal plasticity FEM / D.-K. Kim [et al.] // J. Alloys Compd. 714. 2017. P. 687-697.
4. Nuland T.F.W. Microstructural modeling of anisotropic plasticity in large scale additively manufactured 316L stainless steel / T.F.W. Nuland [et al.] // Mech. Mater. 153. 2021. P. 103664.
5. Romanova V. Micromechanical simulations of additively manufactured aluminum alloys / V. Romanova [et al.] // Comput. Struct. 244. 2021. P. 106412.

UDC 539.422.22

NUMERICAL STUDY OF THE INFLUENCE OF RESIDUAL THERMAL STRESSES ON THE FRACTURE OF METAL MATRIX COMPOSITES

A.V. Zemlianov[1,2*], D.D. Gatiyatullina[1,2], R.R. Balokhonov[2]

[1]National Research Tomsk State University (Tomsk, Russia)

[2]Institute of Strength Physics and Materials Science of Siberian Branch of Russian Academy of Sciences (Tomsk, Russia)

*E-mail: zem.aleks99@ispms.tsc.ru

Abstract. A numerical study of the mechanical behavior of the «aluminum-boron carbide» composite material under different thermomechanical loading is performed. Complex structure of the composites is explicitly taken into account in the calculations. Isotropic elastoplastic and elastic-brittle constitutive models are used to describe the mechanical response of the aluminum matrix and ceramic particles, respectively. Dynamic boundary value problems are solved numerically by the finite element method in the ABAQUS / Explicit software package.

Keywords: numerical simulation, metal matrix composites, mechanics of non-homogeneous materials, residual thermal stresses, fracture.

At present, composite materials are widely used in various industries, including aerospace, energy, and automotive [1–2]. Composites have significant structural inhomogeneity, which is due to the presence of curvilinear interfaces (“coating-substrate”, “matrix-particles”), as well as the difference in mechanical and thermal properties of the components (elastic moduli, tensile strengths, thermal expansion coefficients, etc.).

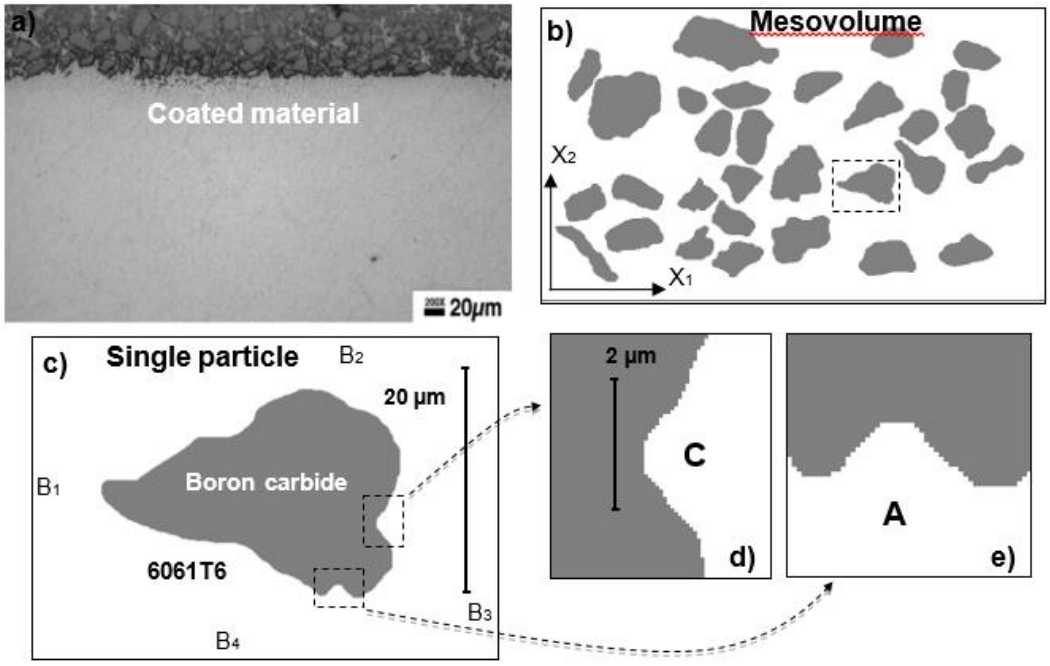

Figure 1 – Experimental (a) [3] and model structures of the coated material (b-e)

Previously, numerical studies of deformation and fracture of composite materials and coatings were carried out without taking into account residual stresses [4], as well as the evolution of residual stresses during cooling of the three-dimensional structure of a composite material with a single particle of titanium carbide of a complex experimentally observed shape [5].

Figure 1a shows a cross-sectional image of a composite coating made by laser deposition. On the scale of a single particle, when a structure with a single particle is considered (Figure 1c), one can distinguish a hierarchy of finer structural inhomogeneities, near which a stress concentration arises (Figure 1d, e).

To set the constitutive ratios of materials in the ABAQUS / Explicit software package, user subroutines have been developed. The physical and mechanical properties of the aluminum matrix and boron carbide and the experimental constants used in the calculations are presented in Table 1. A representative volume of the composite material containing several boron carbide particles located in the microvolume of aluminum alloy 6061T6 is considered.

Table 1 – Mechanical properties of the compound materials

Material	ρ, г/см^3	K, ГПа	μ, ГПа	σ_S, МПа	$\sigma_{0,2}$, МПа	ε_r^p, %	C_{ten}, МПа	C_{com}, ГПа	α, 10^{-6} °C^{-1}
Al6061T6	2.7	66	26	332	234	9.5	-	-	22
B_4C	2.6	235	197	-	-	-	500	5	4.5

Modeling of residual stresses (RS) involves the introduction of a step with cooling of the structure from a temperature close to the aluminum recrystallization temperature to room temperature. When modeling residual stresses, the Duhamel-Neumann relations are solved taking into account the plasticity of the matrix. When carrying out the calculation taking into

account residual stresses, at the first step of the calculation the structure is cooled, at the next step a load is applied to it.

The work was supported by the Russian Science Foundation (grant No. 18-19-00273, https://rscf.ru/en/project/18-19-00273/).

REFERENCES

1. Garg P. Advance research progresses in aluminium matrix composites: manufacturing & applications / P. Garg [et al] // Journal of Materials Research and Technology. 2019. Vol. 8. № 5.

2. Cao D. Effects of thermal residual stresses and thermal-induced geometrically necessary dislocations on size-dependent strengthening of particle-reinforced MMCs / D. Cao [et al] // Composite Structures. 2018. Vol. 200. P. 290-297.

3. Kadolkar P. B. State of residual stress in laser-deposited ceramic composite coatings on aluminum alloys / P. B. Kadolkar [et al] // Acta Materialia. 2007. Vol. 55. Issue 4. P. 1203-1214.

4. Balokhonov R. R. A numerical study of plastic strain localization and fracture across multiple spatial scales in materials with metal-matrix composite coatings / R. R. Balokhonov [et al] // Theoretical and Applied Fracture Mechanics. 2019. Vol. 101. P. 342-355.

5. Balokhonov R. R. Computational microstructure-based analysis of residual stress evolution in metal-matrix composite materials during thermomechanical loading / R. R. Balokhonov [et al] // Facta Universitatis, Series: Mechanical Engineering. 2021. Vol. 19. № 2. P. 241-252.

UDC 538.9

THE RVE SIZE DEFINITION AND DIFFERENT SLIP SYSTEMS CONTRIBUTION TO THE DEFORMATION RESPONSE OF ALPHA-TI AT THE MESOSCALE

M. Pisarev [1,2*], E. Emelianova [1,2], V. Romanova [1]

[1]Institute of Strength Physics and Materials Science SB RAS, Tomsk, Russia

[2]Tomsk State University, Tomsk, Russia

*E-mail: pisarev@ispms.ru

Abstract. The deformation behavior of polycrystalline α-titanium is studied numerically in the crystal plasticity framework. The step-by-step packing method is used to generate the experimental based reference polycrystalline model. The material texture, grain structure and dislocation slip along prismatic, basal and pyramidal systems are taken into account in calculations explicitly. The boundary value problem is solved numerically in Abaqus/Explicit finite-element analyzer for four polycrystalline models.

Keywords: Micromechanics, crystal plasticity theory, polycrystalline structure, numerical simulation, slip systems.

Proper description of the deformation behavior of commercially pure α-titanium at the mesoscale requires taking into account of the physical mechanism of plasticity associated with slip geometry. The polycrystalline model (Figure 1) is generated based on the crystal plasticity theory that explicitly allows the dislocation slip geometry. Then this model is translated in two

directions to obtain larger models. The orientation of grains relative to the global coordinate system is specified by Euler angles to simulate the basal texture in accordance with the experimental data for rolled titanium [1].

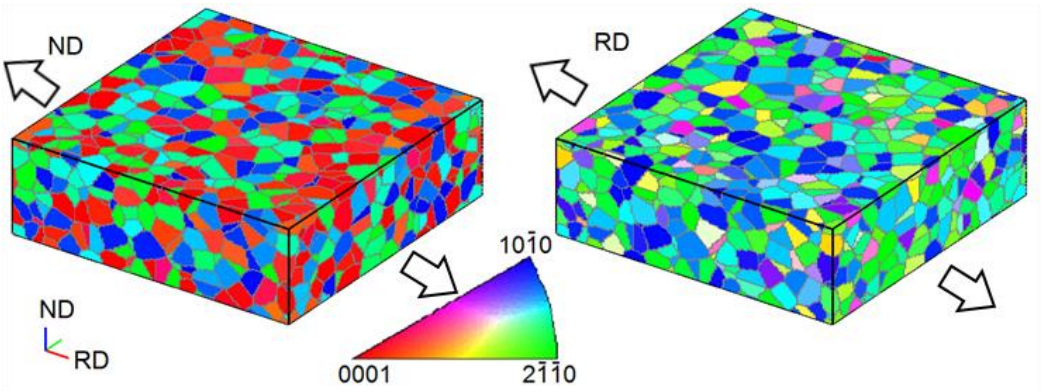

Figure 1 – Microstructural polycrystalline model.

The plastic strain rate components within crystal plasticity theory are related to shear on active slip systems by geometrical relations

$$\dot{\varepsilon}_{ij}^{p} = \sum_{\alpha} \dot{\gamma}^{(\alpha)} \Theta_{ij}^{(\alpha)} \tag{1}$$

The shear strain rate $\dot{\gamma}^{(\alpha)}$ is proposed in [2] as the function of resolved shear stresses $\tau^{(\alpha)}$ on the α-slip system

$$\dot{\gamma}^{(\alpha)} = \dot{\gamma}_0 \left| \frac{\tau^{(\alpha)}}{\tau_{CRSS}^{(\alpha)}} \right|^{\nu} \operatorname{sign}\left(\tau^{(\alpha)}\right) \tag{2}$$

Potentially active slip systems of commercially pure titanium included in this work are 3 prismatic, 3 basal, 6 <a> pyramidal and 12 first-order <c+a>-pyramidal. The values of critical resolved shear stresses among with the other model parameters are shown in Table 1.

Table 1 – Material constants and model parameters

Parameter	Value
C_{1111}, GPa	162
C_{1133}, GPa	92
C_{1122}, GPa	69
C_{3333}, GPa	181
C_{2323}, GPa	47
$\tau_0^{prismatic}$, MPa	60
τ_0^{basal}, MPa	120
$\tau_0^{pyramidal}$, MPa	180
k, MPa	145

Generated geometrical and constitutive models are implemented in Abaqus/Explicit and solved numerically. The boundary volume problem simulates uniaxial tension along RD

(Figure). The top and lateral surfaces are free from external loading and the bottom one is a symmetry plane.

Analysis of the results shows that at the initial deformation stage (up to 10%) all four models show similar plastic strain evolution. In further deformation smaller models fail to properly demonstrate deformation behavior due to the early necking. Therefore, representative volume element size should be chosen in accordance with the maximum strain that occurs during the uniaxial tension.

This work is supported by Russian Science Foundation (Project No. 20-19-00600).

REFERENCES

1. Romanova V. Micro- and mesomechanical aspects of deformation-induced surface roughening in polycrystalline titanium / V. Romanova [et al.] // Mater. Sci. Eng. A. 2017. Vol. 697. P. 248-258.

2. Roters F. Overview of constitutive laws, kinematics, homogenization and multiscale methods in crystal plasticity finite-element modeling: Theory, experiments, applications / F. Roters [et al.] // Acta Materialia. 2010. Vol. 58. № 4. P. 1152-1211.

UDC 533.9:539.4.015.2

MULTILAYER AMORPHOUS-CRYSTALLINE HIGH-ENTROPY FILMS

Ivanov Yu.F., Prokopenko N.A., Petrikova Ye.A.,
Shugurov V.V., Teresov A.D., Tolkachev O.S.

Institute of High Current Electronics, Siberian Branch, Russian Academy of Sciences,
Tomsk, Russia

E-mail: yufi55@mail.ru

Abstract. As a result of the performed studies, the purpose of which was to obtain new knowledge about the structure and properties of high-entropy films synthesized on a substrate during the deposition of a multi-element metal plasma in an argon environment. A deposition regime has been revealed that makes it possible to form multilayer nanostructured amorphous-crystalline films with high (up to 14 GPa) hardness.

Keywords: multilayer nanostructured amorphous-crystalline films, high-entropy alloy, phase composition, structure, properties.

High-entropy alloys (HEA) are multi-element materials and contain at least five elements of similar concentration. HEAs are, as a rule, single-phase thermodynamically stable substitutional solid solutions, mainly based on BCC or FCC crystal lattice. Stabilization of the solid solution during crystallization is provided mainly by the high entropy of mixing and the low rate of diffusion of the components, and the low rate of growth of crystallites from the melt.

The purpose of the performed research is to obtain new knowledge about the structure and properties of high-entropy alloys. Synthesized in the form of thin (up to 5 microns) films by the ion-plasma method. Which consists in the deposition of a multi-element metal plasma created by an electric arc plasma assisted simultaneous independent sputtering of the cathodes of the selected elementsю Ti, Al, Cu, Zr, and Nb were used as elements that form HEAs. The substrate was samples of steel of the austenitic class 321, titanium alloy VT1-0 and hard alloy WC-8%Co. The formation of HEA films was carried out on the «QUINTA» ion-plasma

installation developed at the Laboratory of Plasma Emission Electronics of the IHCE SB RAS and included in the «UNIQUUM» complex in the list of unique electrophysical installations in Russia (https://ckp-rf.ru/usu/434216/) [1]. Part of the HEA films was additionally irradiated with a pulsed electron beam (SOLO setup [1]).

In the course of the work, experiments were carried out on the deposition of multi-element metal films. The modes of generation of gas-metal plasma have been studied. The radial distribution of the ion current density from the plasma for sources of metallic and gaseous plasmas has been studied. The film deposition rates of individual components were measured. The elemental composition of the film was determined using X-ray microanalysis. The optimum mode of deposition of HEA films is revealed. Using the methods of scanning and transmission electron microscopy, X-ray diffraction analysis, studies of the elemental and phase composition, the state of the defective substructure (relative concentration of atoms, sizes, shape, location and volume fraction of phases, scalar dislocation density and type of dislocation substructure, grain and subgrain size) of the formed HEAs and HEAs irradiated with a pulsed electron beam were carried out. It has been shown that the HEA films are a multilayer X-ray amorphous material (Figure 1a). The layer thickness varies from 12 nm to 23 nm. The size of the crystallites forming the layers is (2-3) nm. It has been established that the hardness of HEA films varies from 12.0 GPa to 14.0 GPa; Young's modulus - from 230 GPa to 310 GPa. Irradiation of the HEA film with a pulsed electron beam (20 J/cm^2, 50 μs, 3 pulses) is accompanied by high-speed crystallization of the material with the formation of a cellular structure (Figure 1b). The cell size varies from 300 nm to 600 nm. The cells are bordered by interlayers of the second phase. The thickness of the interlayers varies within (20-110) nm. The volume of the cells is formed by the α-NbZrTiAl composition phase, which has a BCC crystal lattice with a parameter of 0.32344 nm; the interlayers of the second phase are formed by the CuZr alloy (simple cubic lattice). The hardness of the films, measured at an indenter load of 30 mN, varies from 6.9 GPa to 8.8 GPa and decreases with increasing electron beam energy density. It has been established that the high values of the hardness of the material under study are due to substructural (hardening by the boundaries of subgrains, high-speed crystallization cells), dispersion (hardening by nanosized particles of the second phase located along the boundaries of crystallization cells) and solid solution (hardening due to distortion of the crystal lattice by the atoms of the elements forming the alloy) mechanisms. Hardening by internal stress fields, which are formed due to the presence of phases with different coefficients of thermal expansion in the material, should also not be ruled out.

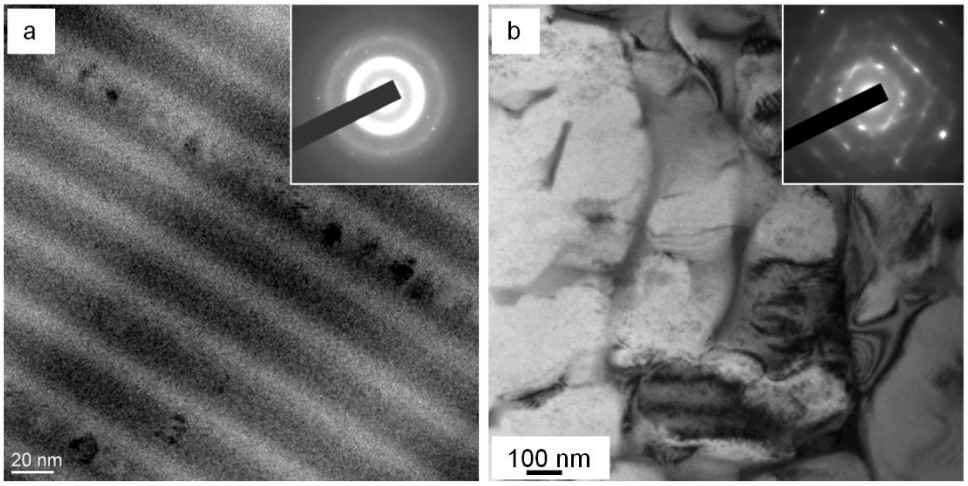

Figure 1 – Electron microscopic image of a multilayer HEA film before (a) and after (b) irradiation with a pulsed electron beam

The optimal regime for the deposition of HEA films (from the standpoint of minimizing the energy consumption of the formation of an HEA of an elemental composition close to equiatomic, with high strength properties) has been revealed, which makes it possible to form HEA films of the following elemental composition: 25.4Ti-17.0Al-21.9Nb-22.3Zr-13.4Cu. The results obtained make it possible to recommend an environmentally friendly, fully automated electron-ion-plasma method for the formation of wind farms for the provision of scientific and technological services aimed at improving the service characteristics of parts and products for various purposes.

Acknowledgements.

The study was carried out with the financial support of the Russian Foundation for Basic Research within the framework of scientific project No. 20-58-00006.

REFERENCES

1. Evolution of the structure of the surface layer of steel subjected to electron-ion-plasma processing methods / Edited by N.N. Koval, Yu.F. Ivanova. Tomsk: NTL, 2016. 304 c. ISBN 978-5-89503-577-1.

UDC 538.9

EXPERIMENTAL STUDY AND NUMERICAL SIMULATIONS OF THE INFLUENCE OF TEXTURE SEVERITY ON THE DEFORMATION-INDUCED SURFACE ROUGHENING IN AN ALUMINUM ALLOY

V. Shakhidzhanov[1]*, O. Nekhorosheva[12], V. Romanova[1]

[1]Institute of Strength Physics and Materials Science SB RAS, Tomsk, Russia

[2]Tomsk State University, Tomsk, Russia

* E-mail: arm3n1an@mail.ru

Abstract. Experimental and numerical studies are performed to reveal an interrelation between mesoscale deformation-induced surface roughening and in-plane plastic strain in an aluminium alloy. The experimental and numerical roughness patterns were evaluated in terms of a relative roughness parameter calculated as a ratio of the rough profile lenght to the profile evaluation lenght. Special attention was given to the numerical study on the effect of the texture severity on the roughness characteristics.

Keywords: deformation-induced surface roughness; aluminum alloys; mesoscale; plastic strain localization; micromechanical simulations; crystal plasticity.

Experimental and numerical investigations have been performed for a commercial purity aluminum alloy to reveal a correlation between deformation-induced surface roughening and in-plane plastic deformation at the mesoscale. These investigations have been performed to reveal an interrelation between mesoscale deformation-induced surface roughening and in-plane plastic strain in an aluminum alloy. In the present study the method of step-by-step packing (SSP) [1] was employed to generate a three-dimensional (3D) aluminum alloy polycrystalline model periodical in three directions. Roughness evolution in selected

subsections of a uniaxially loaded specimen is examined experimentally using a stop-and-study technique. The experimental analysis is complemented by the micromechanical simulations for deformation-induced surface roughening in model polycrystals. In this case special attention is paid to the effect of texture on the roughness characteristics. The experimental and numerical roughness patterns are analyzed in terms of a relative roughness parameter calculated as a ratio of the rough profile length to the profile evaluation length. It has been found that this parameter correlates exponentially with in-plane plastic deformation with a determination coefficent 0.99, which implies a strong interrelation between the two quantities. The results prove the assumption that in-plane plastic strains accumulated in a loaded material can be evaluated from the estimations of mesoscale surface roughness.

The experimental and numerical roughness patterns were evaluated in terms of a relative roughness parameter calculated as a ratio of the rough profile length to the profile evaluation length. In the present work special attention was given to the numerical study on the effect of texture severity on the roughness characteristics. Experimental and numerical roughness patterns represent contributions of out-of plane surface displacements of smaller and larger grain clusters. It was revealed that the larger surface undulations intensify when smaller ones retard their growth or are suppressed. It has been found experimentally that the relative roughness values and in-plane strains developing at the mesoscale correlate exponentially with the coefficient of determination 0.99. The latter implies a strong interrelation between the two quantities which supports an assumption that in-plane plastic strains accumulated in a loaded material can be evaluated from the estimations of mesoscale surface roughness. The texture severity noticeably affects the mesoscale roughness patterns. A common tendency is the sharper the texture, the smoother the surface. In particular, the presence of a sharp axial texture suppresses the development of an orange peel pattern but leads to pronounced waviness and strain localization at a larger scale. It was also noticed that roughness intensity correlates with the deviation of local stresses developing in the material under loading from the mean values.

The work was supported by the Russian Science Foundation (No. 20-19-00600).

REFERENCES

1. V. Romanova, R. Balokhonov, A method of step-by-step packing and its application in generating 3D microstructures of polycrystalline and composite materials, Eng. Comput. (2019), 1-10.

UDC 538.9

CORRELATION BETWEEN MESOSCALE DEFORMATION-INDUCED SURFACE ROUGHNESS AND IN-PLANE STRAINS IN ALPHA-TITANIUM

E. Emelianova[1,2*], M. Pisarev[1,2], V. Romanova[1]

[1]Institute of Strength Physics and Materials SB RAS, Tomsk, Russia

[2]National Research Tomsk State University, Tomsk, Russia

*E-mail: emelianova@ispms.ru

Abstract. The correlation between mesoscale deformation-induced surface roughness and in-plane strains in α-titanium is investigated experimentally and numerically. Based on the experimental data of EBSD analysis, three-dimensional models taking an explicit account of grain morphology and crystallographic orientations of grains are developed in the framework of

the crystal plasticity theory. It has been shown that a series of out-of-plane surface displacements characterized by different amplitudes and frequencies are formed in the experimental and computational specimens under tension. The results support the assumption that the plastic strain localization and fracture can be predicted early from estimations of mesoscale surface roughness.

Keywords: micromechanics, crystal plasticity theory, polycrystalline structure, numerical simulation, surface roughness

Microstructure of commercially pure titanium is studied experimentally by the EBSD analysis. This analysis has revealed the presence of predominantly quasi-equiaxed grains with two characteristic sizes: large grains with a diameter of 40 μm, surrounded by smaller grains with a diameter of 20 μm. The analysis of pole figures has shown that the material has a split basal texture with the prismatic axes of hexagonal grains being deviated within ±15˚ from the direction normal to the free surface (Figure 1).

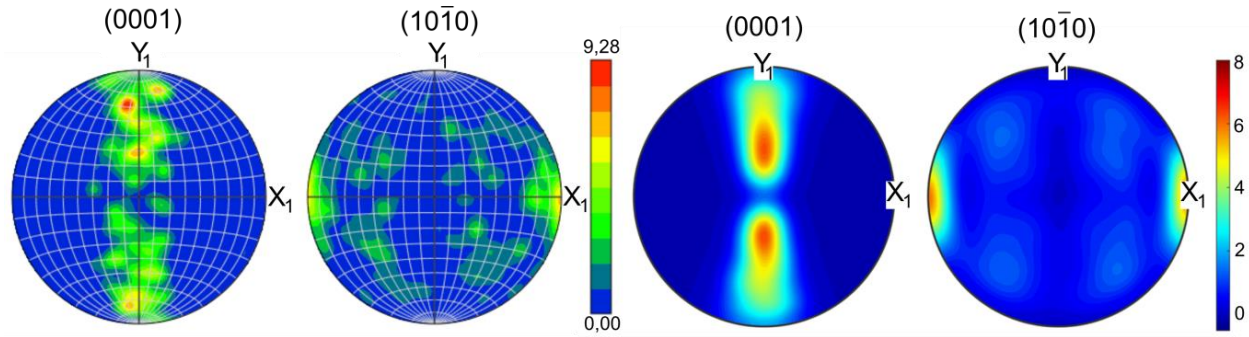

Figure 1 – Pole figures obtained in experiments (a) and calculations (b)

Commercial purity titanium specimens were cut from a 8 mm thick sheet, their surfaces were mechanically polished prior to tensile tests. Uniaxial tension tests were performed at room temperature using an INSTRON universal testing machine.

The mesoscale surface roughening developing in the specimens under tension was studied by a stop-and-study technique [1]. After certain stretching, the specimens were retrieved from the testing machine to analyze their surface morphology with an optical microscope and a contact surface profiler with a step of 1 μm. Then the specimens were placed into the testing machine again and their tensile loading was further continued. The gage section of each specimen was divided into five subsections where surface roughness was investigated. A set of control marks was drawn on the surface to trace local strains of each subsection. The local strains of the subsections were measured as a ratio of the current distances between the marks to the reference subsection lengths.

A quantitative comparison of the experimental and numerical roughness patterns is provided in terms of the dimensionless roughness parameter proposed in [2]. By analogy with a strain measure, the dimensionless roughness parameter R_d is calculated as the ratio of the rough profile length L_r to the profile evaluation length L_e:

$$R_d=L_p/L_e-1. \quad (1)$$

Based on the EBSD data, three-dimensional models taking an explicit account of grain morphology and crystallographic orientations of grains are developed in the framework of the crystal plasticity theory [2]. Model microstructures are generated by the method of step-by-step packing [3]. Grain orientations are set by Euler angles to simulate a split basal texture in accordance with experimental data (Figure). The boundary-value problems of uniaxial tension

of model microstructures along and perpendicular to the rolling direction are solved within a dynamic approach using the ABAQUS / Explicit finite-element package.

Calculated roughness patterns are in a qualitative and quantitative agreement with the experimental data. The deviation of peaks and valleys from the average level, as well as the characteristic period of the frequency components of the profilograms at the same degrees of deformation, vary within the same limits both in the experiment and calculation. Qualitative and quantitative agreement was obtained for the experimental and numerical dependences of the dimensionless roughness parameter on the plastic strain, as well as for the loading curves. The dimensionless roughness parameter is shown to be sensitive to and well correlated with the local plastic strains. The results support the assumption that the plastic strain localization and fracture can be predicted early from estimations of mesoscale surface roughness.

This work is supported by Russian Science Foundation (Project No. 20-19-00600).

REFERENCES

1. Romanova V. Micro- and mesomechanical aspects of deformation-induced surface roughening in polycrystalline titanium / V. Romanova [et al.] // Material Science and Engineering A. 2017. Vol. 697. P. 248-258

2. Romanova V. Early prediction of macroscale plastic strain localization in titanium from observation of mesoscale surface roughening / V. Romanova [et al.] // International Journal of Mechanical Sciences. 2019. Vol. 161–162. P. 105047–105012.

3. Romanova, V., Balokhonov, R. A method of step-by-step packing and its application in generating 3D microstructures of polycrystalline and composite materials. / V. Romanova, R. Balokhonov, // Engineering with Computers. 2021. Vol. 37. № 1. P. 241–250.

UDC 538.911

MODELING OF STRUCTURAL CHANGES IN METALS UNDER HIGH-INTENSITY EXTERNAL ACTION

A.N. Gostevskaya[1], A.V. Markidonov [1,2]

[1] Siberian State Industrial University, lokon1296@mail.ru

[2] Kuzbass Humanitarian Pedagogical Institute of Kemerovo State University

E-mail: lokon1296@mail.ru

Abstract. The study of the structure of metals at the nanoscale using real experiments is difficult due to the size of the particles. The use of computer simulation methods to study and study the effect of high temperatures on the atomic mechanisms of change in a bcc crystal makes it possible to investigate problems that are difficult to solve experimentally. In this regard, conducting a study by computer simulation is the most rational. In the present work, an atomistic simulation of structure ablation, which occurs when materials are irradiated with femto- and picosecond laser pulses, is carried out. The method of molecular dynamics was chosen as a research method. Using a computer model, studies of the influence of the laser ablation process on the change in the internal structure of materials were carried out using computer modeling by the molecular dynamics method.

Keywords: Lab-stable states of the system, condensation of a cloud, interacting defects, nanoclusters.

The physics of ablation regimes inherent in laser irradiation of metals is modeled using the molecular dynamics method [1, 2]. Laser ablation, or irradiation with ultrashort laser pulses, is of practical interest, affecting both experimental and theoretical studies [3 – 5]. At the moment, there are theoretical methods based on the construction of thermal models [6], analysis of the laser emission energy balance [7], which makes it possible to evaluate the effect of laser ablation on the surface structure of the material. In the course of the literature analysis, it was found that the method of molecular dynamics modeling makes it possible to combine theoretical predictions in the field of laser ablation physics and compare them with experimental data.

In the present study, we studied the effect of ultrashort laser pulses on changes in the atomic structure of metals under high-temperature exposure during ablation.

As a mechanism for the formation of cluster particles, the processes of condensation of a cloud of ejected particles, a phase explosion are considered. Considering that most of the computational cell does not change structurally during modeling, it was decided to change the dimensions of the computational cell by $20\times40\times20$ a_0. In this case, the proportion of surface particles increases, but their total number does not change significantly.

To identify clusters, the particle system was divided into separate groups based on distance criteria. This distance is equal to twice the value of the lattice parameter. By different clusters we mean a group of particles, each of which moves away from the particles of this group at a distance not exceeding the cutoff region. After identifying the particle clusters, they are colored in a specific color according to their size. As the number of particles belonging to the cluster increased, the color scheme changed from magenta to red.

To conduct this study, heating was simulated, where the process itself is determined by an increase in the number of clusters, which are individual particles (Figure 1, a). Upon cooling, the number of determined clusters decreases, and the size of these clusters increases, more precisely, previously ejected particles are combined into groups. It was found that with a change in the density of laser radiation, the number of clusters increases. In Figure 1, the number of detected clusters decreased from 32 to 24. Thus, based on the considered model, the mechanism of condensation of ablation products is realized. It is for this mechanism that the formation of small clusters of particles is characteristic.

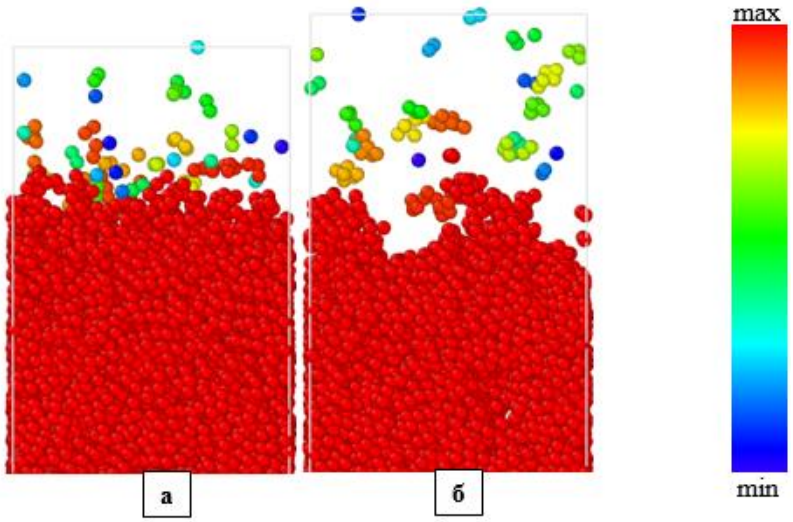

Figure 1 – Representation of recognized clusters after 10 (a) and 18 (b) ps of the time specified in the simulation ($q = 5$ MW/cm^2). Color visualization matches cluster sizes

It can be seen from the figure that the number of clusters decreases with increasing pressure. The change in their number during the simulation is shown in Figure1.

It follows from the above that the constructed molecular dynamics model makes it possible to estimate a part of the ejected particles as a result of heating the computational cell. A study was made of the formation of particle clusters during ablation.

The research was carried out within the framework of the competition of the Ministry of Science and Higher Education of the Russian Federation for the creation of new youth laboratories «Scientific Research Laboratory of EMIP» (project №0809-2021-0013)

REFERENCES

1. Gostevskaya, A. N. Molecular dynamics modeling of laser ablation / A. N. Gostevskaya // Science and youth: problems, searches, solutions : Proceedings of the All-Russian scientific conference of students, graduate students and young scientists, Novokuznetsk, May 12–14, 2021 of the year. – Novokuznetsk: Siberian State Industrial University, 2021. – P. 14-18.

2. Tabetah M., Matei A., Constantinescu K., Mortensen N., Dinescu M., Shaw J., Zhigilei L.V. The minimum amount of "matrix" required for matrix pulsed laser deposition of biomolecules // Journal of Physical Chemistry B. 2014. Vol. 118. Pg. 13290 – 13299. Conv.: https://doi.org/10.1021/jp508284n

3. Song C. Lin T., He P., Zhen J. Molecular dynamics simulation of linear friction welding between dissimilar Ti-based alloys // Computational Materials Science. 2014. Vol. 83. Pg. 35 – 38. Conv.: https://doi.org/10.1016/j

4. S. I. Anisimov and B. S. Luk'yanchuk, "Selected questions of the theory of laser ablation," UFN. 2007. Volume 45. p. 293

5. Bauerle D. Laser processing and chemistry // Luxembourg: Springer Science Business Media, 2011. 851 p.

6. Willis D. A., Grosu V. Influence of melting-induced volume expansion on the initiation of laser-induced forward transfer // Applied Surface Science. 2007. Vol. 253. No. 10. Page 4759 - 4763.

7. Fardel R., Nagel M., Newesh F. Energy balance in laser-induced direct transmission process studied using shadow photography // Journal of Physical Chemistry C. 2009. Vol. 113. Pg. 11628 – 11633

UDC 538.9

NUMERICAL STUDY OF GRAIN STRUCTURE EFFECTS ON THE ELASTIC PROPERTIES OF 316L AUSTENITIC STAINLESS STEEL

O. Nekhorosheva[1,2]*, O. Zinovieva[3], R. Balokhonov[1], V. Romanova[1]

[1] Institute of Strength Physics and Materials Science SB RAS Tomsk, Russia

[2] Tomsk State University Tomsk, Russia

[3] School of Engineering and Information Technology, University of New South Wales, Canberra, Australia

*E-mail: olga0810.00@mail.ru

Abstract. A computational approach providing the whole processing-microstructure-property linkage is used to evaluate the elastic properties of 316L austenitic stainless steel specimens produced by powder bed based additive manufacturing. The computational procedure involves physically-based simulations of grain structure evolution during additive manufacturing and subsequent micromechanical calculations of the deformation response under uniaxial tension. Young modules and Poisson coefficients are obtained by averaging the mechanical properties over the computational domains.

Keywords: additive manufacturing, 316L steel, microstructure-based simulation, grain solidification, elastic anisotropy.

Due to the numerous advantages, including design freedom, time- and resource-efficient production, the dynamically developing additive manufacturing (AM) technology is gaining a significant uptake in many industries. Despite not yet reaching the full potential, flexibility remains one of the main benefits of this technology, from the production of highly complex geometries up to the possibility of engineering microstructures and material properties. That is why the process-structure-property relationship is a critical item to explore in metal AM space. The knowledge gained in this area is crucial to lay the groundwork for process design and property tailoring.

Along with experimental methods of research, microstructure-based numerical simulations are considered as a promising tool to gain valuable information on the processing-microstructure-property link. An attractive idea is to reproduce numerically the whole chain "AM processing – microstructure – mechanical behavior" which would enable substituting high-cost experimental research by computational design.

In this paper, we develop a computational approach providing the whole processing-microstructure-property linkage, including physically-based simulation of grain structure evolution during the laser powder bed fusion (LPBF), and subsequent micromechanical calculations for the deformation behavior at the grain scale and calculation of a homogenized response by averaging the mechanical properties over the representative volume element. The computational approach is used for evaluating elastic properties of 316L austenitic stainless steel. The models of three-dimensional grain structures produced by the LPBF are constructed in terms of a multiphysics methodology which combines the physically-based cellular automata for simulation of the grain structure evolution and finite-difference calculations of heat transfer (Figure1 a-c). Unidirectional and bidirectional scanning strategies are applied as processing conditions. The grain structures obtained are characterized by bi-component crystallographic

textures. While the specimen printed using a bidirectional strategy demonstrates the major {011}⟨100⟩ Goss and minor {001}⟨100⟩ cube texture components, the unidirectional scanning pattern leads to the rotation of both grain arrangement in space and crystallographic texture. The specimen produced with a unidirectional strategy tends to have coarser grains and more severe texture.

The micromechanical finite-element analysis for the microstructures subjected to uniaxial tension along the build (BD), scan (SD) and transverse (TD) directions is performed in the framework of anisotropic crystal elasticity. The stress and strain field analyses show an essential anisotropy of the mechanical properties at the grain scale (Figure1 d-f). It is demonstrated that the stress-strain state of the material under uniaxial tension is complex and all stress tensor components make a comparable contribution to the deformation behavior. It has been found that the unidirectional scanning strategy leads to more pronounced anisotropy of elastic properties than bidirectional scanning.

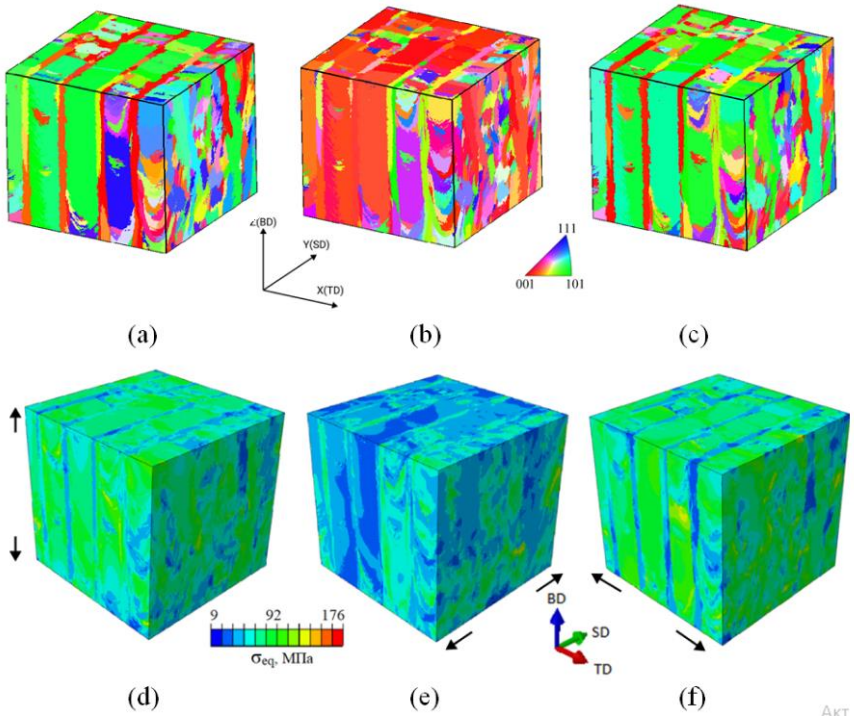

Figure 1 – computational grain structure for bidirectional scanning strategy plotted in IPF colors for BD(a), SD(b) and TD(c), and equivalent stress distributions under tension along BD(d), SD(e) and TD(f)

The funding provided by the Government of the Russian Federation through the research assignment for ISPMS SB RAS (№FWRW-2021-/0002/) is acknowledged.

UDC 538.951 : 616.31

THE EFFECT OF BIOINERT ELECTROEXPLOSIVE COATINGS ON THE STRESS DISTRIBUTION AT THE DENTAL IMPLANT – BONE TISSUE INTERFACE

A.D. Filyakov, K.V. Sosnin, D. A. Romanov

Siberian State Industrial University, Novokuznetsk, 654007, Russia

E-mail: filyakov.1999@mail.ru, k.sosnin@mail.ru, romanov_da@physics.sibsiu.ru

Abstract. In the present work, the first time, it was provided a computer modelling of the stress-strain state of bone tissue located near the implant was carried out, with an electro-explosive coating of the Ti-Zr or Ti-Nb. All materials used in this study were assumed to be linearly elastic, homogenous, and isotropic to simplify the calculation. The stress distribution in the implant and bone tissue located near is uniform. The largest von Mises stress was obtained near the bone-implant interface in the implant area. It has shown that the stress pattern changed in the models with bioinert coatings. The second stress maximum appeared on the boundary between titanium subtract and the coating layer. The most significant changes in stress distribution were reached in the model with Ti-Zr coating.

Keywords: finite element method, dental implants, stress distribution, bioinert coating, electroexplosive spraying.

The difference between Young's modulus of bone and implant leads to a change in force distribution between metal and bone. According to Wolff's Law, bone tissue near implant remodels in response to stress. This effect, known as stress shielding, increases the risk of implants failure.

Electroexplosive method, developing nowadays intensively, is used for spraying different coatings and also can be appeared for Ti-Zr и Ti-Nb coatings development. The result archived by studying electro explosive Ti-Zr, Ti-Nb coating, shows that Young's modulus of these coatings is lower as compared to Ti6Al4V titanium alloy or commercially pure titanium Young's modulus. However, the stress distribution between implant with electro explosive bioinert coatings and the bone study does not exist, because of it, this investigation is important.

The aim of this work is the determinate effect of bioinert electro-explosive coatings on stress distribution near the dental implant-bone interface by means of FEA.

A dental implant made of Ti6Al4V titanium alloy was used as the substrate. The explosive spraying of Ti–Zr and Ti–Nb coatings were carried out on the electro electroexplosive installation EVU 60/10M by an electric explosion of zirconium or niobium foils. The power density was 2.0 GW/m^2. The weight of zirconium or niobium foils were 850 mg. The structure and morphology of sprayed coating and layer located near were analysed by means of scanning electron microscopy (Carl Zeiss EVO50 SEM).

The coatings' thickness was studied on the cross-sections by digital solutions Leica Application Suite. The thickness of the obtained coating is about 63 μm. The Young's module investigation of Ti–Zr and Ti–Nb coating was provided at low indenter load 50 mN by NHT-S-AX-000X Nano Indentation Tester.

The Hounsfield values of cancellous and cortical bone density are 1362.94 and 472.21, respectively. The relationship between HA and kg/m3 is $\rho=a+b\cdot H$ [1], where a=527, b=0.44 are coefficients, H is Hounsfield units (table 1).

The three 2d models were created to investigate the effect of the electro-explosive bioinert coating on the stress distribution near the implant-bone interface.

The length of studying models is 1000 μm, the thickness is 300 μm, while the titanium surface thickness is 87 μm, the intermediate layer thickness is 63 μm, and bone layer thickness is 150 μm. In the third model, also known as the reference model, the intermediate layer, as well as the substrate, is Ti–6Al–4V alloy (figure 1).

The boundary BE is fixed. The compressing force F1 parallel to the x-axis and equal 114.6 N. The bending strength F2 is parallel to the y-axis and equal 29N. The general force F is the geometric sum of F1 and F2, which value is 118.2 N [2]. Two forces are directed to the JF boundary on the other side of the models. The groups of boundaries AB, JC, HD, FE and AJ is free. All models were developed and performed in COMSOL Multiphysics® 5.5.

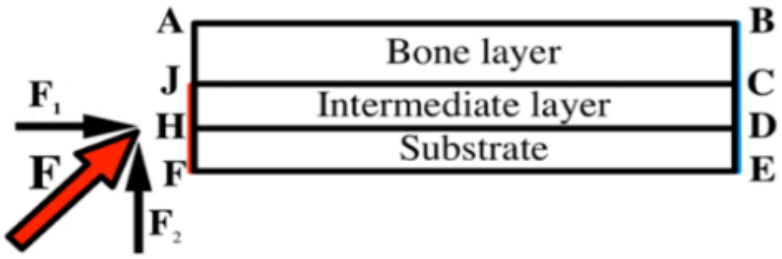

Figure 1 – Boundary and loading conditions

All materials used in this study were assumed to be linearly elastic, homogenous, and isotropic to simplify the calculation (table 1).

Table 1 – Main characteristics of the materials

Material	Young's modulus, GPa	Poisson's ratio	Density, kg/m^3
BT6	110	0.3	4470.5
Ti-Zr	73.8	0.36	6520
Ti-Nb	84.3	0.35	8750
Cortical bone	14.8 [2]	0.3 [2]	1126.28
Cancellous bone	1.85 [2]	0.3 [2]	734.77

In this study was found that the von Mises stress distributes in studied model unequal. The maximum values located in the implant area near the bone-implant interface (JC) and the boundary FE. The layer of bioinert Ti-Zr or Ti-Nb coating changes the stress distribution in the model. The stress values decrease in implant area and grow in bone tissue. The second region with maximum stress value is exist because of the studied model geometry. These changes contribute to reducing stress shielding.

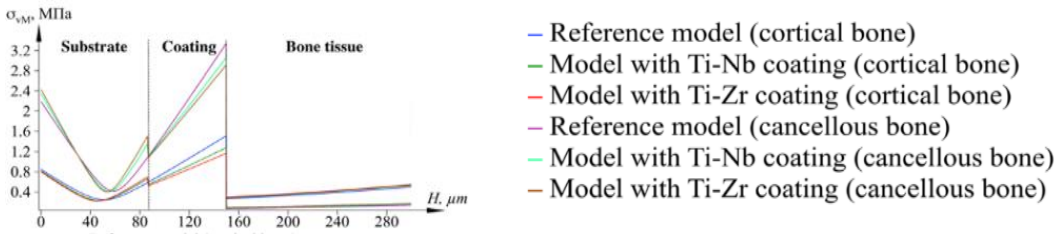

Figure 2 – Cross-section of Von Mises stress distribution

It should be noted that, because of the different coating and subtract Young's module, the second stress peak was found at the coating-subtract interface.

Ti-Zr coating has the most significant impact on stress distribution because of its lower Yong's module.

The average shear stress values are higher in variants with bioinert coating. However, maximum stress values are higher in the reference model.

These results were achieved for both bone tissue types.

Despite the simplicity of the studied model, it possible to conclude, that studied coating can favourably change the life cycle of the implant.

The study was conducted in the framework of the competition new young youth laboratories' creation "Research laboratory of EM&IP".

References

1. S.N. Khan, R.M. Warkhedkar, A.K. Shyam, Analysis of Hounsfield Unit of Human Bones for Strength Evaluation, Procedia Mater. Sci. 6 (2014) 512–519. https://doi.org/10.1016/j.mspro.2014.07.065.

2. A.M. O'Mahony, J.L. Williams, P. Spencer, Anisotropic elasticity of cortical and cancellous bone in the posterior mandible increases peri-implant stress and strain under oblique loading, Clin. Oral Implants. Res. 12 (6) (2001) 648–657. https://doi.org/10.1034/j.1600-0501.2001.120614.x.

UDK 539.214

MECHANICAL PROPERTIES OF RAIL STEEL IN COMPRESSION

Aksenova K.V.[1], Vashchuk E.S.[2], Gromov V.E.[1], Semin A.P.[1]

[1]Siberian State Industrial University, Novokuznetsk

[2]Branch of T.F. Gorbachev Kuzbass State Technical University in Prokopievsk town

E-mail: vaschuk@bk.ru, 19krestik91@mail.ru

Abstract. Mechanical properties of rail steel under conditions of tests for uniaxial compression are determined.

Keywords: rail steel, deformation, uniaxial compression, strength, hardness.

The Russian railways are the second in size transport system of the world. Nowadays the Russian Federation carries out more than 20 % of a freight turnover and 10 % of a passenger turnover of all railroads of the world. A construction of high-loaded railways and an increase in a volume of railroad cargo transformation toughen the requirements to a quality of rail steels. A service life of rails depends on different factors: the purity of steel, technology of rail head quenching, lubrication, operating conditions, etc. A formation of numerous defects in operation is one of the main reasons for a failure of rails. In this context rails should process required mechanical properties such as: hardness, strength, plasticity, impact toughness [1-3].

The P65 type railway rails differentially thermo-strengthened from a rolling heat of a general purpose of the DT350 category we used as a material under study. They were

manufactured at “EVRAZ WSMP” Ltd. Their chemical composition is presented in Figure 1 [4].

The present research concerns the studies of mechanical properties of rail steel under conditions of tests uniaxial compression on an universal testing machine Instron 3369 at a rate of 1.2 mm/min with an automatic recording of load and sizes of sample. Three samples in the form of parallelepiped 9.7 mm in height and cross-section area of 22 mm2 were subjected to tests. It is convenient to use compression as a technique of deformation because, in this case, it is possible to reach deeper deformations than in tension.

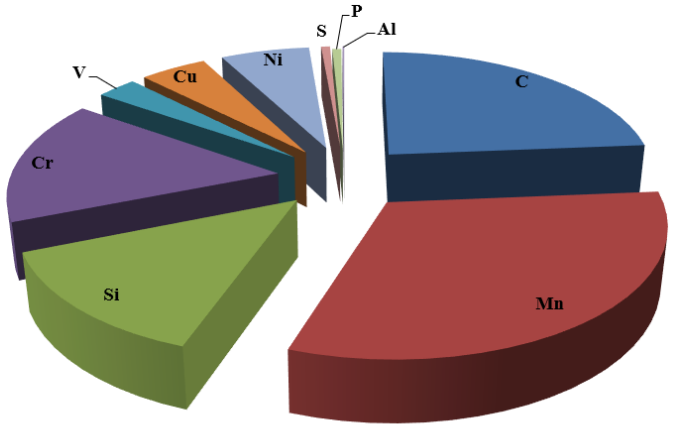

C	Mn	Si	Cr	V	Cu	Ni	S	P	Al
0.71-0.82	0.75-1.25	0.25-0.60	0.20-0.80	0.03-0.15	0.05-0.25	≤0.2	≤0.02	≤0.02	≤0.004

Figure 1 – Chemical composition of rail steel (balance Fe, mas.%)

Machine deformation curves in coordinates ‘load P – total elongation Δl’ (Figure 2, a) were calculated and plotted in dependence ‘true stress σ – true strain ε’ (Figure 2, b). The samples of the studied steel during the compression test could not be brought to failure, i.e. for them, the compressive strength cannot be determined. This is explained by the fact that the steel under study is capable of very strong deformation without destruction, and the samples are flattened.

A mathematical treatment of curves of cold hardening shows that the relation σ-ε has a parabolic form and is described by a fourth-degree polynomial. Mathematical processing of strain hardening curves shows that on the dependence σ-ε it is possible to distinguish the stage of elastic deformation (I) and the stage of plastic deformation (II) with a parabolic functional dependence σ-ε (Figure 2, b). The yield strength is $\sigma_0 \approx 930$ MPa (Figure 2, b).

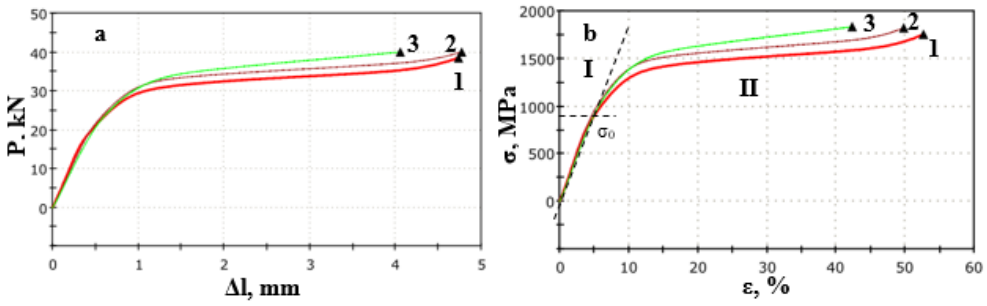

Figure 2 – Machine diagrams of compression (a) and strengthening in compression (b) of a rail steel subjected to loading by uniaxial compression. The dotted lines indicate the yield strength of the material

As a rule, the strain hardening of steel is characterized by the strain hardening coefficient $\theta = \frac{\partial \sigma}{\partial \varepsilon}$, which is determined by differentiating the σ-ε dependence. Analyzing the given in Figure 3 results, the following stages of strain hardening of rail steel can be distinguished: a stage with constant or almost constant high hardening (ε = 0-4%), a stage with a parabolic dependence σ-ε or a decreasing hardening factor Θ (ε = 4-15%) and stage with a weakly changing and low value of the hardening coefficient (ε = 15-45%). If we compare the type of dependence σ-ε and Θ-ε with what is observed at this stage in fcc alloys, where the staging of flow curves is well studied by now, then the above stages should be called stages II, III and IV [5].

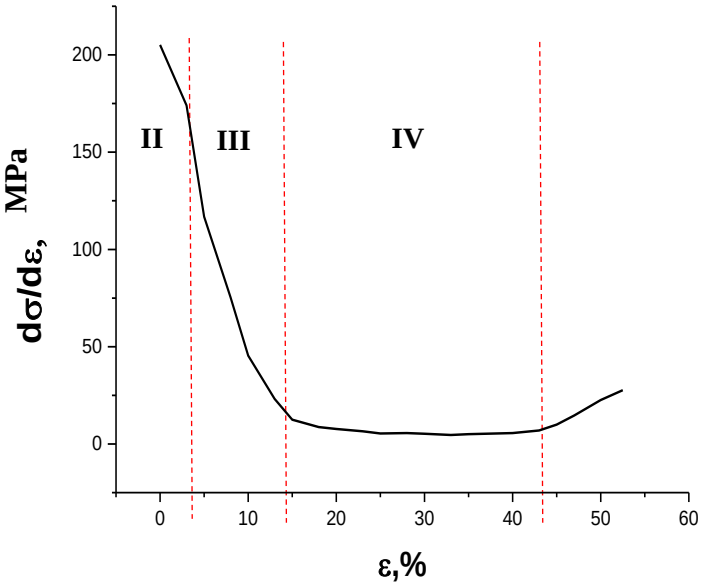

Figure 3 – Dependence of the strain hardening coefficient of sample No. 1 on the degree of deformation of the rail steel subjected to loading by uniaxial compression

References:

1. E.A. Shur, Failures to rails / E.A. Shur. – Moscow: Intekst, 2012. – 192 p.

2. Lengthy rails: structure and properties of ultralong operation: Monograph / A.A. Yuriev, R.V. Kuznetsov, V.E. Gromov [et al.]. – Second edit, supplemented and revised. – Novokuznetsk: Polygraphist, 2022. – 311 p. – (Fundamental problems of modern materials science).

3. Structural-phase state and strengthening of rails after extreme long-term operation / R.V. Kuznetsov, V.E. Gromov, Yu.F. Ivanov [et al.] // Fundamental problems of modern materials science. – 2021. – V. 18. – No. 3. – P. 328-337.

4. GOST P 51685–2013. Railway rails. General specifications. M: FGUP "Standartinform". – 2013.

5. The nature of the stages of plastic deformation / N.A. Koneva // Soros Educational Journal. – 1998. – No. 10. – P. 99-105.

UDC 669.539.381.296

MACROSCALE PLASTICITY PARAMETER: LIGHT AND HEAVY METALS

L. B. Zuev, S. A. Barannikova, S. V. Kolosov

Institute of Strength Physics and Material Science, SB RAS, Tomsk, Russia

E-mail: bsa@ispms.ru

Abstract. It is shown that throughout the process plastic deformation develops in a localized manner at the macroscale level. At the same time, the shape of the observed patterns localization is associated with the stages of strain hardening of the material. Patterns are projections different modes of autowaves of localized plastic flow to the observation surface. Introduced elastic-plastic strain invariant, which is different for light and heavy metals. The invariant is considered as the basic equation of the autowave models of plasticity, and its physical nature is discussed.

Keywords: plasticity, strength, localization, self-organization, autowaves, defects.

During recent decades, it was found that the plastic flow would exhibit an inhomogeneity at all its stages [1]. These processes appear to involve simultaneously micro-, meso- and macro-scale mechanisms. It is of importance that the macro-localization phenomena would emerge at different loading conditions, with the kinetics and distribution of localization nuclei evolving in accordance with plastic flow curve stages. The experimental observations suggests that the plastic deformation would exhibit a localization autowave behavior over the entire process, as one can see in Figure 1.

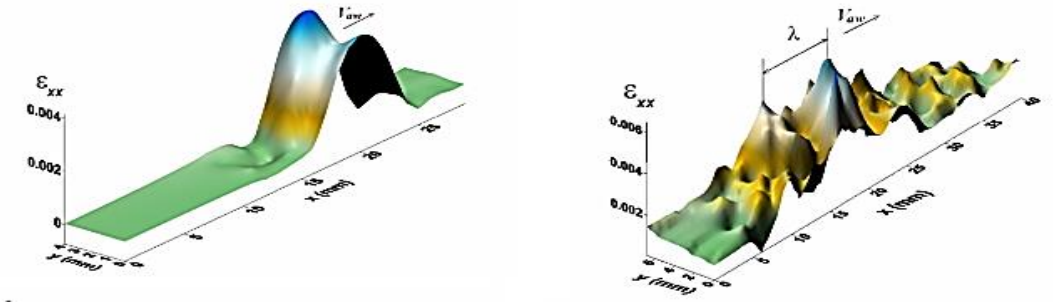

a) b)

Figure 1 – Autowaves of plasticity at the deformation. *a*–yield plateau; *b* – linear hardening

Viewed in this way general regularities of this phenomenon, we proposed an autowave approach in which the deforming media is considered as a nonlinear system with the continuously altering structure on micro- and macroscopic space-temporal scales. Series expansion parameters are selected, characterized the kinetics of structure relaxation in deforming media. The kinetics of structure relaxation is des a)ribed by the system of two nonlinear differential equations of parabolic type. The conditions of the origination are defined exactly for autowave modes on the stages of easy glide, linear work hardening and for stationary dissipative structures on parabolic work hardening stage with the help of the analysis and solution of these equations.

The fact that the plastic flow in solids is an autowave process is arrived at by a simple generalization from the above. By analogy, the evolution of elastic deformation is known to involve elastic wave propagation. A comparison was drawn between the quantitative characteristics of elastic waves and those of localized plasticity autowaves. It was found that a close linear correlation exists between the two-factor product of the macro-parameters λ and V_{aw} (here λ and V_{aw} are, respectively, the length and rate of autowaves propagating at the linear work hardening stage) and the two-factor product of the crystal lattice characteristic *d* or r_{ion} and the quantity $V_{\perp}$ (here $d \approx 10^{-10}$ m is the spacing between close-packed planes of the crystal lattice; $r_{ion} \approx d/3$ is the Pauling ionic radius and $V_{\perp} \approx 10^3$ m/s is the transverse rate of sound). For all the metals studied, the following equality holds true:

$$\lambda \cdot V_{aw} \approx \frac{1}{2} d \cdot V_{\perp} \approx \frac{3}{2} r_{ion} \cdot V_{\perp}. \qquad (1)$$

The average value calculated for ten metals investigated is $\langle 2\lambda \cdot V_{aw} / d \cdot V_{\perp} \rangle \approx 1.07 \approx 1$.

An exponential dependence on the density of the studied metals has been established, from which it can be seen that the value is different for light and heavy metals. An oscillating nature of the plasticity parameter was found as the atomic number of the Periodic Table of Elements increases (Figure 2). The oscillations correlate with similar behavior of a number of other independently determined lattice characteristics, such as the Debye characteristic parameter.

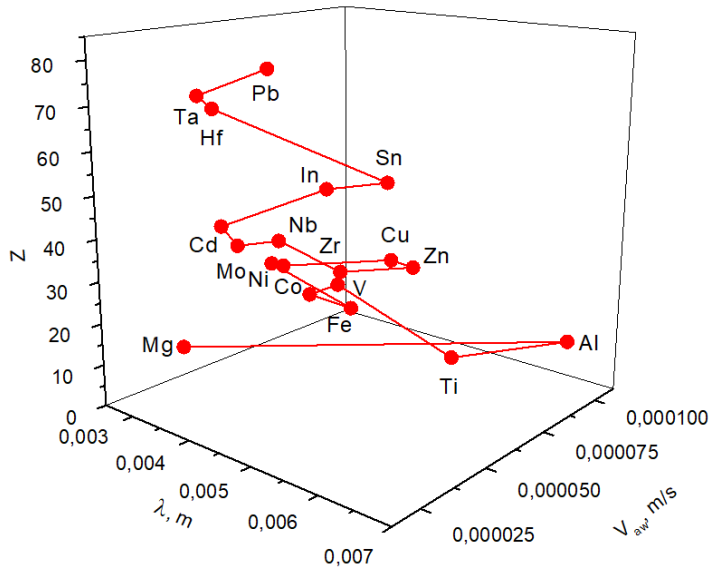

Figure 2 – Variation of macroscale plasticity parameters for light and heavy metals

Of great importance is the empirical equation (1) which for the first time establishes a quantitative relationship between the characteristics of elastic waves, *d* and $V_{\perp}$, and those of localized plastic flow autowaves, λ and V_{aw}. The products $\lambda \cdot V_{aw}$ and $d \cdot V_{\perp}$ could be regarded as invariants of elastic and plastic deformation processes occurring simultaneously in the deforming medium. The above correlation is particularly informative since it accounts for the interrelation between the elastic and plastic strains $\varepsilon_e \ll 1$ and $\varepsilon_p \approx 1$, respectively. Equation (1) presupposes a connection between the elastic and plastic processes, which control the deformation in a consistent manner. However, the rates of these two kinds of processes differ

significantly. Thus the rate of redistribution of elastic stresses, $V_{\perp}$, and the rate of redistribution of localized plasticity regions, V_{aw}, are in the ratio $V_{\perp}/V_{aw} \approx 10^7 \ldots 10^8$.

The existence of invariant (1) suggests that, by addressing the problem of plastic deformation description, one proceeds based on incorrect conventional assumption. Usually, one supposes that the contributions of the elastic, ε_e, and plastic, ε_p, strains to the total deformation are additive, i.e. $\varepsilon_{tot} = \varepsilon_e + \varepsilon_p$. In view of $\varepsilon_e \ll \varepsilon_p$ and $\varepsilon_{tot} \approx \varepsilon_p$, the contribution of elastic strains is generally neglected. However, invariant (1) is suggestive of a close relation between the above deformation characteristics, which should be taken into account by an explanation of the localized plastic flow. One of the fundamental implications of such a model should be the notion of interdependence between the mechanisms of elastic and plastic deformation involved in the process of plastic form changing.

The work was performed according to the Government research assignment for ISPMS SB RAS, project FWRW-2021-0011 and has been supported partially by the grants the Russian Foundation for Basic Research (grant no. 20-08-00305-A).

REFERENCES

1. Zuev L.B. Quasi-particle approach to the autowave physics of metal plasticity / L.B. Zuev // Metals. 2020. V. 10. P. 1–15.

UDC 669.539.381.296

STRESS – STRAIN RESPONSE OF AUSTENITIC STEELS

P. V. Iskhakova, S. A. Barannikova

Institute of Strength Physics and Material Science, SB RAS, Tomsk, Russia,
E-mail: bara71s@yandex.ru

Abstract. The study presented in this paper focuses on the role of temperature on the stress-strain response of Fe-18%Cr-9%Ni austenitic steel polycrystals under extension loading. Stress-strain response exhibits strong dependence on temperature. Mechanical properties and ultrasound wave measurements showed that the hardening was promoted the volume fraction of α′ - martensite for the steel samples with decreasing temperature. γ - α′ martensitic transformation has been observed at T = 180-423 K during plastic deformation in austenitic stainless steel.

Keywords: stress, plasticity, strength, mechanical properties, ultrasound velocity.

At present, the problem of elucidating the causes of macroscopic inhomogeneity of plastic deformation is becoming increasingly important. Both experimental and theoretical studies have been carried out, in which the formation of spatially inhomogeneous structures due to the self-organization of structural defects is studied. It has been established that the patterns of macroscopic localization arising during plastic deformation quantitatively depend on the structure and type of the crystal lattice of the material under study, and their form is completely determined by the laws of strain hardening operating at this stage [1]. This work is devoted to studying the parameters of the macroscopic localization of plastic deformation and ultrasound velocity at the stages of work hardening of Fe-Ni-Cr alloy in the temperature range of 180–423 K. Martensitic mechanisms are effective mechanisms for increasing the strength properties of alloys, which depend on the thermodynamic stability of austenite and deformation conditions. The study of the kinetics of these processes at different temperatures will make it possible to establish the patterns of macroscopic localization of plastic deformation. Mechanical tests for

uniaxial tension were carried out on flat samples of austenitic Fe-Ni-Cr alloy in the form of a double blade with dimensions of 40×5×2 mm at a constant speed of the movable gripper of 0.2 mm/min. Visualization of patterns of localized plastic deformation on the working surface was carried out with an interval of 30 seconds by the method of photographic speckle imaging [1] when the samples were in a transparent flask (a glass Dewar vessel) in the temperature range of 180–423 K using a chromel-alumel thermocouple placed inside the flask on the sample. The rate of nitrogen vapor supply was set using a heating element located inside the Dewar vessel. The temperature in the range of 180–423 K was measured with a chromel-alumel thermocouple located on the non-deformable part of the sample. The temperature was maintained constant throughout the experiment by blowing hot air over the sample inside a thermally insulating box with a transparent window. As a result of the analysis of the distributions of local strains at the stages of linear strain hardening, the dependences of the parameters of localized plasticity on temperature, the strain hardening coefficient, and acting stresses were established. The activation energy of the plastic deformation localization process was also estimated. Simultaneously with the registration of loading curves, the speed of ultrasonic Rayleigh waves was measured using a separate-combined sensor consisting of emitting and receiving piezoelectric transducers installed in the same housing based on piezoceramics with a resonant frequency of 5 MHz [2]. Simultaneously with measurements of ultrasonic wave velocity, magnetic phase analysis of samples (determination of the volume fraction of ferrite) was carried out using a multifunctional eddy current device MVP-2M (ferritometer). Analysis of the change in the velocity of propagation of ultrasound depending on the temperature at the value of the total plastic deformation e = 0; 0.05; 0.1; 0.015; 0.2; 0.25; 0.3 showed that in the studied temperature range, the dependences Vs (T) are linear,

$$V_s = V_{S_0} + \gamma T \,, \qquad (1)$$

here γ = 4.8 m/(s·K) – coefficient. The correlation coefficients of the dependences V_s (T) amounted to ~ 0.97. A decrease in the test temperature from 297 to 180 K causes a change in velocities $(V_s - V_0)/V_0$ by 18% in the undeformed sample and by 16% in the deformed one (e = 0.3), where V_0 is the speed of sound in the undeformed material at room temperature. Measurements carried out throughout the entire process of stretching samples of the Fe-Ni-Cr alloy led to the discovery of the dependence of the ultrasonic propagation velocity Vs and the volume fraction of martensite (formed as a result of the γ-α'-phase transformation) on the magnitude of the applied stress (Figure 1). At the initial stage of deformation up to the yield point, the changes in the ultrasound velocity are insignificant, while after the transition to plastic deformation, a sharp change in V_s occurs. The decrease in the deforming force at the end of the stretching process, which is known to be associated with the formation of a macroscopic neck, corresponds to a slight increase in V_s. An increase in the propagation velocity in this region of deformation indicates a pre-critical state of the deformed material.

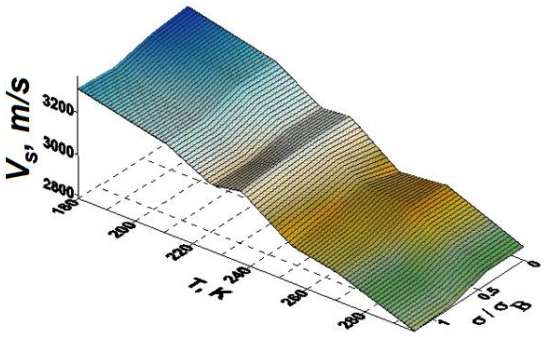

Figure 1 – Variation of ultrasound velocity with an increase in the normalized stress and temperature

Studies of the change in the speed of ultrasound during the stretching of the Fe-Ni-Cr alloy in a wide temperature range of 180–423 K showed that lowering the temperature has a significant effect on the speed of propagation of ultrasonic waves in the samples. An increase in the velocity of propagation of ultrasonic waves in non-deformable samples with decreasing temperature may be due to the fact that the velocity of an ultrasonic wave in a metal is determined by elastic moduli, which increase with decreasing temperatures, as well as the occurrence of compressive stresses arising in the sample against the background of a significant change in the coefficient of linear expansion in the studied temperature range. It has been established that in deformable specimens the dependences of the propagation velocity of ultrasound on the magnitude of the applied stress have a sigmoidal shape and correlate with changes in the volume fraction of α′ - martensite. The stresses corresponding to the maximum growth of the α'-phase and the decrease in the ultrasound velocity were determined.

This work has been supported by the grants the Russian Science Foundation (grant No. 22-29-01608).

REFERENCES

1. Zuev L.B. Quasi-particle approach to the autowave physics of metal plasticity / L.B. Zuev // Metals. 2020. V. 10. P. 1–15.
2. Lunev A.G. Acoustic parameters as criteria of localized deformation in aluminum alloys / A.G. Lunev [et al] // Acta Phys. Polonica A. 2018. V. 134. P. 342–345.

UDC 538.9

CORROSION RESISTANCE OF ZR-BASED BULK AMORPHOUS ALLOYS

Fedorov V.A., Yakovlev A.V., Balybin D.V., Pluzhnikova T.N., Fedotov D.Yu., Berezner A.D., Shlikova A.A.

Derzhavin Tambov State University, Tambov, Russia

E-mail: fedorov-tsu.tmb@inbox.ru

Abstract. The impact of corrosion solution, simulating biological liquid, is investigated for the surface reaction of Zr-based amorphous alloy. The potentiometric investigations have been carried out. It is shown that the corrosion resistance of mentioned alloy increases significantly through the complication of metal ionization.

Keywords: corrosion resistance, amorphous alloys, potentiometric investigations, fractography.

Because of its perfect properties and [1] high corrosion resistance [2] with biocompatibility [3], zirconium amorphous alloys are used in practical medicine [4]. In this work, the experiments on corrosion resistance are carried out on Zr-Cu-Ni-Ti-Ag bulk amorphous system in the biosimilar solutions. The potentiometric investigations have been carried out.

At the experiments on corrosion resistance, two methods were used. At the first one, the specimens of 5×5×2 mm sizes were etched in solution for a long time. Fractography was investigated periodically with a week interval. By the second method, a drop of solution was put on the sample surface. After drying the drop, the next one was put in the same place. For the

experiments, we used the as-cast specimens and ones treated by the ion beam. Ar and N_2 ionic beaming was made by the «Pion/Pulsar» universal source.

The potentiometric investigations have been carried out in water-based and ethylene glycol-water-based (with 50% of H_2O mass) solutions, imitating a biological liquid. Electrochemical kinetics was investigated with Zr-based amorphous and crystalline electrodes during potentiodynamic polarization (with 0.66 mV/s rates of reaction at room temperature and standard hydrogen scale) without forced deaeration by Solartron 1257.

The as-cast specimens had been put in solution, and their surface was investigated after 168 hours of treatment. It leads to a smoothing of the surface relief, observed before etching in solution. Growth of the treatment up to 1512 hours leads to dissolution of the surface layer. A saline cover forms on the surface and corrosion cracking occurs. All of this leads to irreversible changes of the properties (tribological, for example) of bulk metallic glasses.

In the second part, we investigated the local impact of biosimilar liquid on as-cast bulk metallic glasses. After treatment, the outgrowths, corresponding with salts from the solution, are observed on the surface (Figure1). The explicit structure grains stand out.

Then, we investigated the specimens, which underwent ionic beaming. After mentioned treatments, despite the regimes, the formation of some periodic subgrain structure, which can give the materials with new properties, is observed on the surface.

The salt-type structures also occur on the surface, but they have less explicit geometry with weak reaction boundaries. Herewith, it occurs better in the specimens with more fluence, i.e. crystallization is difficult in the second case. Saline outgrowths are observed mainly at the boundary of local etching, while the distribution of the outgrowths is much lesser in the central areas.

During the potentiometric investigations, the polarization curve with standard anodic and cathode branches has been plotted (Figure2).

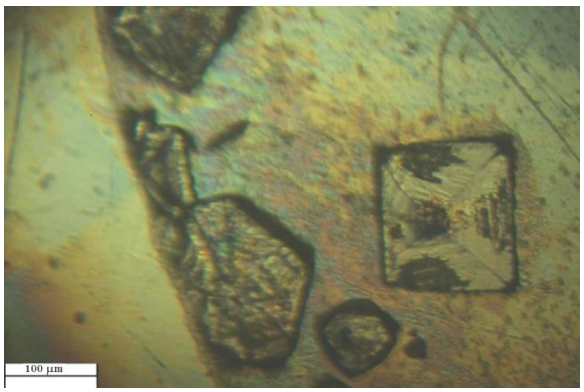

Figure 1 – Surface outgrowths after local treatment by solution

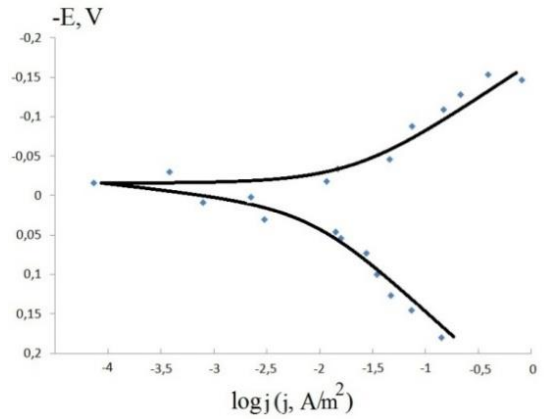

Figure 2 – The electrochemical dynamic of $Zr_{46}(Cu_{4/5}Ag_{1/5})_{46}Al_8$ amorphous alloy in biosimilar water-based solutions

By analysis of the plotted curve, we have established the corrosion potential, which is -0.17 V and current is $3.78 \cdot 10^{-4}$ A/m^2, that is less than standard value (Zr —4 e ↔ Zr^{4+}, E_0= -1,53 V). Tafel angles are b_k = -0.08 V and b_a=0.100 V. By the ennoblement of corrosion potential of amorphous zirconium alloy, its corrosion resistance increases significantly.

Thus, local solution etching does not affect the surface properties of specimens. Long exposure to the biosimilar solution leads to corrosion cracking. Preliminary argon and nitrogen ionic beaming leads to a decrease of biosimilar impact on specimens as in the case of the local etching. The disordered structure of the electrode can be a cause of corrosion resistance of amorphous zirconium alloy where the metal ionization is more complicated.

This work has been financially supported by the RFBR (grant №19-42-680001 p_a).

REFERENCES

1. Suryanarayana C., Inoue A. Bulk metallic glasses. Boca Raton. CRC press. 2017. C. 542.
2. Scully J.R., Gebert A., Payer J.H. Corrosion and related mechanical properties of bulk metallic glasses //Journal of Materials Research. – 2007. – T. 22. – №. 2. – C. 302-313.
3. Lin C. H. et al. Simulated body-fluid tests and electrochemical investigations on biocompatibility of metallic glasses //Materials Science and Engineering: C. – 2012. – T. 32.– №. 8. – C. 2578-2582.
4. Li H. F., Zheng Y. F. Recent advances in bulk metallic glasses for biomedical applications //Acta biomaterialia. – 2016. – T. 36. – C. 1-20.

UDC 538.913

INVESTIGATION OF THE CHARACTERISTICS OF A DISCRETE BREATHER IN THE CUPT ALLOY

Cherednichenko A.I.[1,2], Starostenkov M.D.[2], Bebihov Ju.V.[3], Semenov A.S.[3], Zakharov P.V.[4]

[1]Shukshin Altai State University for Humanities and Pedagogy, Biysk, Russia

E-mail: anton.chered@mail.ru

[2] Altai State Technical University, Barnaul, Russia

[3]Mirny Polytechnic Institute (branch) of North-Eastern Federal University, Mirny, Russia

[4]Peter the Great St. Petersburg Polytechnic University, St. Petersburg, Russia

E-mail: zakharovpvl@rambler.ru

Abstract. The paper considers setting the initial values for a discrete breather in the CuPt alloy. The offset values are calculated from the Gaussian function. The simulation was carried out using the Lammps software package. The influence of the initial conditions on the characteristics of a discrete breather is studied.

Keywords: discrete breather, molecular dynamics, Lammps, nonlinear dynamics, Gaussian function.

The crystal lattice dynamics is determined by a number of factors. First of all, the rigidity of interatomic bonds and the very geometry of the crystal, which determines the anisotropy of properties. This allows one to consider different crystallographic directions for the formation of localized lattice vibrations. Discrete breathers with a hard type of nonlinearity are considered as such localized modes. A discrete breather is understood as localized oscillations in an ideal but non-linear crystal lattice [1]. We can say that such oscillations are infinite under ideal conditions, but it is an impossible task to select such conditions for all atoms of the system. We consider discrete breathers with a finite lifetime. The hard type of localization implies an increase in the frequency of oscillations with amplitude.

In this work, we study the characteristics of a discrete breather in a CuPt alloy. The alloy model is an fcc crystal of AB-$L1_0$ stoichiometry. The model has dimensions of 10 by 30 by 10, respectively, along the XYZ axes and the crystal lattice parameter a = 3.83 Å. The crystal

structure was obtained using the Phana program. The data was written to the data.pos file, which contains information about the number of atoms in the model, the identification number of each atom and its type, and XYZ coordinates. For modeling by the molecular dynamics method, the Lammps software package [2] was used. To set the pair interaction between atoms, we used the EAM potential obtained according to the procedure [3]. A script was written for Lammps that sets the initial conditions for modeling a discrete breather. In our model, the discrete breather was not a single atom, but a group of 14 Cu sublattice atoms located along the <110> direction. The atoms of the discrete breather were displaced along the Y axis in pairs, so that the vibrations of neighboring atoms occurred in antiphase. The initial values of the amplitudes for each atom in the discrete breather were calculated from the Gaussian function [4]:

$$f(x) = A_0 e^{-\frac{(x-b)^2}{2C^2}} \quad (1)$$

As a result of calculations by the Lammps program, we obtained a file with data of the following form: time in picoseconds, the position along the Y axis of the central atom in the discrete breather, and the total energy of the discrete breather.

In the course of calculations, the dependence of the discrete breather frequency on the initial amplitude was obtained (Figure 1).

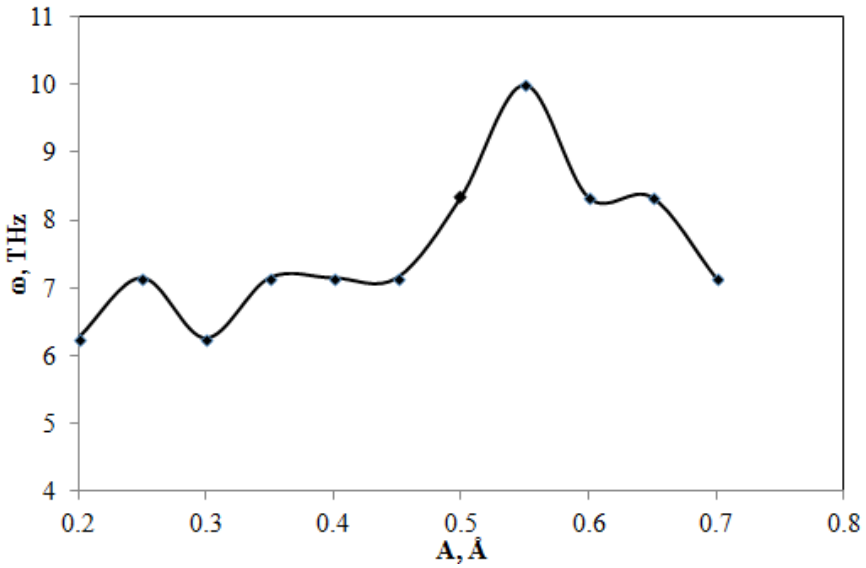

Figure 1 – Dependence of the frequency of a discrete breather on the initial value of the amplitude

Characteristic is the increase in frequency from amplitude from 0.2 to 0.55 angstroms. Then there was a rather sharp decline, which is due to the dissipation of the initial energy of oscillations. An increase in the amplitude leads to significant displacements of atoms in neighboring layers and does not provide conditions for energy localization.

Analyzing the effect of the initial conditions on the duration of oscillations of the atoms that make up the discrete breather, the curve was plotted in Figure 2a. It has been established that the discrete breather exists for the longest time, about 13 ps, at the initial amplitude A = 0.35 Å and the value of the parameter C = 1.9. There are no beats in the system, and the oscillation amplitude remains stable for 10 ps (Figure 2b).

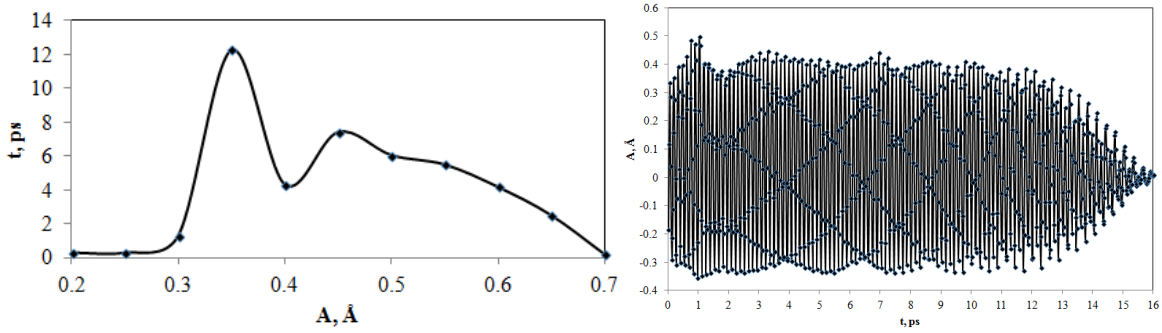

a b

Figure 2 – Duration of oscillations of a discrete breather: a) dependence of the lifetime of a discrete breather on the initial value of the amplitude; b) the dependence of the coordinate on time at the initial value of the amplitude equal to 0.35 Å

Thus, in this work, the conditions for the existence of localized excitations, in the form of a discrete breather, in a CuPt crystal are considered by the method of atomistic simulation. The main characteristics of such objects are the amplitude-frequency dependence, which makes it possible to draw a conclusion about the type of nonlinearity.

The work was supported by the Russian Science Foundation, project no. 21-12-00275.

REFERENCES

1. Flach S. Discrete breathers advancer in theory and application / S. Flach, A.V. Gorbach // Phys. Rep. 2008. 467. P. 1-116.
2. LAMMPS Molecular Dynamics Simulator. URL: https://lammps.org/
3. Zhou X.W. Misfit-energy-increasing dislocations in vapor-deposited CoFe/NiFe multilayers / X.W. Zhou, R.A. Johnson, H. N.G. Wadley // Physical Review B. 2004. V. 69. P. 144113.
4. Zaкharov P.V. Discrete breathers in the crystal CuAu / P.V. Zaкharov [et al] // Lett. Mater. 2016. V. 6. № 4 (24). P. 294-299.

UDC 538.913; 539.8

STUDYING THE EFFECT OF CNT AS A REINFORCING ELEMENT ON THE PROPERTIES OF COMPOSITES WITH A METAL MATRIX

Yankovskaya U.I. [1], Starostenkov M.D.[2], Zakharov P.V. [3]

[1]Altai State Medical University of the Ministry of Health of Russia, Barnaul, Russia

[2]Altai State Technical University, Barnaul, Russia

[3]Peter the Great St. Petersburg Polytechnic University, St. Petersburg, Russia

E-mail: zalaevau@gmail.com

Abstract. In this paper, using the Pt crystal model as an example, we consider the efficiency of strengthening pure platinum when reinforced with a single-layer carbon nanotube. Within the framework of the embedded atom model for the proposed crystal model, the EAM potential was considered. In this work, the melting point of pure Pt and Pt-C composite was studied.

Keywords: modelling, molecular dynamics simulation, metal-matrix composites, melting temperature, CNT.

The work [1] considers nanocarbon materials such as graphene, carbon nanotubes and their derivatives, which are considered to be highly efficient strengthening elements in metals. One of the most important criteria for choosing a reinforcing material is the thermodynamic stability of the reinforcing particles with respect to the material of the crystal under study. The absence of mutual solubility and the possibility of chemical interaction (up to the melting temperatures of the hardened metal). It is also important that with an increase in temperature, the process of diffusion coalescence of particles should not be observed. [2]. Currently, the possibility of using nanostructures as reinforcing additives in the production of composites is being actively studied. [3].

To study the mechanical and thermal properties of CNT-reinforced nanocomposites, there are a number of models considered in [4]. In the presented work, the method of molecular dynamics was used. A crystal of pure platinum was created through Atomsk [5]. The resulting crystal was reinforced with the single-layer carbon nanotube of the "zigzag" type with chiral indices (8.0).

When modeling in the Pt crystal, the size of the hole was varied with respect to the CNT diameter. After that, the system was relaxed within the framework of the NVE ensemble. The model with the most stable structure was chosen for further research. In this case, the diameter of the CNT was 3.31 Å, and the diameter of the hole in the platinum crystal was 6 Å.

The study compared the melting point of the pure Pt crystal and the CNT-reinforced platinum crystal. The simulation conditions were as follows: for 0.3/ns, the model was in equilibrium at the temperature of 300K; then the system was heated for 3/ns from 300K to 3500K, after which the model was relaxed for 1/ns at the temperature of 3500K. After that, the model was cooled at the temperature from 3500 K to 300 K for 30.5/ns. Modeling of heating and cooling processes of pure platinum and Pt-C system was carried out using the LAMMPS package. To calculate the melting temperature, the temperature dependence of the potential energy was studied, which made it possible to monitor phase transformations.

According to the data obtained, the melting point of platinum can be determined by the formula:

$$T = T_{heating.} + T_{cool.} - \sqrt{T_{heating.} \cdot T_{cool.}},$$

where T is the melting temperature, $T_{heating}$. - melting temperature when the model is heated, $T_{cool.}$ is the crystallization temperature during model cooling. For pure platinum (Pt), was obtained the value of 2392 K, which is 15% higher than the experimental value. This is due to the ideal crystal lattice, the absence of defects and free surfaces.

For a CNT-reinforced crystal, it was experimentally found that nanotubes are very good heat conductors. [6]. According to the data obtained at the heating stage, the melt of the crystal with CNTs occurs faster (at a temperature of 2600 K), which indicates a lower melting temperature of the considered composite. It was found that the cooling curves up to 1400 K for both models run in parallel. Cooling of the Pt-C composite occurs at a lower value of potential energy, there is no phase transition. However, it was not possible to achieve the presence of an ordered structure. This is due to the presence of free volume, which was originally enclosed in the nanotube.

Reinforcement of CNT metal leads to a change in material properties that affect the melting temperature. In this work, it was established that the introduction of the carbon nanotube into the model leads to a decrease in the melting temperature.

The work was supported by the Russian Science Foundation, project no. 21-12-00275.

REFERENCES

1. Zhao L. Mechanical Robustness of Metal Nanocomposites Rendered by Graphene Functionalization / L. Zhao // Nano Letters. 2021. №13. С. 5706-5713.
2. Sokolovskaya E. N. Physicochemistry of composite materials: textbook / E. N. Sokolovskaya, P. S. Guzey. M.: Publishing House of Moscow University, 1978. 255 с.
3. Tjong S.C. Novel nanoparticle-reinforced metal matrix composites with enhanced mechanical properties // Advanced Engineering Materials. 2007. V. 9. Issue 8. P. 639−652.
4. Ahmed K. S. Advanced nanoindentation simulations for carbon nanotube reinforced nanocomposites / K. S. Ahmed [и др.] // Heliyon. 2020. № 6(8). E04575.
5. Atomsk: A tool for manipulating and converting atomic data files Pierre Hirel, Comput. Phys. Comm. 197. 2015. pp. 212-219.
6. Suk M. E. Effect of the Nanotube Radius and the Volume Fraction on the Mechanical Properties of Carbon Nanotube-Reinforced Aluminum Metal Matrix Composites // Molecules. 2021. №26(13). С. 3947.

UDC 666.775-798.2:539.9:666

SYNTHESIS OF SIALON BASED ON THE USE OF HIGH-TEMPERATURE PLASMA

V.A. Vlasov[1], A.A. Klopotov[1], K.A. Bezukhov[1], N.N. Golobokov[2], G.G. Volokitin[1], S.A. Buinovskii[3], Litvinova V.A.[1]

[1]Tomsky State University of Architecture and Building, Tomsk, Russia

[2]Tomsk branch of the Institute of structural Macrokinetics SB RAS, Tomsk, Russia

[3]Seversk Technological Institute NRNU,MEPI, Tomsk, Russia

E-mail: victorisain@mail.ru

Abstract. The paper presents the data of an X-ray diffraction study of a SiAlON-based ceramic material obtained by a plasma-chemical method using the energy of a low-temperature arc plasma. It has been established that the addition of a fine powder of an alloy based on (Fe,Co)(REE) to a mixture of aluminum and silicon nitrides leads to the formation of two forms of SiAlON by the plasma-chemical method: β−SiAlON and 16H-SiAlON.

Keywords: β−SiAlON, high-temperature plasma, plasma-chemical method, structure.

SiAlON four-component ceramics belongs to the class of high-temperature materials. About 10 types of SiAlONs with different crystal structures have been established. On figure 1 shows the unit cell of a β−SiAlON of the composition Si_5AlON_7. The composition of β−SiAlON is described by the formula $Si_{6-x}Al_xO_xN_{8-x}$($1\leq x \leq 4.2$). The composition of α−SiAlON is described by the formula $Si_{12-(x+y)}Al_{x+y}O_xN_{16-x}$. The composition of α−SiAlON is described by the formula $Si_{12-(x+y)}Al_{x+y}O_xN_{16-x}$. The composition of O′−SiAlON is described by the formula $Si_{2-x}Al_xO_{1+x}N_{2-x}$. ($1\leq x \leq 0.2$). The main and widely used are α−, β− and O'−SiAlON.

The active use of α- SiAlON is due to a good set of physical and mechanical properties: high hardness and good heat resistance. The use of β−SiAlON ceramics is due to high strength and toughness. Such a difference in the physical and mechanical properties of α− and

β–SiAlONs leads to the fact that a material consisting mainly of β–SiAlON exhibits high viscosity. On the other hand, the material based on α- SiAlON (with a low content of β–SiAlON) has a high hardness. At the same time, ceramics based on α– and α/β – SiAlON have good resistance to corrosion in alkalis. Therefore, the development of new methods for the synthesis of SiAlON ceramics with different structural and phase compositions is topical.

The aim of this work is to use the energy of low-temperature arc plasma for the synthesis of a ceramic material based on SiAlON with the addition of metal powder.

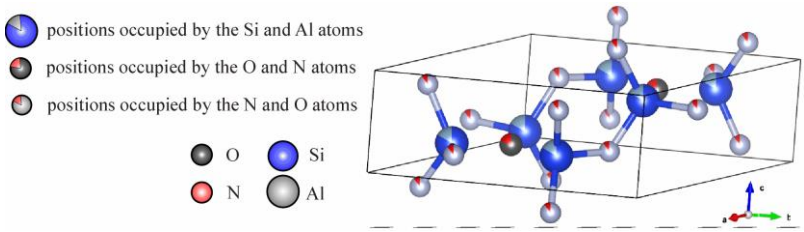

Figure 1 – Unit cell β–Si_5AlON_7

The following components were used as starting materials: powders of β–Si_3N_4, AlN, and REM-Fe(Co), urea solution (H_2NCoNH_2) and liquid glass (Na_2SiO_3). Powders of REM-Fe(Co) alloy were obtained by secondary calcethermal reduction we eat from fluorides at JSC «Siberian Chemical Combine». The total amount of all rare earth elements in the samples of this alloy was in the range of 35-40% wt. (REM = Nd, Pr, La, Dy).

Table 1 – Composition of components in samples for plasma chemical synthesis, weight. %

Compounds	β-Si_3N_4	AlN	P3M-Fe(Co)	H_4NCoNH_2	Na_2SiO_3
Composition 1	25	25	–	25	25
Composition 2	44	44	4	–	8

The creation of a low-temperature plasma beam was carried out in a plasma generator of the VPR-410 type. Technical parameters of the plasma generator: mains voltage 380 V; operating voltage on the arc 120 V; rated operating current 220 A. The plasma gas was nitrogen. Under such regimes, the temperature in the region of the middle part of the plasma beam reaches the value T = 6100÷7300 K. In Figure 2 shows a photograph of the plasma-chemical reactor.

The exposure of the plasma beam to the sample was carried out for three minutes. After plasma exposure, the sample was cooled in air to room temperature. On Figure 3 shows a briquette after plasma treatment. For X-ray diffraction study, the melted part of the sample was mechanically crushed to a powder.

Figure 2 – Photo of the plasma chemical reactor:1 – plasmatron; 2 – reactor; 3 – nitrogen supply pipeline to the reactor; 4 – plasma jet; 5 – nitrogen supply piping to the plasmatron; 6 and 7 – reactor water cooling pipes

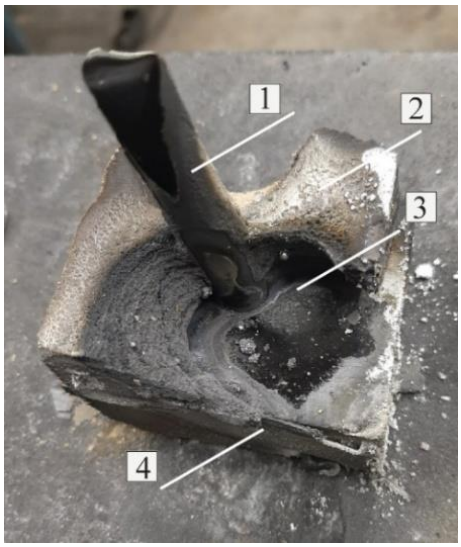

Figure 3 – Photo of the sample after exposure to high-temperature plasma: 1 – graphite electrode; 2 – sample; 3 – reflow zone; 4 – graphite plate

X-ray diffraction study was carried out on DRON-3 and SHIMADZUXRD-7000S diffractometers using $Co_{K\alpha}$ and $Cu_{K\alpha}$ radiations.

Based on a qualitative X-ray phase analysis, it was found that the formation of the composition AlN_7OSi_5 with hexagonal syngony (Pearson symbol *h*P14, space group $P6_3/m$) occurred by the β–SiAlON plasma-chemical method.

The introduction of REM-Fe(Co) metal powder into the mixture led to the formation of additional lines on the diffraction patterns, which belong to other SiAlON phases. It is most likely that these additional lines belong to 16H-SiAlON. This assumption is based on the fact that the phase transition between two types of SiAlON ceramics when heated to temperatures above 2000 °C satisfies the following conditions: α–SiAlON+$O_2\rightarrow\beta$–SiAlON и β–SiAlON+$N_2\rightarrow\alpha$–SiAlON. This also does not exclude the formation of compounds 16H–SiAlON, O′–SiAlON, 15R–SiAlON, etc.

The work has been conducted with the financial support of the Government Assignment of the Ministry of Education and Science of the Russian Federation (project No. FEMN-2020-0004).

UDC 620.171.2:620.186.8

ELECTROPLASTIC AND THERMAL ACTION OF THE CURRENT IN THE EXTENSION OF TITANIUM

Korolkov O.E.[1], Pakhomov M.A.[2], Stolyarov, V.V.[2]

[1]Moscow Polytechnic University, Moscow, Russia

[2]Mechanical Engineering Research Institute of RAS, Moscow, Russia

Moscow, Russia, korolkov_oleg@vk.com

Abstract. The effect of single-pulse and multi-pulse current modes on the tensile mechanical behavior of commercially pure titanium Grade 4 is shown. To assess the relative contribution of the electroplastic effect to the decrease in flow stresses, the current exposure is compared with thermal heating from an external source.

Keywords: tension, pulsed current, electroplastic effect, Joule heating, titanium

The electroplastic effect (EPE) is a phenomenon in which a decrease in the resistance of a metal to deformation is observed, as well as an improvement in its ductility under the influence of an electric current of a sufficiently high density or intense electron radiation [1]. The most common theories explaining the effect of EPE are electron-dislocation interaction and local heating on structural in homogeneities [2]. The treatment of titanium and its alloys by metal working, mainly at room temperature, is a promising field of application for EPE due to low thermal conductivity, polymorphism, and a tendency to oxidization [3]. Some features of EPE in titanium and other materials were demonstrated in [4]. The purpose of this study was to compare the contributions of the electroplastic and a thermal effect in Grade 4 titanium using the example of powerful single current pulses and a multipulse modes.

Annealed, commercially pure Grade-4 titanium (ASTM F67-06) was chosen as the material for the study. Diameter and gauge length of tensile specimens were ∅2x12mm according to GOST 1497-84. Tension was performed on a horizontal tensile testing machine IR - 5081/20 with electrically isolated clamps. The test speed was 1.7 mm/min. Current was supplied to the clamps of the tensile testing machine in a multipulse mode with a frequency of 1 kHz, a pulse duration of 100 μs, a density of 60 A/mm^2, and in the form of single pulses with a duration of 1000 μs, a density of 220 and 860 A/mm^2 injected every 5 seconds. A technical dryer was used to separate EPE and Joule heating MAKITA HG6530VK, with which the sample was heated to a temperature corresponding to the temperature of the sample when current was passed. Sample temperature was controlled with a Digital Thermometer UT320 and a chromel-alumel thermocouple at the center of the sample with an accuracy of ± 2°C. The amplitude current density was monitored using an AKIM-4131/2 oscilloscope. The current was introduced into the sample before the start of tension which was performed after the temperature stabilized.

Introduction of single current pulses with a density of 220 A/mm^2 and a duration of 1000 μs. (Figure1a, curve 2) leads to a decrease in flow stresses and decrease relative elongation relative to curve 1 obtained during the test in the absence of current. In addition, downward stress jumps appear with amplitude increasing with strain from 5 to 35 MPa in the elastoplastic region. A fourfold increase in current density up to 860 A/mm^2 while maintaining the pulse duration (Figure 1a, curve 3) leads to a further decrease in flow stresses and an increase in the amplitude of stress jumps by an order of magnitude, from 90 to 350 MPa.

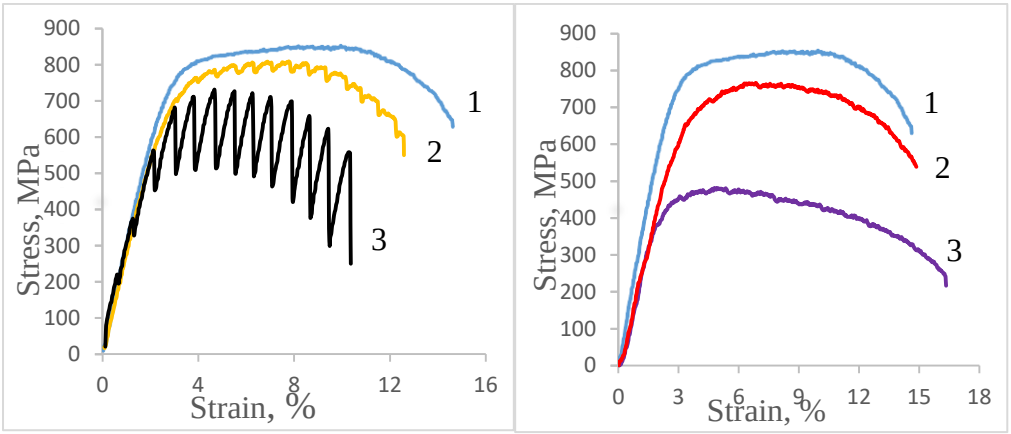

Figure 1 – Tension curves of titanium: a) single impulses: 1 - without current, 25ºC; 2 - 220 A/mm^2, 1000 μs, 25ºC; 3 - 860 A/mm^2, 1000 μs, 58ºC; b) multipulse current: 1 - without current, 2 - hair dryer, 110 ºC; 3 - 60 A/mm^2, 100 μs, 1 kHz, 110ºC

In addition, jumps with an amplitude of 15–40 MPa are also noted in the elastic region. The temperature during this test rose to 58 ºC. Jumps in the elastic region were also observed earlier, for example, in shape memory alloys [5]. It is believed that they are due only to the thermal effect of the current, and the EPE is added to the thermal effect of the current in the elastoplastic region [6]. The introduction of a multipulse current with a density of 60 A/mm^2 (Figure 1b, curve 3) led to an increase in the sample temperature to 110 °C, a sharp decrease in the flow stress ($\Delta\sigma$= 350 MPa), strain hardening and a noticeable increase in elongation to failure. Tension without current, but with heating by a hair dryer to the same temperature (curve 2), led to a decrease in the flow stresses $\Delta\sigma$=90 MPa, which is much less than for curve 3.

The results of the deformation behavior of titanium under the influence of different current modes are discussed from the standpoint of a thermal contribution of EPE.

REFERENCES

1. Troitsky O. A. Electroplastic effect in metals / Monograph. M.: Kim L.A. 2021. 468 p.

2. Minko D. V. Analysis of the prospects of the application of the electroplastic effect in the processes of processing metals with pressure / D. V. Minko // Litiyo i Metallurgiya. 2020. 4. 125-130.

3. Illarionov A. G. Technological and operational properties of titanium alloys: textbook / A. G. Illarionov, A. A. Popov. Yekaterinburg: Ural University, 2014. 137 p.

4. Stolyarov V. V. Features of the interaction of plastic deformation and pulse current in various materials / V. V. Stolyarov, I. Calliari, C. Gennari // Mater. Lett. 2021. 299. 130049

5. Frolova, A.V. Strain of Alloys with the Martensitic Transformation under the External Impact / A.V. Frolova [et al] // Bulletin of the Russian Academy of Sciences: Physics. 2019. 83. 1289-1293.

6. Okazaki K. An Evaluation of the Contributions of Skin, Pinch and Heating Effects to the Electroplastic Effect in Titanium / K. Okazaki, M. Kagawa, H. Conrad // Materials Science and Engineering. 1980. 45. 109-116.

UDC 539.382

DEFORMATION OF SAMPLES OF SILUMIN AK5M2 DOPED WITH TITANIUM BY IRRADIATION OF THE FILM/SUBSTRATE SYSTEM WITH A PULSED ELECTRON BEAM

Ivanov Yu.F.[1], Klopotov A.A.[2], Zaguliaev D.V.[3], Ustinov A.M.[2], Prokopenko N.A.[1], Teresov A.D.[1], Abzaev Yu.A.[2], Klopotov V.D.[4]

[1]Institute of High Current Electronics SB RAS, Tomsk, Russia

[2]Tomsk State University of Architecture and Building, Tomsk

[3] Siberian State University of Industry, Novokuznezk

[4]National Research Tomsk Polytechnic University, Tomsk

E-mail: zagulyaev_dv@physics.sibsiu.ru

Abstract. The paper presents the results of a study of the effect of surface modification of samples of silumin A319.0 by irradiation with a pulsed electron beam of samples of the "film (Ti)/(silumin A319.0) substrate" system on mechanical properties, distribution of deformation fields at the meso- and macroscale levels by the digital image correlation method.

Keywords: silumin, deformation, intense electron beam irradiation, VIC-3D system

Recently, an approach based on surface modification by irradiating alloys with high-energy electronbeams has been widely used. The composite material "film (Ti)/(silumin A319.0) substrate" irradiated with a pulsed electron beam was chosen for the study. Deformation effects by uniaxial tension on flat proportional specimens were carried out on an «INSTRON 3386» testing machine. The speed of movement of the active grip of the machine is constant and equal to 0.0025 s^{-1}. The evolution of deformation fields during testing was recorded using a VIC-3D optical measuring system [1, 2]. The study of deformation using a measuring system was carried out on the basis of an extensometer installed within the working part of the test sample from the upper to the lower clamp of the testing machine. The deposition of a titanium film 0.7 μm thick on silumin samples was carried out on the KVINTA installation. The samples were irradiated with a pulsed electron beam using a SOLO setup (30 J/cm^2, 200 μs, 3 pulses).

Figure 1 shows strain diagrams obtained by stretching silumin samples in the cast state and silumin samples, the surface of which was modified by irradiating samples of the “film (Ti)/(silumin A319.0) substrate” system with a pulsed electron beam. On the deformation curves, three stages of deformation can be distinguished: I – the stage of elastic deformation; II – stage with a parabolic functional dependence of the form:

$$\sigma = \sigma_0 + \theta\varepsilon^n, \quad (1)$$

where σ_0 – yield strength; $\theta(\varepsilon)=d\sigma/d\varepsilon$ – strain hardening factor; $n<1$ – strain hardening index [3]. Stage III – the stage of sample pre-fracture. The numerical values of the parameters from equation (1) for the original and modified samples are given in the table 1.

Table 1 – Parameters characterizing the strength properties of A319.0 silumin

Sample	σ_0, MPa	n	σ_t, MPa
Initial	24±3	0.44±0.02	90±15
Modified	45±3	0.36±0.02	140±15

It can be seen that the modification of the surface layer of samples of A319.0 silumin led to an increase in the strength properties of the material.

Points 1, 2, 3, 1', 2', 3' on the deformation curves $\sigma=f(\varepsilon)$ in Figure 1 correspond to the patterns of distributions of longitudinal relative strains shown in Figure 2. An analysis of the patterns of distributions of longitudinal ε_{YY} relative strains on the surface of the original and modified samples made it possible to establish the following regularity. The modification of the surface led to the fact that the rupture of the sample occurred in that local place where a significant localization of the deformation centers manifested itself (Figure 2, pattern 2). The destruction of the original sample occurs in the place where there was no significant localization of deformation centers (Figure 2, pattern).

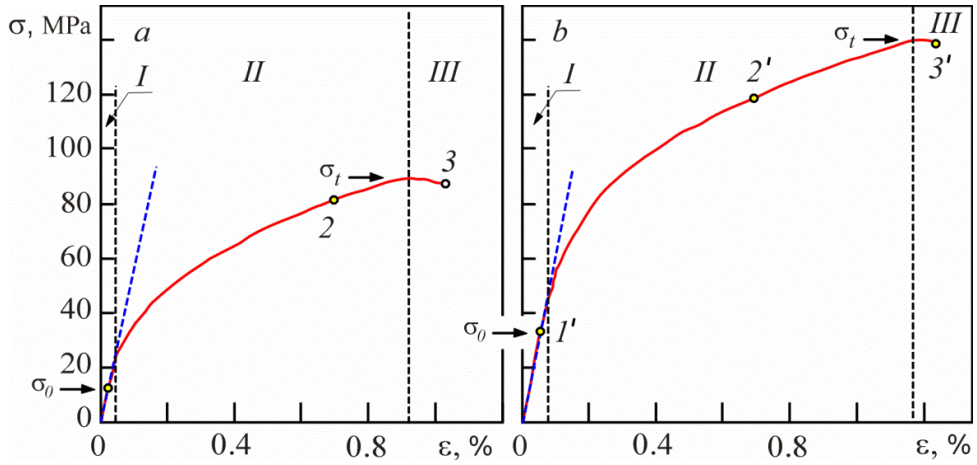

Figure 1 – Deformation curves of the original (a) and modified (b) samples of A319.0 silumin. Points 1, 2, 3, 1′, 2′, 3′ highlight the states for which the distribution patterns of deformation fields are shown in Figure. 2

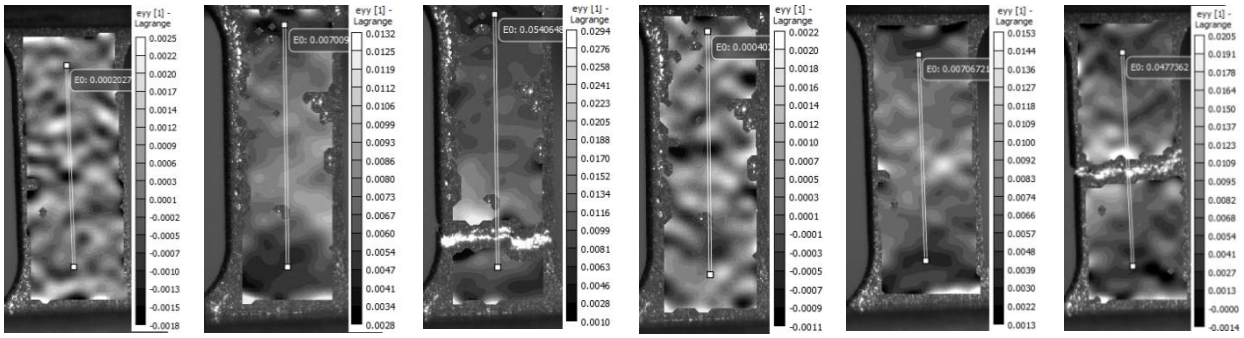

1 *2* *3* *1′* *2′* *3′*

Figure 2 – Patterns of distributions of longitudinal ε_{YY} relative strains on the surface of the original and modified samples. These patterns correspond to points 1, 2, 3 (Figure 1,*a*) and 1′, 2′, 3′ (Figure 1, *b*)

Acknowledgments. The research was financially supported by the Russian Science Foundation (RSF) (project № 19-79-10059).

REFERENCES

1. Klopotov A., Sharkeev Y., Potekaev A. and et. al. Speckle Structures of Surface Layer of Zr-1Nb Alloy Samples in Micro- and Ultrafine-grained States under Deformation. AIP Conference Proceedings. 2019. 2167, 020161.

2. Sutton M. A., Orteu Jean-Jose, Schreier H. W. Image Correlation for Shape, Motion and Deformation Measurements. Basic Concepts, Theory and Applications. Springer Science, Business Media. 2009. P.332.

3. Honeycombe R. W. K. The plastic deformation of metals. Edward Arnold. 1984, 483 p.

UDC 621.785.53; 539.25

SURFACE HIGH SPEED STAINLESS STEEL ALLOYING WITH COPPER

Ivanov Yu.F.[1], Petrikova E.A.[1], Ivanova O.V.[2], Teresov A.D.[1], Prokopenko N.A.[1], Petyukevich M.S.[1]

[1]Institute of High Current Electronics, Siberian Branch of the Russian Academy of Sciences

[2]Tomsk State University of Architecture and Building, Tomsk, Russia

E-mail: yufi55@mail.ru

Abstract. A two-stage mechanism of solid solution decomposition in the Fe-Cu system was revealed as a result of the studies performed. The purpose of this studies was to establish the patterns of the structure and properties evolution of 321 steel subjected to high-speed surface alloying with copper as a result of irradiation of the “film/substrate” system with a pulsed electron beam.

Keywords: film/substrate system, pulsed electron beam, steel, copper, structure, properties.

The using copper as an alloying element, the addition of which in small concentrations to low-carbon steel instead of expensive elements - niobium, titanium and vanadium, leads to the appearance of high corrosion and mechanical characteristics associated with the formation of Fe-Cu precipitates in the bulk of the material [1-3]. It has been established that these precipitates are nanosized particles of a saturated (more than 1% at.) solid solution of copper in iron, while in the equilibrium state the maximum solubility of copper in iron does not exceed 0.38% at. In this case, one should speak about the properties of the material as a function of near-surface transition states. Nanosized copper-enriched particles in α-Fe formed during cooling provide high ductility and fracture toughness and cause dispersion strengthening of the steel.

The formation of the "film (Cu)/(steel 321) substrate" system was carried out on the QUINTA installation [4] by sputtering copper films 0.5 μm thick onto steel specimens. High-speed alloying of steel with copper was carried out by irradiating the "film (Cu)/(steel 321) substrate" system with a pulsed electron beam using a SOLO setup [4]. The irradiation mode corresponded to the liquid-phase alloying of the steel surface layer with copper.

Studies performed by scanning electron microscopy showed that at an electron beam pulse duration of 50 μs (15 J/cm^2, 15 pulses, 0.3 s^{-1}) a nanocrystalline structure with a crystallite size of (80-120) nm is formed on the specimen's surface (Figure 1a). At an electron beam pulse duration of 200 μs (30 J/cm^2, 15 pulses, 0.3 s^{-1}), regions with a lamellar structure are formed on the specimens surface. A structure of cellular crystallization is observed in the bulk of the plates (Figure 1b). The cell sizes vary within (0.58-0.81) μm.

X-ray microanalysis revealed a decrease (more than 4 times) in the concentration of copper in the steel surface layer with an increase in the duration of exposure to the electron beam from 50 μs to 200 μs.

Using X-ray phase analysis methods, it was shown that at an electron beam pulse duration of 50 μs, a solid solution of copper in a crystal lattice based on γ-Fe and a $Fe_{0.5}Cu_{0.5}$ phase with a bcc crystal lattice are formed in the surface layer. With an increase in the pulse duration to 200 μs, a two-phase structure is formed in the surface layer - γ-Fe and a phase of $Fe_{0.7}Cu_{0.3}$ composition, which has an fcc crystal lattice.

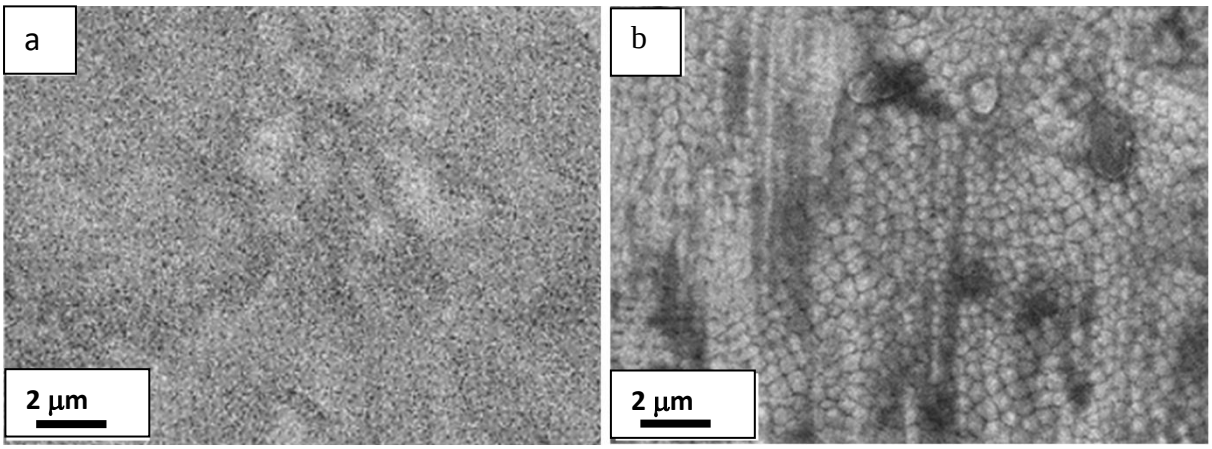

Figure 1 – Electron microscopic image of the steel modification surface structure of specimens by irradiating the "film (Cu) / (321 steel) substrate" system with a pulsed electron beam with parameters: 50 μs, 15 J/cm^2, 15 pulses, 0.3 s^{-1} (a) and 200 μs, 30 J/cm^2, 15 pulses, 0.3 s^{-1} (b)

Cu as a separate phase is not detected. An increase in the electron beam pulse duration from 50 μs to 200 μs leads to an increase in the crystal lattice parameter of γ-Fe from 0.35191 nm to 0.35300 nm. Taking into account the ratio of the sizes of the atomic radii of Fe (R(Fe) =

0.126 nm) and Cu (R(Cu) = 0.128 nm), we can conclude that the process of replacing iron atoms in the crystal lattice of the γ-phase by copper atoms increases with an increase in the duration of the electron beam pulse, which leads to an increase in the lattice parameter.

Thus, a two-stage mechanism of solid solution decomposition in the "film (Cu) / (steel 321) substrate" system irradiated with a pulsed electron beam was revealed, as a result of the performed studies. At an electron beam treatment duration of 50 μs, the formation of nanosized particles of the $Fe_{0.5}Cu_{0.5}$ phase, which has a bcc crystal lattice, is observed. With an increase in the duration of exposure to the electron beam to 200 μs, the formation of $Fe_{0.7}Cu_{0.3}$ composition phase, which has an fcc crystal lattice, is recorded in the steel surface layer.

Acknowledgements. The work was supported by the Ministry of Science and Higher Education of the Russian Federation (Number: FWRM-2021-0006).

REFERENCES

1. Dreval L.A. Thermodynamic properties of liquid alloys of copper and iron with chromium, cobalt and nickel / L.A. Dreval. Abstract of the dissertation of Cand. chem. Sciences. Kiev: Kiev National University. 2011 20 p.
2. Gornostyrev Yu.N. Interaction of dislocations with nanoscale precipitates of the metastable phase and dispersion strengthening of the Fe-Cu alloy / Yu.N. Gornostyrev, I.N. Karkin, L.E. Karkina // Solid State Physics. 2011. V.53. No. 7. S. 1317-1324.
3. Saltykov S.N. On the issue of polymorphic modifications of iron in a thin-film state / S.N. Saltykov, A.M. Hoviv, A.A. Maksimenko // Journal of Inorganic Chemistry. 2011. V. 56. No. 3. P. 373–376.
4. Evolution of the Steel Surface Layer Structure Subjected to Electron-Ion-Plasma Processing Methods, Ed. N.N. Koval, Yu.F. Ivanova. Tomsk: NTL, 2016. 304 p.

UDC 669.713.017:538.9

DYNAMICS OF LEAD MICROHARDNESS IN AN EXTERNAL MAGNETIC FIELD WITH INDUCTION UP TO 0.5 T

Serebryakova A. A., Zaguliaev D. V., Shlyarov V.V.

Siberian State Industrial University, Novokuznetsk, Russia

E-mail: aserebrakova87@gmail.com

Abstract. The microhardness of samples of technically pure lead was measured without exposure and under the influence of an external magnetic field with an induction of up to 0.5 T. Dependences are obtained that establish the effect of the magnetic treatment time on the microhardness of C2 grade lead. The exposure time at which the maximum effect of the influence of the magnetic field on microhardness is observed is revealed.

Keywords. Lead, magnetic field, microhardness.

The issues of controlling the plastic and strength properties of metals and alloys through external energy influences are relevant in the field of materials science and metalworking, one of such influences is the magnetic field [1]. In this paper, such a type of external influence as a weak magnetic field (up to 0.5 T) will be considered. Magnetic fields are often used in the processing of materials, since according to research, it is known that magnetic processing allows to improve the quality of the material [2]. Studies performed with the use of strong magnetic fields for processing materials are widespread [3]. The effect of a constant magnetic field allows you to control the mechanical properties (strength, ductility and hardness) and the

processes of plastic deformation of various materials and alloys [4]. As is known, metals are divided into ferromagnets, paramagnets, antiferromagnets and diamagnets by their magnetic nature. In this paper, the influence of a magnetic field on a diamagnet, technically pure C2 grade lead, is investigated [5]. The purpose of this work is to study the dynamics of microhardness of C2 grade lead under the influence of a magnetic field with different induction values of 0.3 Tl, 0.4 Tl and 0.5 Tl. This study is relevant, since various results of the influence of a strong magnetic field on materials and alloys are known, and the area of influence of weak magnetic fields on materials remains poorly studied.

For microhardness tests, lead samples were used in the form of a rectangular parallelepiped, 12 mm high, 5 mm wide, 15 mm long. In the studied samples, the lead content was 99.98%, the impurity content did not exceed 0.12%. Lead samples previously subjected to recrystallization annealing at a temperature of 200℃ for two hours, were subsequently cooled 24 hours to room temperature.

As a source of the magnetic field, a permanent electromagnet was used, which has the ability to regulate the induction of the magnetic field. In this work, the induction was adjusted by changing the current strength in the coils. The magnitude of the magnetic field induction was measured by a TPU milliteslameter. The tests were carried out at room temperature.

In microhardness studies, the samples were placed in a magnetic field so that the induction lines were perpendicular to the side of the sample with dimensions of 1.5 × 1.2 cm and penetrated it. Magnetic field treatment in this work was carried out in four modes. Mode 1, 2, 3 and 4 were exposure within the field with an induction of 0.3, 0.4 and 0.5 T for 1 hour, 2 hours, 3 hours, 4 hours.

The microindentation procedure was carried out on the HVS-1000 Vickers microhardness meter. Test load: 10 g. The loading time and under load was 10 s. The unloading time was 5 s., the number of loads was 20 (for each measurement). Data processing based on the results of micro-identification is performed in Excel and Origin Pro 8 programs.

As a result of tests of lead C2 after exposure in a magnetic field of various inductions, dependences were obtained showing the nature of the initial effect of influence on the material (Figure1). The initial effect of the influence of the magnetic field on microhardness was revealed by measuring microhardness immediately after exposure in a magnetic field.

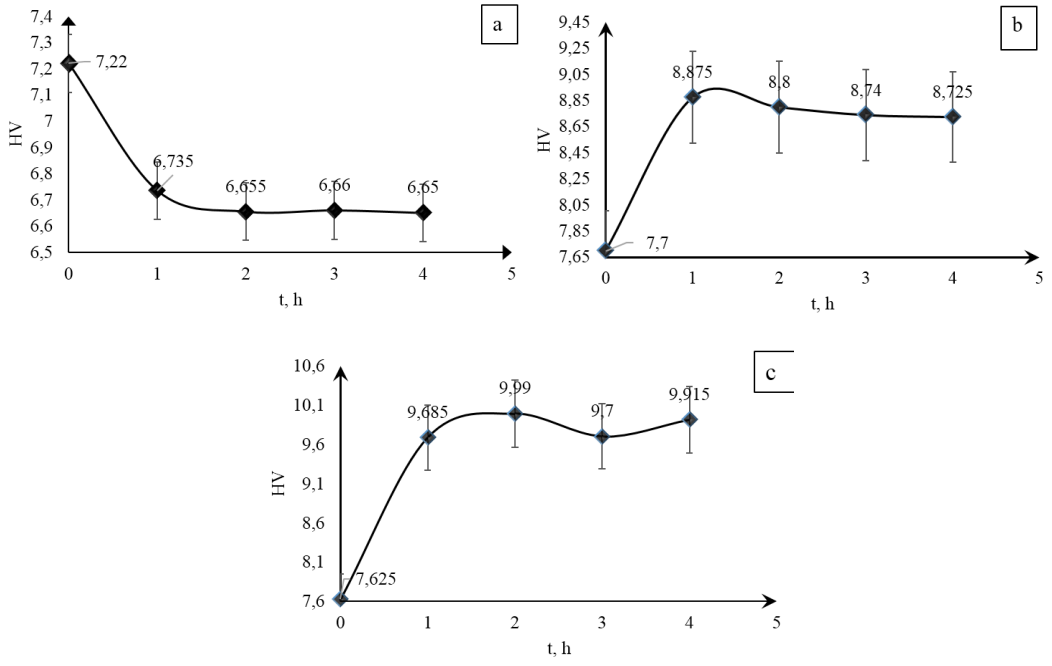

Figure1 – Initial effect of 0.3 Tl (a), 0.4 Tl (b), 0.5 Tl (c) MP on lead samples

According to the data obtained, it can be seen that the magnetic field has the greatest effect on microhardness during the first hour of exposure in a magnetic field at all values of magnetic induction. Further exposure in a magnetic field for 2, 3, 4 hours does not significantly affect the microhardness of lead. The initial effect of the influence of the magnetic field on the microhardness of lead C2 shows a different result, depending on the magnitude of the magnetic field induction, namely, there is both a decrease (Figure1a) and an increase (Figure1b, c) of the microhardness value under the influence of the magnetic field. From the analysis of the graphs in Figure 1, it can be seen that at a magnetic induction value of 0.3 T (Figure1a), the microhardness decreased during the first hour of exposure. At magnetic induction values of 0.4 and 0.5 T, the microhardness increased during the first hour of exposure (Figure1b, c). A similar non-monotonic character of the microhardness dynamics was discovered when studying the dynamics of the crystal microhardness under the influence of a magnetic field [6].

Thus, based on the experiments performed, it can be concluded that the initial effect of magnetic treatment obtained is ambiguous depending on the value of the magnetic field induction. At a magnetic induction value of 0.3 T, the microhardness decreases by 6.7% compared to the initial one. At induction values of 0.4T and 0.5T, an increase in microhardness was revealed by 14.2% and 27.1%, respectively.

The research was carried out at the expense of a grant from the Russian Science Foundation (project No. 21-79-00118).

REFERENCES

1.Ida, N. The Static Magnetic Field / N. Ida // In book: Engineering Electromagnetics. 2021. - pp.377-418.

2.Gillon P. Uses of intense d.c. magnetic fields in materials processing / Materials Science and Engineering: A. – 2000. - №287. – pp. 146-152.

3.Watanabe K., Motokawa M. Materials Science in Static High Magnetic Fields. -2002.-10.1007

4. Kraev M., Kraeva V. The influence of a constant magnetic field on the deformation resistance and hardening of metals. - 2018

5. Romanteev Yu.P. Metallurgy of heavy non-ferrous metals. Lead. Zinc. Cadmium. - MISIS - M., 2010. - 374 p.

6. Reversible and irreversible changes in the plastic properties of NaCl crystals, caused by the action of a magnetic field / Yu.I. Golovin, R.B. Morgunov, D.V. Lopatin, etc. //FTT. 1998. No. 11. pp. 2065-2068

UDC 539.31

INVESTIGATION OF THE DEPENDENCE OF THE LÜDERS BAND FRONT SLOPE ON THE PARAMETERS OF UP-DOWN-UP EQUATION

Chirkov A.O.[1], Eremin M.O.[2] and Pazhin A.[1]

[1] National Research Tomsk State University, Tomsk, Russia

[2] Institute of strength physics and materials science of the Siberian branch of the Russian academy of sciences, Tomsk, Russia

E-mail: chirkovartyem@gmail.com

Abstract. In this work, the computational study of yield point phenomenon is performed. The low-carbon steel demonstrating the yield point phenomenon is chosen as material for investigation. Judging by the literature review, there is a lack of papers addressing numerically the curves of dependences of Lüders band inclination on parameters of up-down-up constitutive equation. It is shown that the difference between the true upper and lower yield stresses has an unclear effect on the slope of the Lüders band when the J_2-plasticity is employed as a part of the model.

Keywords: Plastic strain, Lüders bands, up-down-up constitutive equation, yield stress

Lüders bands appear in the yield plateau stage of loading diagram as the switching waves transferring the gauge section of the sample of some low-carbon steels from elastic to plastic state. One of the explanations of the transition to a plastic state in the form of Lüders band is a local loss of stability. Meanwhile the front continues its motion due to regularities of the relaxation and recovery of stress behind the front. Notably, that the Lüders band inclination angle to the loading axis might exhibit a sufficient change during propagation. The inclination angle of the Lüders band was calculated numerically in many works (e.g. Zhang et al., 2008; Johnson, 2012; Yu et al., 2021). However, the topic of the dependence of the Lüders bands inclination angle on the parameters of the up-down-up (UDU) constitutive equation demands lucidity since some of the results are contradictory. This work is intended to supplement the existing research in order to clarify this issue. We use UDU constitutive equation which was apparently first time used to simulate Lüders banding in (Shaw and Kyriakides, 1997). Its schematic representation is given in Figure 1.

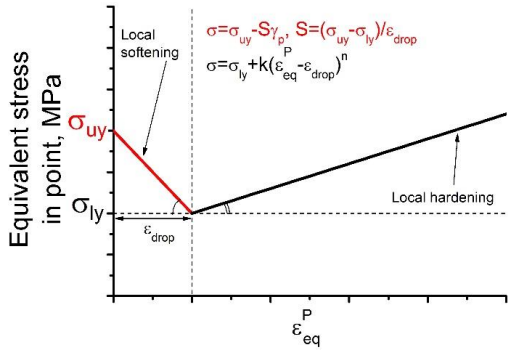

Figure 1 – Schematic representation of "up-down-up" constitutive equation in a point of continuum. An example of linear hardening law is taken when hardening exponent *n* is equal to unity.

Modeling of uniaxial tension was carried out in the framework of three-dimensional finite-difference method. It is based on the explicit time integration scheme of solid mechanics dynamic equations (Wilkins, 1999).

A numerical experiment was carried out so that the parameters of up-down-up equation, namely, the stress drop Δσ and strain hardening factor k were changed in a certain range. To eliminate the influence of the velocity of the Lüders band front on the result, several options were considered, in which the ratio Δσ:k was 4, 6, and 8, and the length of the yield plateau section was ~10%, ~7.5%, and ~6%, respectively.

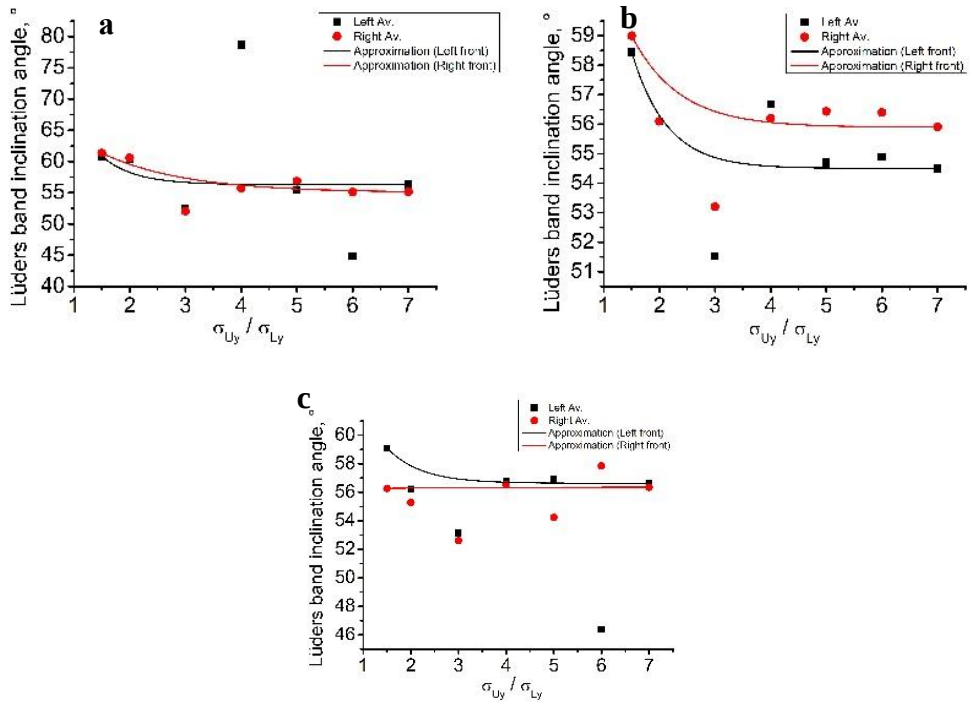

Figure 2 – Dependence of the Lüders band inclination angle on the ratio of the upper and lower yield stresses at Δσ:k=1:4(a), Δσ:k=1:6(b); Δσ:k=1:8(c). Black and red points correspond to average inclination angle of left and right Lüders band fronts, respectively

Upon reaching the upper yield point two bands of strain localization originate near the sample supports and start to propagate towards each other. The dependences of inclination angle of Lüders bands on the ratio of the upper and lower yield stresses for different ratios of Δσ:k are illustrated in Figure 2.

There is a section distinguished in the beginning of all diagrams, which is characteristic of a relatively small difference between the upper and lower yield stresses. The higher values of the inclination angles of the Lüders bands can be observed (up to 60°) in this section. An increase in σUy/σLy ratio does not produce a significant change in the slope of the Lüders band. An inclination angle remains approximately constant ~56°.

If we compare the results obtained in this work with the analytical solution presented in (Schwab and Ruff, 2013) we can conclude that the results are contradictory. The latter might be the result of difference in limit design approaches employed in works. The J2-plasticity approach is employed in this work and Coulomb-Mohr theory was employed in (Schwab and Ruff, 2013).

This work was supported by the Russian Foundation for Basic Research under grant № 20-31-90016.

REFERENCES

1. Johnson D.H., 2012. Lüders bands in RPV steel
2. Shaw, J.A., Kyriakides, S., 1997. Initiation and propagation of localized deformation in elasto-plastic strips under uniaxial tension. International Journal of Plasticity 13 (10), 837-871.
3. Yu K., Hou L., Guo M., Li D., Huang D., Zhuang L., Zhang J., Wu P., 2021. A method for determining r-value of aluminum sheets with the Portevin-Le Chatelier effect. Materials Science & Engineering A 814 (2021) 141246.
4. Zhang Y.T., Ao T., Jiao W. , Cui Y.H., 2008. Prediction of the Lüders band in fine grained steel strips under uniaxial tension. Computational Materials Science 41, 547–552.
5. Wilkins M., 1999, Computer Simulation of Dynamic Phenomena, Springer-Verlag.
6. Schwab R., Ruff V., 2013. On the nature of the yield point phenomenon. Acta Materialia 61(5), 1798–1808.

UDC 669.017.15

INFLUENCE OF ELECTRON-BEAM PROCESSING ON THE PROPERTIES OF CO-CR-FE-MN-NI HIGH-ENTROPY ALLOY

Kirillova A.[1], Konovalov S.[2], Gromov V.[2], Osintsev K.[1,2], Ivanov Y.[2,3], Bessonov D.[2], Panchenko I.[2]

1 - Samara National Research University, Samara, Russia,

2 - Siberian State Industrial University, Novokuznetsk, Russia,

3 - Institute of High Current Electronics SB RAS, Tomsk, Russia,

E-mail: ksv@ssau.ru, gromov@physics.sibsiu.ru, yufu55@mail.ru

Abstract. The article is devoted to a comprehensive study of the effect of electron-beam processing on the mechanical properties of a high-entropy alloy of the Co-Cr-Fe-Mn-Ni system obtained using additive manufacturing technology. The study consisted in evaluating the chemical composition of the alloy obtained by twisting wires of various compositions of the initial components. An assessment of the structural-phase composition of the alloy and its mechanical properties after processing by electron beams has been carried out.

Keywords: high-entropy alloy, structure, microhardness, phase composition, additive manufacturing.

High-entropy alloys (HEAs) are relatively new and understudied structural materials consisting of 5 or more main components. HEAs are metal materials with enhanced performance characteristics, and their formation is based on a fundamentally new technology that excludes the presence of a basic component.

In this paper, a high-entropy alloy of the Co-Cr-Fe-Mn-Ni system, obtained using modern additive manufacturing technologies, is analyzed. The multicomponent wire of this system is made by twisting wires of different chemical composition on the original installation in several

modes. To select the optimal twisting mode, which ensures the passage of the wire in the guide channel and the burner nozzle, the rotational speed of the receiving and supply coils was varied.

To obtain an alloy of this composition, the following wires were chosen: cobalt wire (Co ≈ 99.9 at. %) with a diameter of 0.47 mm; welding wire Autrod 16.95 (Fe ≈ 65.3 at. %, Cr ≈ 19.6 at. %, Ni ≈ 7.3 at. %, Si ≈ 1.6 at. %, Mn ≈ 6.2 at. %), 0.74 mm in diameter; chromium-nickel wire Ni80Cr20 (Cr ≈ 22.5 at. %, Fe ≈ 1.5 at. %, Ni ≈ 72.1 at. %, Al ≈ 0.8 at. %, Si ≈ 2.9 at. %, Mn ≈ 0.2 at. %) with a diameter of 0, 4 mm. The calculated elemental composition, expressed in atomic percent, using these wires as the starting material, was: Co 25.0 at. %, Cr 14.9 at. %, Fe 37.9 at. %, Mn 3.5 at. %, Ni 17.9 at. %, Al 0.1 at. %, Si 0.9 at. %, where Al and Si are possible impurities. As a result, the diameter of the resulting combined Co-Cr-Fe-Mn-Ni cable was ≈ 1.2 mm, with a laying length of 10 mm. On samples from the obtained alloy, before electron-beam processing, studies were carried out to determine the chemical, structural-phase composition and mechanical properties. The results of studies of mechanical properties are shown in table 1.

Table 1 – Results of changes in mechanical properties under compression depending on the manufacturing mode

№ Reqme	Tensile strength, MPa	Relative deformation, %	Microhardness, HV
1	1689	54	174
2	1690	56	176
3	1720	56	178

Due to the fact that the samples obtained by mode No. 1 demonstrated the best mechanical properties, they were chosen for surface treatment with a pulsed electron beam. The surface treatment of the resulting alloy was carried out by a pulsed electron beam with different parameters. The irradiation of the samples was carried out on the SOLO facility, designed and manufactured at the ISE SB RAS. Sample irradiation mode: accelerated electron energy 18 keV, electron beam energy density 10, 15, 20, 25, 30 J/cm^2, beam pulse duration 50 μs, pulse repetition rate 0.3 s^{-1}, number of pulses irradiation 3, irradiation was carried out at a residual pressure of an inert gas (argon) in the working chamber of the installation $2 \cdot 10^{-2}$ Pa. After surface treatment, studies of the mechanical properties of the alloy were also carried out.

Table 2 – The results of measuring the mechanical properties in tension depending on the energy density of the electron beam

Electron beam energy density, J/cm^2	Conditional yield strength, MPa	Tensile strength, MPa	Relative deformation, %	Microhardness, MPa
0	279	499	63	3,1
10	284	442	53	2,7
15	298	341	33	1,7
20	355	472	53	1,8
25	285	320	45	1,7
30	240	312	35	1,8

Mechanical tests of a high-entropy alloy of the Co-Cr-Fe-Mn-Ni system in irradiated states, performed by uniaxial tension of flat samples, showed that irradiation of the alloy with a

pulsed electron beam in the mode of high-speed melting and subsequent high-speed crystallization of the surface layer leads to a decrease in the strength and ductility of the material. The tensile strength and relative strain decrease nonmonotonically with an increase in the energy density of the electron beam and reach their minimum values at 30 J/cm^2. The highest values were observed in the sample treated with an electron beam with an energy density of 20 J/cm^2 and reached the following values: ultimate strength 472 MPa, yield strength 355 MPa, relative strain 53%.

At the same time, irradiation of a high-entropy alloy of the Co-Cr-Fe-Mn-Ni system is accompanied by a 1.6-fold decrease in the microhardness of the treated layer (from 3.1 GPa before treatment to 1.8 GPa after).

Acknowledgement Study was supported by the Russian Science Foundation (project 20-19-00452).

UDC 539.3

CHANGE IN THE VALUE OF THE REGION OF COHERENT SCATTERING AND MICRODISTORTIONS OF THE CRYSTAL LATTICE OF AL-20%SI ALLOY SUBJECTED TO COMPLEX PROCESSING

Shliarova Yu.A.[1], Zaguliaev D.V.[1], Gromov V.E.[1], Ivanov Yu.F.[2], Shlyarov V.V.[1]

[1]Siberian State Industrial University, Novokuznetsk, Russia

[2]Institute of High-Current Electronics SB RAS, Tomsk, Russia

E-mail: rubannikova96@mail.ru

Abstract. The paper investigates the analysis of changes in the region of coherent scattering and microdistortions of the crystal lattice of an alloy subjected to complex processing. As a result, it was found that the size of the coherent scattering regions and the ratio of the silicone lattice microdistortions are larger in sample № 2. This can be determined by greater concentration of yttrium oxide powder introduced into the surface layer of silumin during the electroexplosive doping.

Keywords: electron beam, modified layer, Al-20%Si.

Modification of the surface layer of silumin was completed in two stages. At the first stage electroexplosive doping of Al-20%Si was done, aluminum foils were used as the material for exploding conductors, Y_2O_3 was used as the test charge. At the second stage the modified surface was irradiated by a pulsed electron beam.

Table 1 – The conditions of electroexplosive doping and further treatment by electron beam

Mode №	Mass of the aluminum foil, m_{Al} (mg)	Mass of the powder Y_2O_3, $m_{Y_2O_3}$ (mg)	Discharge voltage, U (kV)	Electron beam energy density, J/cm^2	Energy of accelerated electrons keV	Electron beam pulse duration, μs	Number of current impuses	Pulse repetition rate, s^{-1}
1	58.9	58.9	2.8	35	18	150	3	0.3
2	58.9	88.3	2.6	25				

Study of the phase composition and structural parameters of the samples was completed by the methods of X-ray structure analysis (X-ray diffraction meter XRD-6000 on CuK_{α}-radiation).

As a result of the research, it was found that the main phases in the initial state of the Al-20% Si alloy are a solid solution based on aluminum and silicon. After complex treatment in the Al-20% Si alloy, the size of the coherent scattering region (CSR) changes. At an electron beam energy density of 25 J/cm^2, the CSR size for the Al phase reaches its maximum value and amounts to 320.53 nm (Figure 1). An increase in the energy density of the electron beam to 35 J/cm^2 leads to a decrease in CSR to a value of 94.31 nm. For the Y_2O_3 phase, the size of the CSR changes insignificantly. At an electron beam energy density of 25 J/cm^2, the CSR reaches a minimum value of 13.08 nm, and at 35 J/cm^2 it reaches 24.09 nm. At an electron beam energy density of 25 J/cm^2, the CSR size for the Si phase is 41.92 nm, and at 35 J/cm^2 it decreases to 16.27 nm (Figure 1).

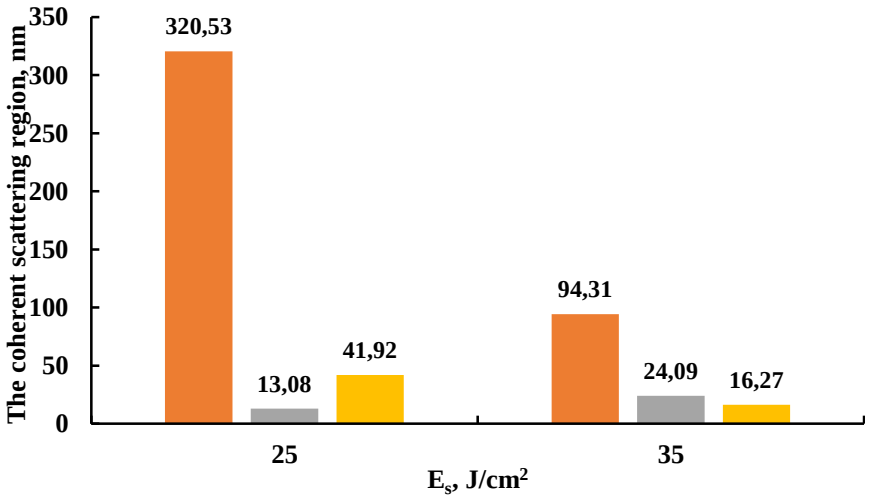

Figure 1 – Dependence of the size of the coheret scattering region on the energy density of the electron beam

The microdistortions of the crystalline lattice of yttrium oxide change significantly: they increase by three times when the energy density of the electron beam grows from (25 to 35) J/cm^2 (Figure 2). The microdistortions of the crystalline lattice of Al and Si phases change in an opposite way: they reduce as the energy density of the electron beam increases.

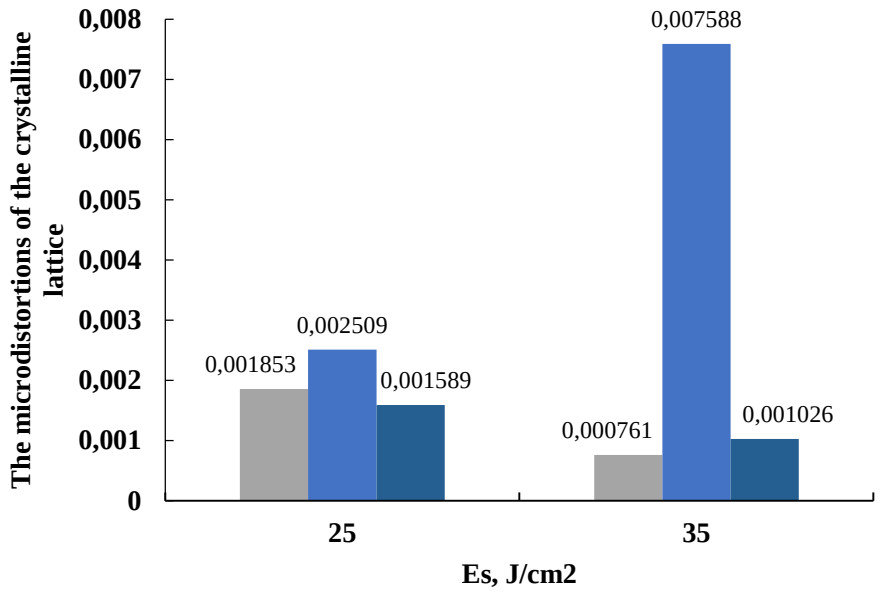

Figure 2 – Dependence of the mictodistortions of the crystalline lattice upon the energy density of the electron beam for Al-20%Si alloy

The size of the coherent scattering regions and the ratio of the silicone lattice microdistortions are larger in sample № 2. This can be determined by greater concentration of yttrium oxide powder introduced into the surface layer of silumin during the electroexplosive doping.

The research was granted by the Russian Science Foundation (project No. 19-79-10059).

UDC 538.913

A REVIEW OF THE ELECTROPULSING EFFECT ON EVOLUTION OF TEXTURE IN SILICON STEEL

Guoliang Hu[1,2], Jianxiu Liu[1], Baofeng Zhang[1]

[1]Huanghe Science and Technology College, China

[2]Shenzhen Sanpin Hulian Technology Co., Ltd

Keywords: electropulsing; recrystallization; texture; Fe-Si steel

As a new developing process, electropulsing has been found to be more powerful than the thermal energy in improving microstructure and the properties of the alloys, and in strengthening the metallurgical processes [1 – 5]. Electropulsing treatment (EPT) has been applied to obtain well recrystallized grains and to retard the formation of annealing twins in the cold-worked alloys [6,7].

Grain-oriented electrotechnical steel sheets are mainly used as a core material for transformers and other electrical equipment because of their high magnetic induction and low watt losses during premagnetization [8–11]. The recrystallization texture of grain oriented Fe-3 pct Si steel has long been a subject of research. It has been reported that a major driving force for recrystallization was the stored energy generated during deformation, and the textures of the recrystallization were related to the grain stored energy, rolling reduction, annealing temperature, and so on [8 – 11]. Also, it was indicated that

the stored energy of grains was closely related with the orientations in the shear bands. Goss texture (110) <100> was a typical microtexture of the GO silicon steel. The formation and growth of the Goss texture {110} <001> occurred in sequence during recrystallization, i.e., in the primary and secondary stages [8,9]. As a new developing process, electropulsing was found to be more powerful than the thermal energy in improving microstructure and the properties of the alloys, and in strengthening the metallurgical processes[12 – 16]. Electropulsing treatment (EPT) was applied to obtain well-recrystallized grains and to retard the formation of annealing twins in the cold-worked alloys [12,17-19].

The electropulsing induced texture evolution during recrystallization was studied by EBSD. Shown in Figures.1a and b are the EBSD mapping and ODF by EBSD of the EPT specimens with various voltages and temperatures, respectively. During 74.0V/510℃-EPT, with the additional electropulsing induced Gibbs free energy, recrystallization of those high energy stored γ-grains took place firstly. The γ- (111)<112> (dark blue in color) and (111) <110> texture (light blue in color) vanished, and left only partially recrystallized α (100)<110> texture (green in color) in the specimen, as shown in Figure 1a1. The $\varphi_2 = 45^O$ section of ODF by EBSD confirmed what was obtained from the EBSD mapping, as shown in Figure 1b1. The (100)<110> texture is indicated by white arrows, as shown in Figure 1 b1 [20, 21].

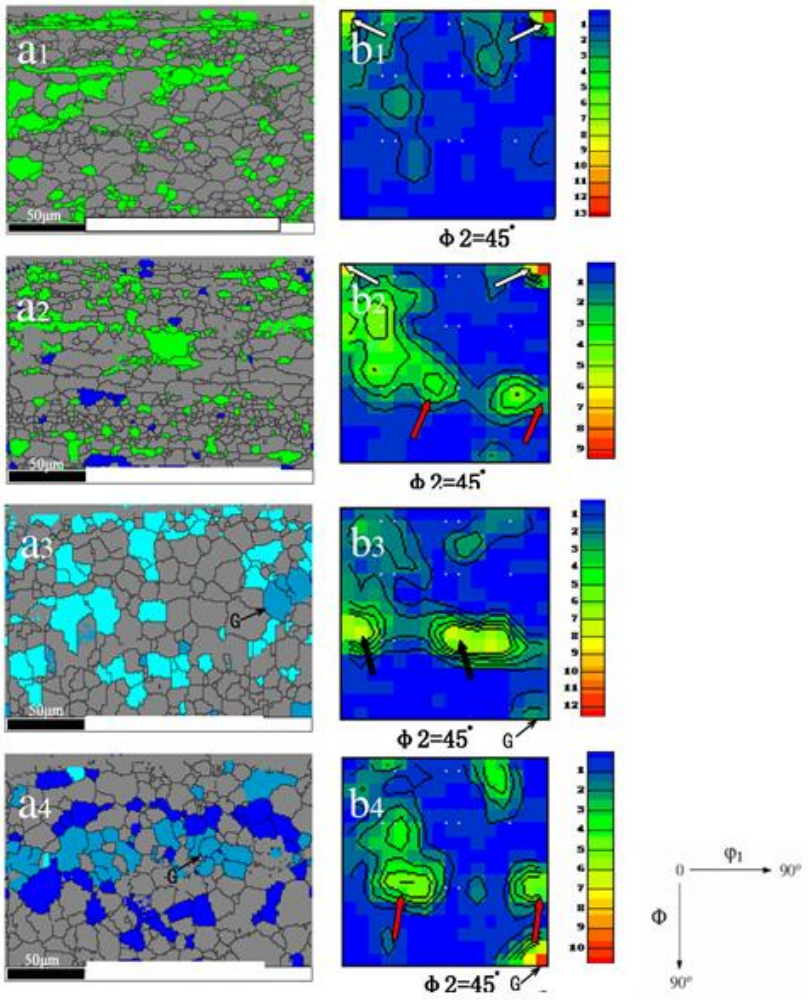

Figure 1 – EBSD mapping and ODF Figureure examined by EBSD

(a1) EBSD mapping after 74V/510℃;((b1) ODF Figureure after 74V/510℃
(a2)EBSD mapping after 76V/580℃; (b2) ODF Figureure after 76V/580℃
(a3)EBSD mapping after 77.5V/750℃; (b3) ODF Figureure after 77.5V/750℃
(a4) EBSD mapping after 79V/850℃; (b4) ODF Figureure after 79V/850℃

Compared with the textures in the 620℃/20 mins-annealed specimen, the recrystallization was apparently accelerated in the EPT specimen. It is supposed that the deformed γ textures, such as the (111)<110> and (111)<112> decreased rapidly during the early stage of recrystallization . This implies that the textures of the74V/510℃-EPT specimens were developed to the middle stage of recrystallization.

Under 76.0V/580℃-EPT, electropulsing accelerated the movement of dislocation and caused vacancies to pile up and to block at the grain boundaries and other structural distorted sites. This resulted in a local high strain-concentration and facilitated forming the (111)<112> texture. A small amount of the recrystallized grains with (111)<112> texture (dark blue in color) was observed, as shown in the EBSD mapping (Figure 1 a2). Meanwhile the (100)<110> texture (green in color) reduced, as shown in Figure 1 a2.

The φ2 = 45^{O} section of ODF by EBSD illustrates what was observed in the EBSD mapping (Figure 1a2), as shown in Figure 1b2. The (100)<110> and (111)<112> textures are indicated by white and red colored arrows of colors, respectively.When the intensity of the electropulsing increased to 77.5V/750℃-EPT, a new balance between the accumulation and the annihilation of the dislocations was established . Both the texture (100)<110> (green in color) and the higher energy stored (111)<112> texture (dark blue in color) vanished. The textures consisted of mainly (111)<110> (light blue in color) and a small amount of G (110)<100>, as shown in EBSD mapping (Figure 1(a3)). The related φ_2 = 45^{O} section of ODF by EBSD ODF are shown in Figure 1(b3), where the **G** texture (110)<001> and the (111)<110> texture are indicated by " **G** " and black arrows, respectively.

Upon increasing the intensity of the electropulsing to 79.0V/850℃, the high energy stored γ-grains with (111)<112> texture formed prolifically again. Meanwhile, the **G** texture (110)<001> was well developed together with a few recrystallized (111)<110> grains remained, as shown in the EBSD mapping (Figure 1(a4)). The texture induced by the

79V/850℃-EPT was similar to that which was observed in the 850℃-annealed specimen (Figure2 (a1)). The related φ_2 = 45^{O} section of ODF by EBSD ODF is shown in Figure1 (b4), where the **G** texture (110)<001> of a volume fraction of Fe[13.9%] and the (111)<110> texture are indicated by " **G** " and red arrows. Then under the annealing, the related φ_2 = 45^{O} section of ODF by EBSD ODF is shown in Figure 2 (b1), where the **G** texture (110)<001> of a volume fraction of Fe is only about 3%.The (111)<110> texture,(110)<001> texture are indicated by red arrows and " **G** " [20,21].

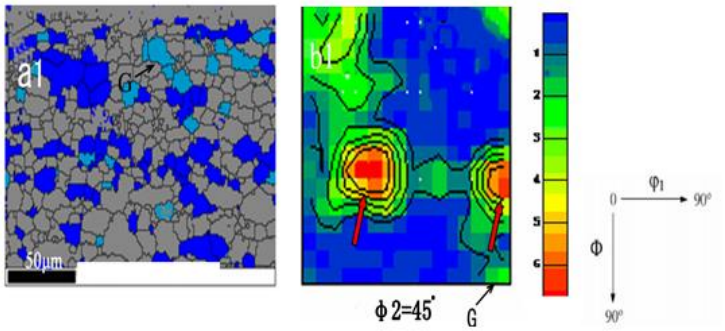

Figure 2 – Texture distributions and ODF Figureures examined by EBSD

(a1) texture distribution after annealing at 850
(b2) ODF Figureure after annealing at 850℃

As can be seen from the above, the electropulsing tremendously accelerated formation of the G texture. At the same temperature of recrystallization, compared with the annealing, the electropulsing is conducive to promote the formation of the **G** texture (110)<001> .

REFERENCES

1. Y.H. Zhu, S. To, W.B. Lee, X.M. Liu, Y.B. Jiang, G.Y. Tang, Mater, Sci. Eng.A, 2009, vol.501, pp 125-132.

2. S. To.Y. H. Zhu.W. B. Lee. G. Y. Tang. X. M. Liu. Y. B. Jiang, Mater.Trans., 2009, Vol.50/12, pp 2772-2777.

3. Y.H. Zhu, S. To, X.M. Liu and G.L.Hu, Metall. Mater. Trans.A, "Effects of electropulsing on microstructure and elongation of a Zn-Al based alloy (ZA22) " in press.

4. Y.H. Zhu, S. To, W.B. Lee, X.M. Liu, Y.B. Jiang, G.Y. Tang, J. Mater. Res., 2009. vol.4, pp 2661-2666.

5. S. To. Y.H. Zhu .W.B. Lee .X.M. Liu .Y.B. Jiang .G.Y. Tang, Appl. Phys A, 2009, vol. 96, pp 939-944.

6. Z.H. Xu, G.Y. Tang, F. Ding, S.Q. Tian, H.Y. Tian, Appl. Phys. A, 2007, vol. 88, pp 429-433.

7. V.V. Stolyarov, Mater.Sci.Eng. A, 2009, vol.503, pp 18-20.

8. N.H. Heo: Mater. Lett., 2005, vol. 59, pp. 2827–31.

9. C. Gheorghies and A. Doniga: J. Iron Steel Res. Int., 2009, vol. 16 (4), pp. 78–83.

10. D.N. Lee Intern and H.T. Jeong: Scripta Mater., 1998, vol. 38, pp. 1219–23.

11. J.T. Park and J.A. Szpunar: Acta Mater., 2003, vol. 51, pp. 3037– 51.

12. Y.H. Zhu, S. To, W.B. Lee, X.M. Liu, Y.B. Jiang, and G.Y. Tang: Mater. Sci. Eng. A, 2009, vol. 501, pp. 125–32.

13. S. To, Y.H. Zhu, W.B. Lee, G.Y. Tang, X.M. Liu, and Y.B. Jiang: Mater. Trans., 2009, vol. 50 (12), pp. 2772–77.

14. Y.H. Zhu, S. To, X.M. Liu, and G.L. Hu: Metall. Mater. Trans. A, 2011, vol. 42A, pp. 1933–40.

15. Y.H. Zhu, S. To, W.B. Lee, X.M. Liu, Y.B. Jiang, and G.Y. Tang: J. Mater. Res., 2009. vol. 4, pp. 2661–66.

16. S. To, Y.H. Zhu, W.B. Lee, X.M. Liu, Y.B. Jiang, and G.Y. Tang: Appl. Phys. A, 2009, vol. 96, pp. 939–44.

17. Z.H. Xu, G.Y. Tang, F. Ding, S.Q. Tian, and H.Y. Tian: Appl. Phys. A, 2007, vol. 88, pp. 429–33.

18. V.V. Stolyarov: Mater. Sci. Eng. A, 2009, vol. 503, pp. 18– 20.

19. V.E. Gromov, Y. Ivanov, F.E.V. Kozlov, E.Y. Suchkova, S.V. Konovalov, and V.A. Rybyanets: Proc. Electromagnetic Fields Effect on the Structure and Characteristics of Materials, Novokuznetsk, Russia, D. Yury, V.D. Baranov, V.E. Gromov, and T.G. Tang, eds., 2009, pp. 209–24.

20.G.L.Hu,G.Y.Tang, Y.H.Zhu,and C.H.Shek:METALLURGICAL AND MATERIALS TRANSACTIONS A,Vol.42A,pp.3484-3490.

21.G.L.Hu,G.Y.Tang, Y.H.Zhu,and C.H.Shek, J. Mater. Res., Vol. 26, No. 7,PP,917-922.

UDC 669.71'3:539.89:536.425

THE EFFECT OF PRE-DEFORMATION ON DISSOLUTION OF CU-RICH PRECIPITATES UNDER ELECTROPULSING IN AN AGED FE–CU ALLOY

Shengjun Xia[1,2], Gao Menglin[1,2], Xiaoshi Guan[1,2], Qiulin Li[1,*]

[1] Shenzhen International Graduate School, Tsinghua University, Shenzhen 518055, China
[2] School of Materials Science and Engineering, Tsinghua University, Beijing 100084, China

* E-mail: liql@sz.tsinghua.edu.cn

Abstract. Nanoscale Cu-rich precipitates (CRPs) are one important microstructural nano-features responsible for hardening and embrittlement of reactor pressure vessels (RPV). Pre-deformation of various deformation variables was applied to an aged model Fe-Cu alloy, and the Fe-Cu alloy was treated by electropulsing with same parameters. The dissolution behavior of CRPs under EPT was significantly promoted with the introduction of pre-deformation. The pipe diffusion and the localized Joule heating effect caused by high density dislocations could accelerate the dissolution of CRPs in the aged Fe-Cu alloy on account of the higher atomic drift flux.

Keywords: Cu-rich precipitates (CRPs); pre-deformation; dislocations; electropulsing; diffusion.

Nanoscale Cu-rich precipitates (CRPs) are one important kind of microstructural defects responsible for irradiation embrittlement and hardening of reactor pressure vessels (RPVs), which threaten the safe operation and limit the service time of nuclear power plants[1]. Electropulsing treatment (EPT) is a newly high-energy external field processing method, which has been widely used adjust microstructure and mechanical properties of metallic materials[2-6]. In these researches, EPT can change the microstructure and mechanical properties in short time and at lower temperature than equilibrium transition temperature, showing high efficiency. Therefore, applying EPT to the repair of RPV irradiation damage is expected to be a new idea for extending the life of nuclear reactors. In our previous study[7], an aged Fe-Cu model alloy was treated with EPT, confirming that compared with traditional annealing, EPT could rapidly dissolve the CRPs with lower temperature and shorter time.

Pre-deformation before EPT can introduce many dislocations and change the effect of the pulsed current[8,9]. Until now, the reverse thermodynamic dissolution of nanoclusters under EPT combined with pre-deformation has rarely been reported. Thus, the present work concentrates on the dissolution behavior of CRPs induced by EPT combined with pre-deformation.

A Fe-1.1%Cu alloy smelted with pure iron and pure copper in a 25 kg vacuum induction furnace was used in this study. The alloy ingot was solution treated at 1153 K for 5 h and then quenched into water. Then the alloy was isothermally aged at 773 K for 8 h to form CRPs. After the heat treatment, the Fe-Cu alloy was subjected to cold rolling with reductions of 10%, 40% and 70%. The current parameters and highest temperatures collected during EPT were shown in Table 1.

Table 1 – Current parmeters of EPT.

Sample no.	Frequency(Hz)	Duration(μ s)	j_m (A/mm^2)	Time(s)	Temperature(K)
0	100	73	187	60	930
10%	100	73	191	60	929
40%	100	73	192	60	907
70%	100	73	187	60	935

The Nano-measure software was used to amplify TEM pictures with same multiple, and the size of nanoprecipitates was measured one by one directly. The changes of number density and particle size are shown in Fig. 1. Fig. 1(a) shows that number density of CRPs decreased significantly for samples with pre-deformation after EPT, especially compared with the samples without pre-deformation. Fig. 1(b) shows that after EPT the average particle size increased significantly for pre-deformation samples from about 14nm to 26nm. However, there was only a slight increase in the no deformation sample.

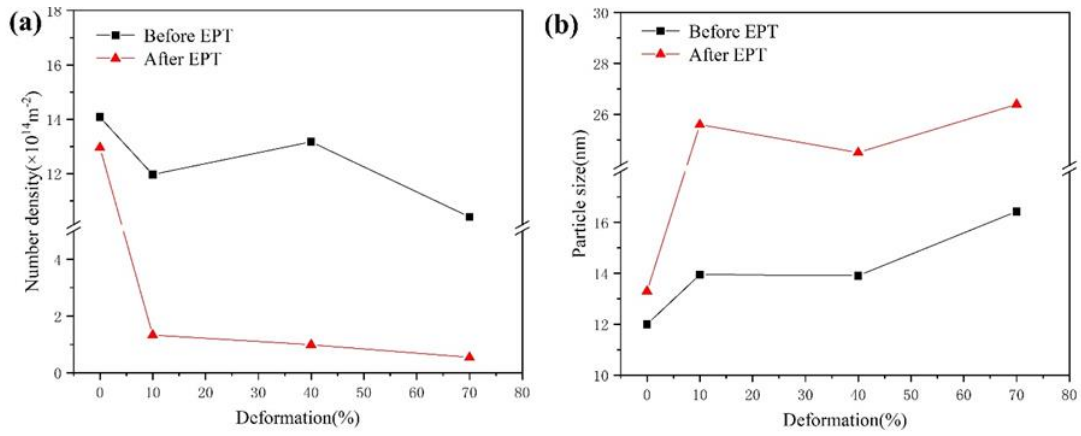

Figure 1 – The number density (a) and particle size (b) of CRPs before and after EPT.

The hardness of the samples before and after EPT is shown in Fig. 2. Cold rolling before EPT made the hardness of the samples increase significantly from 184.3HV to 258.4HV. However, all the samples with pre-deformation showed better hardness property than the sample without pre-deformation after treated with pulse current. The hardness of the sample with 70% deformation decreased the most.

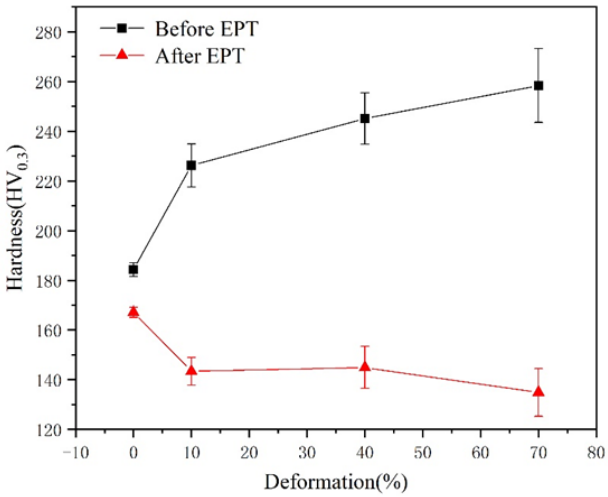

Figure 2 – Hardness of the Fe-Cu alloy before and after EPT

Figures 1 and 2 show that the dissolution behavior of CRPs under EPT was significantly promoted with the introduction of pre-deformation. The recovery of hardness was attributed to the enhanced dissolution of CRPs induced by combination of electropulsing and deformation. The pipe diffusion and the localized Joule heating effect caused by high density dislocations could accelerate the dissolution of CRPs in the aged Fe-Cu alloy on account of the higher atomic drift flux. Although it's difficult to apply deformation on reactor pressure vessels, this study has a guiding significance for the in-situ repair of RPVs due to a large number of dislocations will be introduced in the process of manufacturing and service.

This study was supported by the National Key Research and Development Program under Grant No. 2017YFB0305304.

REFERENCES

1 Odette, G. R. & Lucas, G. E. Embrittlement of nuclear reactor pressure vessels. JOM 53, 18-22, doi:DOI 10.1007/s11837-001-0081-0 (2001).

2 Liang, C. L. & Lin, K. L. The microstructure and property variations of metals induced by electric current treatment: A review. Mater. Charact. 145, 545-555, doi:10.1016/j.matchar.2018.08.058 (2018).

3 Zhou, Y., Xiao, S. & Guo, J. Recrystallized microstructure in cold worked brass produced by electropulsing treatment. Mater. Lett. 58, 1948-1951, doi:10.1016/j.matlet.2003.11.035 (2004).

4 Zhou, Y., Zhang, W., Guo, J. & He, G. Diffusive phase transformation in a Cu–Zn alloy under rapid heating by electropulsing. Philos. Mag. Lett. 84, 341-348 (2004).

5 Liu, X. & Zhang, X. An ultrafast performance regeneration of aged stainless steel by pulsed electric current. Scr. Mater. 153, 86-89, doi:10.1016/j.scriptamat.2018.05.004 (2018).

6 Kapoor, R. et al. Electric current induced precipitation in maraging steel. Scr. Mater. 154, 16-19, doi:10.1016/j.scriptamat.2018.05.013 (2018).

7 Gao, M., Liu, H., Xu, B., Liu, W. & Li, Q. Reverse evolution in nanoscale Cu-rich precipitates of an aged Fe–Cu alloy under electropulsing. Philos. Mag. Lett. 99, 39-47, doi:10.1080/09500839.2019.1615147 (2019).

8 Conrad, H. Effects of electric current on solid state phase transformations in metals. Mater. Sci. Eng. A 287, 227-237, doi:Doi 10.1016/S0921-5093(00)00780-2 (2000).

9 Xiao, H. et al. Study on the microstructure evolution and mechanical properties of an Al-Mg-Li alloy aged by electropulsing assisted ageing processing. Mater. Sci. Eng. A 756, 442-454, doi:10.1016/j.msea.2019.04.049 (2019).

SECTION 3. Problems of materials exploitation in extreme conditions

UDC 669.539.382:669.17:625.1

GRADIENT OF STRUCTURE-PHASE STATE OF RAILS ALONG CENTRAL AXIS OF TREAD SURFACE

Gromov V.E.[1], Kuznetsov R.V.[1], Ivanov Yu.F.[2], Kormyshev V.E.[1], Shliarova Yu.A.[1]

[1]Siberian State Industrial University, Novokuznetsk, Russia

[2]Institute of High-Current Electronics SB RAS, Tomsk, Russia

E-mail: gromov@physics.sibsiu.ru

Abstract. The structure, phase composition, dislocation substructure, mechanical properties in differentially quenched 100-meter rails are studied after their ultra-long-term operation (passed tonnage 1770 million gross tons) using the methods of modern materials science.

Keywords: rails, structure, phase composition, properties, ultra-long-term operation.

The main fraction of pearlite is the pearlite of lamellar morphology whose structure is formed by regular colonies with successive alternation of cementite and ferrite plates.

A long-term operation of rails (passed tonnage of 1770 million gross tons) is accompanied by numerous transformation of pearlite structure. Figure 1 presents metal microstructure of rail under study at a depth of 2 mm and 5 mm from tread surface along vertical axis.

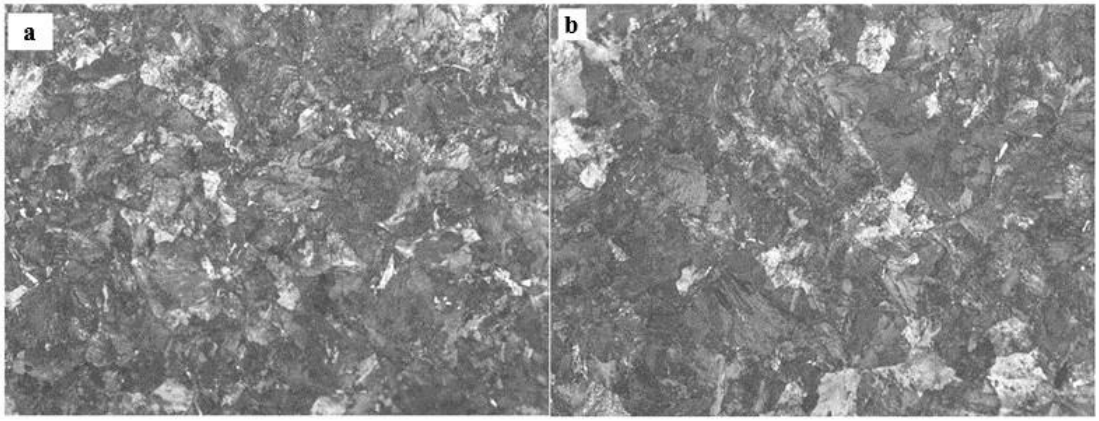

Figure 1 – Microstructure of metal in head of rail under study at a depth of 2 mm (a) and 5 mm (b) from tread surface along vertical axis. x500

TEM studies showed that in the layer not less than 2.0 mm thick a transformation of grains and colonies of lamellar pearlite, taking place in long-term operation, proceeds in the following way.

In the first place, the grains which retained a lamellar pearlite structure are revealed. The dark field analysis shows that ferrite plates in the grains are fragmentary, that is broken into areas separated from each other by low-angle boundaries. As a rule, transverse sizes of fragments correspond to those of ferrite plates, longitudinal sizes of fragments are 2-3-fold larger than their transverse sizes.

In the second place, the pearlite colonies in which cementite plates break into separate fragments, shifted relative to each other, are observed. It is suggested that the structure forms as a result of realization of mechanism of cutting off the cementite plates by moving dislocations.

In the third place, the pearlite colonies, wherein cementite plates are divided into separate particles of rounded shape, are observed. As a rule, the particles are surrounded by a large number of dislocations.

It is suggested that the structure forms as a result of realization of mechanism under action of which a fracture of cementite plates is realized by dissolution of cementite and transition of carbon atoms from lattice of iron carbide to lines of dislocations. In the layer adjacent to tread surface the sizes of the particles, having a globular shape and being revealed by the methods of dark-field analysis, vary in the limits from 10 nm to 25 nm. The sizes of the particles increase to 80-95 nm with distance from tread surface along central axis of rail.

In the fourth place, the material areas containing so-called channels of deformation [55, 56]. In this case, within lamellar pearlite colonies the extended areas, in whose volume a fragmentary substructure forms at the place of lamellar structure.

In the fifth place, the material areas having a subgrain structure whose characteristic image is presented in Figure 2. A quantitative analysis of the structure shows that subgrain sizes vary in the limits from 150 nm to 300 nm. On boundaries and in junctions of ferrite subgrain boundaries the particles of carbide phase locate, they are of globular shape. The sizes of particles vary in the limits from 25 nm to 55 nm. As a rule, the type of structure forms in junctions of pearlite colonies and grains, which may be caused by incompatibility of plastic deformation of the material areas in the process of ultra long-term operation of rails.

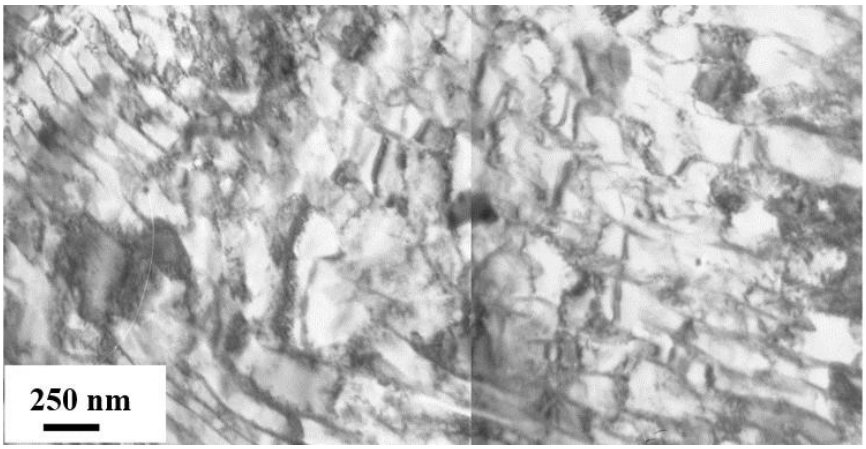

Figure 2 – Structure of tread surface layer of rail head

The research was supported by RFBR grant no. 19-32-60001.

REFERENCES

1. Gromov, V. E. Deformation channels under conditions of electrically stimulated drawing / V. E. Gromov, E. V. Kozlov, V. E. Panin, Yu. F. Ivanov, Yu. P. Sharkeev, G. V. Pushkareva // Metallophysics. 1991. Vol. **13**. No. 11. P. 9-13.

2. Ivanov, Yu. F. Evolution of localized deformation channels in the process of electrically stimulated drawing of low carbon steel / Yu. F. Ivanov, V. E. Gromov, E. V. Kozlov, O. V. Sosnin // Izvestiya. Ferrous Metallurgy. 1997. No. 6. P. 42-45.

Scientific Edition

MATERIALS IN EXTERNAL FIELDS (ISMEF 2022)

Proceedings
of the 11th INTERNATIONAL ONLINE SYMPOSIUM

Under the general editorship of	V.E. Gromov
Desktop publishing	A.N. Gostevskaya
Technical editor	A.A. Serebryakova

Publishing License of 15.03.2022.

Paper format 60x84 1/16. Writing paper. Offset printing.

Conv. print. sheet 8.46 Stand. publ. sign. 8.95 Number of copies 500. Order N° 69

Siberian State Industrial University

654007, Kemerovo region - Kuzbass,
Novokuznetsk, 42 Kirova Str.

SibSIU Publishing Center